DEVELOPMENT OF EXPERIMENTAL RUBBER TOUGHENED BONE CEMENTS

Myfanwy Nicholas

PhD Thesis

2007

School of Engineering

Cardiff University

ProQuest LLC
789 East Eisenhower Parkway
P.O. Box 1346
Ann Arbor, MI 48106-1346

ABSTRACT

Acrylic bone cement is used in orthopaedic surgery for total joint replacements as a means of fixation of the prosthesis to the bone. One of the main problems associated with total joint replacements is aseptic loosening which can be caused by the brittle fracture of the cement.

The purpose of this research was to improve the resistance of bone cement to brittle fracture by creating new experimental cements containing the thermoplastic rubber, acrylonitrile-butadiene-styrene (ABS), and to determine if improvements could be furthered by using ABS surface coated with a silane coupling agent, the latter having never been investigated before. Incorporating the ABS into the cement will affect the cements' rheological/handling characteristics, therefore these properties were investigated over the entire curing process both at 25°C and 37°C.

The results showed that the introduction of either ABS or silane-coated ABS significantly improved the fracture resistance of the cement. The fracture toughness of cements containing 30% ABS increased by 19%, and 40% silane-coated ABS by 31%. There was also a substantial improvement in fatigue crack propagation behaviour with cements containing 30% and 40% ABS or silane-coated ABS showing a minimum three-fold increase in stress intensity at failure. Furthermore, by monitoring changes in the rheological properties over the entire curing process it was found that the incorporation of silane-coated ABS particles increased the maximum complex viscosity by 35% and maximum elastic modulus by 33%. The curing rates of the cements containing 30% and 40% ABS/silane-coated ABS remained comparable with commercial cements.

These results are of major significance as the enhanced ability of the new acrylic cements to resist catastrophic failure by brittle fracture could dramatically lengthen the working lifetime of a total joint replacement.

DECLARATION

This work has not previously been accepted in substance for any degree and is not concurrently submitted in candidature for any degree.

Signed.....Myfanwy Nicholas.....(candidate)

Date.....28/9/07.....

STATEMENT 1

This thesis is being submitted in partial fulfillment of the requirements for the degree of PhD.

Signed.....Myfanwy Nicholas.....(candidate)

Date.....28/9/07.....

STATEMENT 2

This thesis is the result of my own independent work/investigation, except where otherwise stated. Other sources are acknowledged by explicit references.

Signed.....Myfanwy Nicholas.....(candidate)

Date.....28/9/07.....

STATEMENT 3

I hereby give consent for my thesis, if accepted, to be available for photocopying and for inter-library loan, and for the title and summary to be made available to outside organisations.

Signed.....Myfanwy Nicholas.....(candidate)

Date.....28/9/07.....

ACKNOWLEDGEMENTS

I would like to thank my two supervisors Karen Holford and Mark Waters.

CONTENTS

LIST OF FIGURES

CHAPTER 2

CHAPTER 3

CHAPTER 4

CHAPTER 5

LIST OF TABLES

CHAPTER 5

NOMENCLATURE

α	a/w
γ	surface energy of a material (J)
γ	shear strain
γ_o	strain amplitude
δ	phase/loss angle (rads)
θ	angle (^{o})
σ	applied stress (Pa)
σ_a	stress amplitude (Pa)
σ_f	fracture stress (Pa)
σ_{max}	maximum stress amplitude (Pa)
σ_{min}	minimum stress amplitude (Pa)
$\Delta\sigma$	σ_{max} - σ_{min} (Pa)
τ	shear stress (Pa)
τ_o	stress amplitude (Pa)
υ	Poisson's ratio
ω	angular frequency (rads/s)
Δ	deflection at loading point (m)
a	the original length of a central crack or the full length of an edge crack (m)
ABS	acrylonitrile-butadiene-styrene
ANOVA	analysis of variance
B	depth of a CT specimen (m)
C	Carbon
C	empirical constant representing crack growth rate (Pa.m$^{1/2}$)
C	compliance (m/N)
C_0	initial compliance (m/N)
CL	centre line of compact tension specimen
CT	compact tension
d	distance between inner and outer loading points, three-point bending specimen (m)
da/dN	increase in crack length per fatigue cycle (m/cycle)
D	diameter of loading holes in CT specimen (m)

E	Young's modulus (Pa)
f	calibration factor
$f(a/w)$	geometry calibration factor depending on crack length a
F	distance between centre line and centre of loading hole in CT specimen (m)
F	force/load (N)
$F_{5\%}$	load when compliance has increased by 5% (N)
F_{max}	maximum load (N)
F_Q	load at crack growth initiation (N)
G	width of CT specimen (m)
G	dynamic shear modulus (Pa)
G'	real part of the shear modulus (Pa)
G''	imaginary part of the shear modulus (Pa)
G^*	complex shear dynamic modulus (Pa)
G_c	the total work of fracture i.e. the fracture energy (J/m^2)
h	height of specimen (m)
H	half the height of a CT specimen (m)
H	Hydrogen
i	$\sqrt{-1}$
K	stress intensity factor ($Pa.m^{1/2}$)
K_{IC}	fracture toughness ($Pa.m^{1/2}$)
K_{max}	maximum stress intensity factor ($Pa.m^{1/2}$)
K_{min}	minimum stress intensity factor ($Pa.m^{1/2}$)
ΔK	stress intensity factor range, K_{max} - K_{min} ($Pa.m^{1/2}$)
l	length of specimen (m)
L	distance between two outer loading points, three point bending specimen (m)
log	logarithm
m	empirical constant in Paris Erdogan law
MA	methylacrylate
MMA	methylmethacrylate
N	number of fatigue cycles
N_f	number of fatigue cycles to failure
O	oxygen

p	probability
P	load (N)
PMMA	polymethylmethacrylate
ppm	parts per million
R	methacrylate radical
R	ratio of minimum to maximum load
SEM	scanning electron microscope
Si	silicon
t	time (s)
T_{amb}	ambient temperature (^{o}C)
T_{max}	maximum temperature (^{o}C)
TEM	transmission electron microscope
UHMWPE	ultra high molecular weight polyethylene
vol.	volume
W	width of CT specimen from reference plane X (m)
wt.	weight
X	methoxy group
X	Reference plane indicating the centre line through the loading holes in a CT specimen
Y	geometry factor

CHAPTER 1

INTRODUCTION

Bone cement is one of the most widely used non-metallic implant materials in orthopaedic surgery. Its main functions are to stabilize a prosthesis by filling the gap between the prosthesis and surrounding bone, and to transmit load from the prosthesis to the bone.[1, 2] However, one of the main problems associated with total joint replacements is aseptic loosening which can be caused by brittle fracture of the cement.[3]

Fracture is caused by cracks initiating and propagating through the material during cyclic loading. There are several possible crack initiation sites, such as pores introduced during the mixing of the cement and surface irregularities. Cracks can also be initiated as a result of residual stress produced by thermal shrinkage both during and after the polymerization process. Once cracks or micro-cracks have been initiated, cyclic stresses lead to stable or unstable crack propagation resulting in the premature failure of the cement.[4-7]

In order to make bone cement less brittle and more ductile, thereby reducing the risk of brittle fracture, a powdered rubber second phase can be introduced. This is known as rubber toughening and is widely used in engineering polymers.[8] The incorporation of a rubber phase allows the material to yield and deform plastically before eventually fracturing.[9] To improve the effect of rubber toughening yet further, the rubber particles can be covalently bonded into the polymethylmethacrylate (PMMA) matrix thereby creating a strong interface between the particles and matrix. This can be achieved by pre-treating the surface of the rubber particles with a suitable

silane coupling agent capable of bonding with the PMMA matrix during the polymerization process.[10] Incorporating rubber particles into a bone cement will also have an effect on the modulus of the cement as well as its rheological properties such as handling and setting characteristics.

The purpose of this research, therefore, was to investigate the improvement in the resistance of bone cement to brittle fracture with the incorporation of rubber particles, and to examine if this could be further improved by using rubber particles pre-treated with a silane coupling agent, the latter has never been investigated before. The effect these rubber particles had on the flexural modulus was also established. In addition, the rheological properties of cement, with and without rubber particles, were examined in detail over the entire curing process both at room temperature (25°C) and body temperature (37°C). Neither the rheological behaviour of bone cement whilst curing at 37°C nor the rheological behaviour of cement containing rubber particles at 25°C or 37°C had been examined before.

This thesis begins with Chapter 2 by reviewing the mechanical properties of bone cement. This chapter also includes a section on the viscoelastic features of rheology relevant to the current research. A section on rubber toughening as well as a detailed section outlining previous work on the incorporation of rubber compounds into bone cement is also given.

Chapter 3 examines the resistance of currently available bone cements to catastrophic failure via unstable crack growth, by determining the fracture toughness of Palacos R, CMW 1 and Cemex ISOPLASTIC. The rate of sub-critical crack propagation during cyclic loading was also investigated for each of the three cements. The flexural modulus of the three cements was ascertained, along with a detailed analysis of the changes in rheological behaviour during curing, both at room

temperature and body temperature.

Having established the aforementioned mechanical and rheological properties of currently used bone cements a set of experimental cements were formulated, and these are described in Chapter 4. The experimental cements underwent the same mechanical and rheological testing as the commercial cements and the results were analysed to determine which two experimental formulations most closely emulated the commercial cements.

Chapter 5 describes the incorporation of rubber particles into the two selected experimental cement formulations. The resistance of these new cements to fracture by unstable crack propagation, i.e. fracture toughness, was investigated and the effect of the inclusion of the rubber particles examined. The changes in flexural modulus caused by the inclusion of rubber particles were also assessed. By examining these results, the experimental cement formulation which showed the greatest improvement in fracture toughness also underwent cyclic loading to observe if the rubber particles reduced the rate of sub-critical crack propagation. The introduction of rubber particles also had an influence on the handling characteristics and setting time of the cement, therefore these changes in rheological properties are also described.

Chapter 5 also examines the effect of incorporating rubber particles pre-treated with a silane coupling agent. In order to observe any changes as a result of the silane coupling agent, pre-treated rubber particles were added to the same experimental cement formulation which underwent all aspects of mechanical and rheological testing described for the untreated rubber particles. The influence of the silane coupling on these properties is also presented and discussed in this chapter.

Chapter 6 presents the conclusions which can be drawn from this research and makes some suggestions for further work.

CHAPTER 2

BACKGROUND

2.1 INTRODUCTION

Acrylic bone cement or polymethylmethacrylate (PMMA) is commonly used in orthopaedic surgery for total joint replacements as a means of fixation of the prosthesis to the bone.[1] It also stabilizes the prosthesis by filling the gap between the prosthesis and the surrounding bone, and transmits load from the prosthesis to the bone.[1, 2]

Bone cement was first introduced into orthopaedic surgery by Charnley in 1958 when he successfully used PMMA to anchor the femoral component in a total hip replacement.[11] Currently, bone cement is mainly used in hip and knee replacements, and in the repair of spinal fractures.[12, 13] An example of a hip fixation is shown in Figure 2.1.

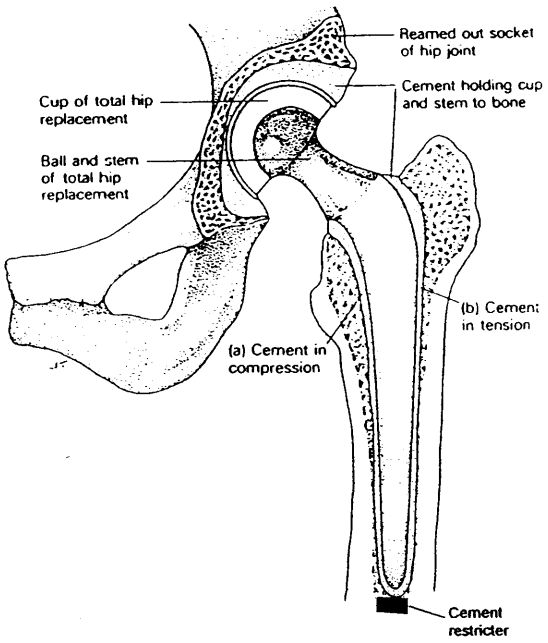

Figure 2.1: Schematic diagram of a hip replacement[14]

2.2 CHEMICAL PROPERTIES

2.2.1 Chemical Composition

PMMA is a self-curing acrylic polymer. In bone cement it consists of a powder component and a liquid component, usually mixed in a 2/1 ratio. Table 2.1 shows the chemicals present in each component of four commercially available bone cements; CMW 1, Palacos R, Simplex P and Cemex ISOPLASTIC.

Table 2.1: Composition of commercial bone cements

	CMW 1[a]	Palacos R[b]	Simplex P[c]	Cemex ISOPLASTIC[d]
Liquid component				
Methylmethacrylate (g)	18.22	18.40	18.31	13.18
N, N-Dimethyl-p-toluidine (g)	0.15	0.38	0.47	0.12
Hydroquinone (ppm)	25	60	80	75
Chlorophyll VIII (g)	-	0.0004	-	-
Powder component				
Polymethylmethacrylate (g)	35.53	-	6.0	33.72
Poly(methylacrylate methylmethacrylate) copolymer (g)	-	33.8		
Poly(methylmethacrylate-styrene) (g)	-	-	29.4	-
Benzoyl peroxide (g)	0.82	0.2	0.6	1.08
Barium sulphate (g)	3.64	-	4.0	5.2
Zirconium dioxide (g)	-	6.0	-	-
Chlorophyll VII (g)	-	0.001	-	-

[a] **CMW, Blackpool, U.K.**
[b] **Schering-Plough Ltd, Brussels, Belgium.**
[c] **Simplex-Howmedica Incorporation, Rutherford, NJ, USA.**
[d] **Tecres S.p.A. Italy**

The basic chemical formula of the methylmethacrylate monomer is:-

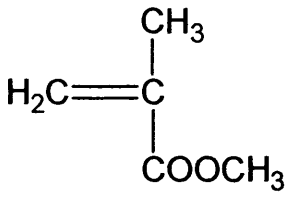

2.2.2 Polymerization

On mixing the powder and liquid component together, free-radical polymerization occurs. This type of polymerization is a chain addition polymerization which requires free-radicals to initiate the start of the growth of the polymer chain. The polymer then continues to grow by the addition of monomer to the end-group of the polymer chain. This results in the polymer having identical molecular repeat units to the initial monomer.[9, 15]

Like most types of chain polymerization the reaction can be divided into three distinct stages; initiation, propagation and termination.[9, 15]

Initiation

This stage involves two processes, the first is the formation of free-radicals. Free-radicals are independently-existing atomic or molecular species which contain an unpaired electron, and are therefore highly reactive with a short life span. During the polymerization of PMMA, the free radicals are produced from the initiator (benzoyl peroxide) according to the following reaction:-[16]

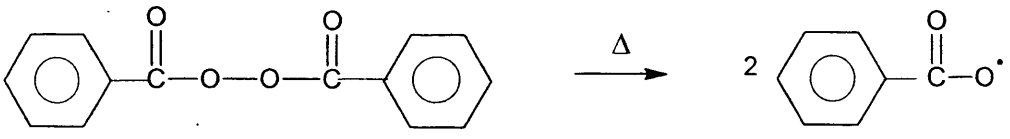

Benzoyl peroxide

Benzoyloxy radicals

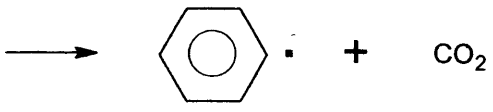

Phenyl radical

The second process involves the free-radicals reacting with the methylmethacrylate monomer to create a free-radical active centre on the monomer:-

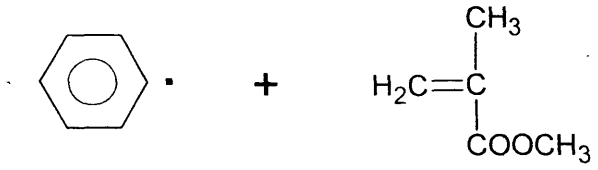

Phenyl radical Methylmethacrylate monomer

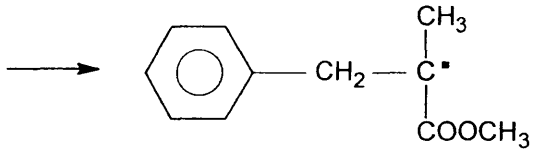

Propagation

The polymer chain grows by the addition of monomer to the free-radical active centre, and with every addition of monomer, the active centre is transferred to the newly bonded methylmethacrylate end group.

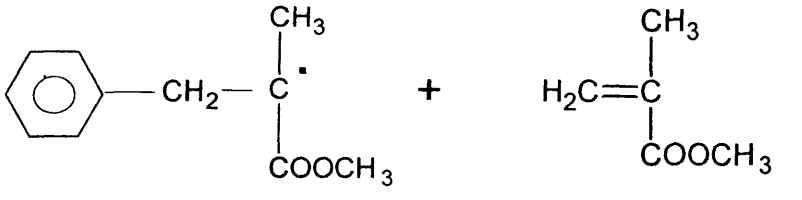

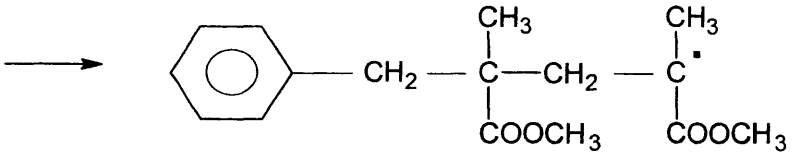

Termination

Termination of the growth of the PMMA chain occurs predominantly by disproportionation, especially at temperatures above 60°C, i.e.

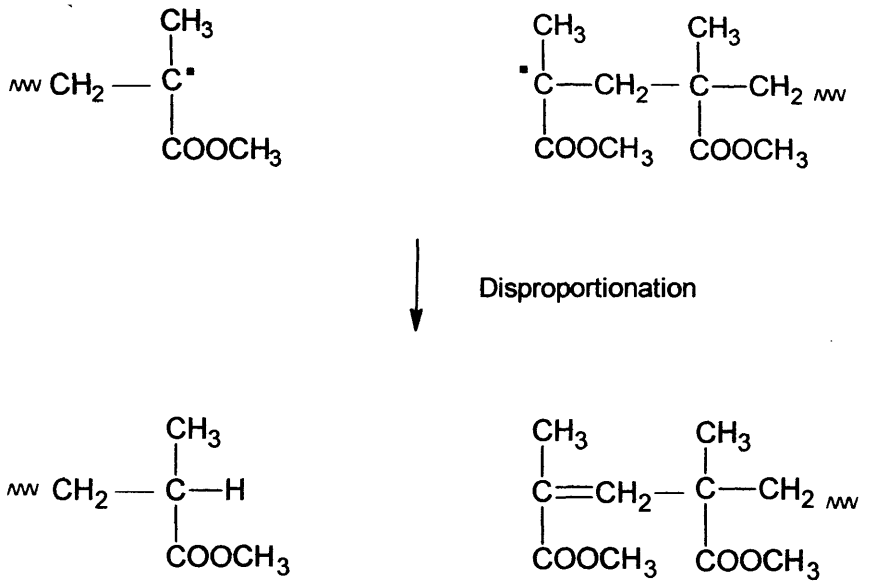

However, at temperatures below 60°C, termination can also occur by combination:-

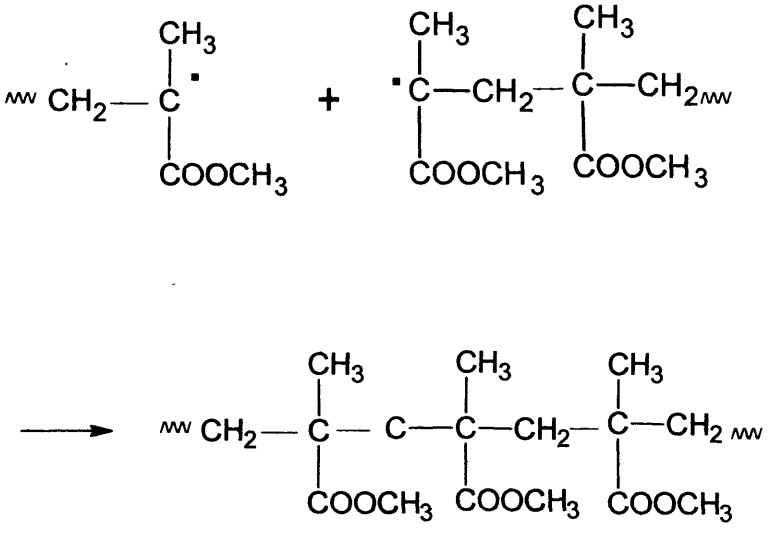

The other chemicals present in the liquid component are N, N-dimethyl-p-toluidine and hydroquinone. N, N-dimethyl-p-toluidine is added to accelerate the polymerization reaction by rapidly decomposing the benzoyl peroxide. Hydroquinone is added to prevent the monomer from polymerizing whilst in storage by absorbing any free radicals which may develop in the liquid. This inhibitory action of the hydroquinone is overcome during the polymerization/mixing of the PMMA by the large quantity of free-radicals produced by the benzoyl peroxide.[16] Barium sulphate or zirconium dioxide is present in the powder component as an opacifier (i.e. to make the cement visible under X-ray). Palacos R cement also contains chlorophyll pigment, this gives Palacos R a distinctive green colour.

The polymerization of bone cement is a highly exothermic process with the average peak temperature being greater than 70°C. However, temperatures can range from 39°C to 124°.[1, 16, 17] Peak temperature is reached after approximately 10 minutes and exposure of the bone to temperatures above 50°C can lead to necrosis of the bone tissue.[15, 16] Figure 2.2 shows how the temperature rises with time.

Polymerization, peak temperature and curing time are affected by temperature, powder to liquid ratio, and composition of the bone cement. Increasing the environmental temperature results in decreased dough, handling and setting time.[18-20] Changing the powder to liquid ratio from the standard 2/1 to 3/1 reduces peak temperature as there is proportionally less liquid monomer generating exothermic heat during polymerization.[18] Decreasing the amount of benzoyl peroxide and/or N, N-dimethyl-p-toluidine also moderately reduces peak temperature and increases the overall setting time.[21-23] In addition, increasing the average diameter of the PMMA particles[22] or partial substitution of the methylmethacrylate monomer with higher molecular weight methacrylates, results in reduced peak temperature.[24, 25]

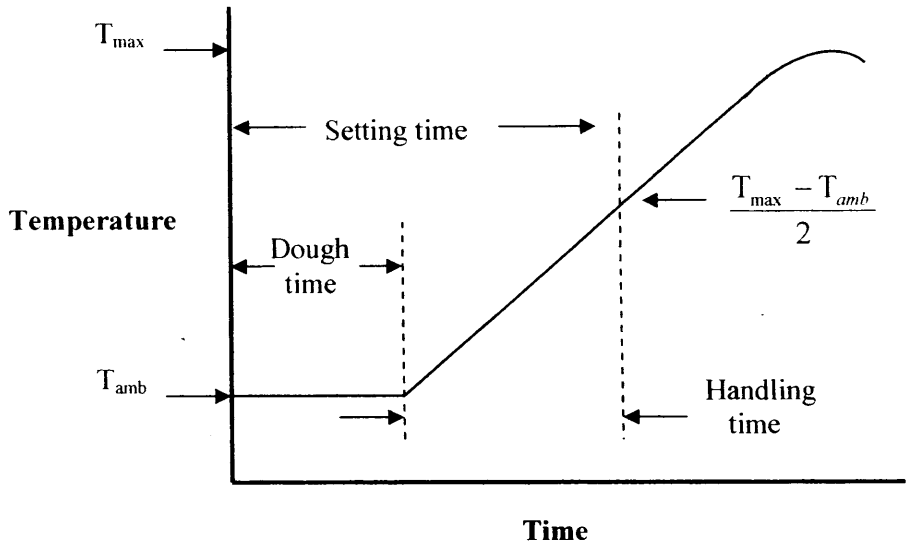

Figure 2.2: Sketch showing the temperature rise due to the exothermic polymerization

Tamb - ambient temperature

Tmax - maximum temperature

Dough time - time from when all of the liquid added to the powder, to the time at which the cement mass no longer adheres to a surgically gloved finger[19]

Setting time - the elapsed time from start of mixing to the temperature midway between peak temperature and ambient temperature[16]

Handling time - difference between dough time and setting time. Handling time includes both the period when the material is readily workable and the subsequent period when it is hardening[19]

2.2.3 Porosity

One of the main problems with bone cement is porosity. Porosity is caused either by the entrapment of air during mixing of the cement, or by the evaporation of some of the monomer due to the high temperatures reached during polymerization. This results in reduced mechanical performance of the cement.[26] To minimize the extent of this porosity, bone cement can be mixed then centrifuged[27] or mixed under vacuum, which has been reported to reduce porosity by between 25%[28] and 89%.[26]

The entrapped air bubbles in the cement can expand by up to 10% as the temperature rises during polymerization.[19] However, during the latter stages of curing,

molecular rearrangement results in an overall decrease in volume of the cement in the range of 1-8%.[19, 29-31] This decrease in volume may cause the cement to retract from the bone and/or prosthesis interface,[29] and induce shrinkage/residual stresses leading to crack initiation.[5] Recent work has shown that bone cements with larger amounts of porosity i.e. hand-mixed cements, undergo less volume shrinkage (1-3.4%) than vacuum mixed cements (6-8%) resulting in less induced residual stresses.[29, 30]

2.3 MECHANICAL PROPERTIES

The mechanical properties of bone cements are determined by powder and liquid composition; powder size, morphology and distribution; liquid/powder ratio, handling conditions; molecular weight; porosity and shrinkage/residual stresses. Extrinsic factors such as mixing and curing environments and techniques also influence the properties of the cement.[2, 19, 22-24, 32]

2.3.1 Static Properties

Static mechanical properties of bone cement are those derived from tests conducted at a slow rate of loading.[1, 33] These properties include ultimate strength in tension, compression, shear and bending/flexure, and also the corresponding moduli of elasticity.[1] The values for commercially available cements mixed by hand and tested in air at room temperature are shown in Tables 2.2 and 2.3.

Tensile Strength

As bone cement is a predominantly brittle material, it is weaker in tension than in compression. The ultimate tensile strength of commercial bone cement lies in the range of 21.8-51.4 MPa and the corresponding elastic modulus is between 2.36-

2.76 GPa or 2.79-3.53 GPa if determined by the secant method. The range of tensile strength values is very wide, and Table 2.2 shows that it is not only the different types of cement which have different values, but each individual type of cement has a huge variation in reported results. Other studies examining experimental cements have revealed that omitting the $BaSO_4$ radiopacifier can lead to an increase in tensile strength.[19, 23]

Table 2.2: Mechanical properties of bone cement hand mixed and stored in air at room temperature

Cement	Tensile strength (MPa)	Compressive strength (MPa)	Shear strength (MPa)	Elastic modulus (GPa)
Palacos R	51.4[34] 22.6[36] 32[37] 46.2[38]	93[35] 65.79[32] 90[37] 79.6[39]	41.4[36]	3.21 (secant)[34] 2.8 (compression)[35] 2.44 (tension)[37] 2.62 (tension)[38] 2.55 (tension)[38]
Zimmer	31.7[34] 22.9[36] 33.9[41]	84.4[40] 86.5[41]	48.3[36]	2.79 (secant)[34]
Zimmer LVC	25.8[36] 31.8[41]	84.7[40] 84.5[41] 88.5[42]	48.3[36] 48.7[42]	2.84 (compression)[42]
Simplex P	50.1[34] 25.1[36] 27.4[44] 33.8[38] 31.6[41] 29.18[46]	80.1[39] 87.8[42] 69.8[45] 89.2[40] 83.9[41] 80.66[46]	49.3[36] 43.14[43] 42.7[42]	3.43 (secant)[34] 2.67 (compression)[42] 2.34 (compression)[45]
CMW 1	21.8[36] 39.1[34] 42.7[38]	86.6[42] 94.4[39]	49.0[36] 44.6[42]	2.76 (tension)[38] 2.96 (secant)[34] 2.36 (compression)[42]
Cemex	52[47]			
Cemex ISOPLASTC		92.2[39]		

Compressive Strength

The compressive strength of bone cement is between 65.79-93 MPa and its corresponding modulus is 2.34-2.8 GPa. There have been various studies examining the effect of different mixing techniques on compressive strength.[26, 42] Dunne and

Orr[32] produced a very comprehensive study examining the effect of using different vacuum mixing systems on the porosity and compressive strength of Palacos R. These mixing systems apply different reductions in air pressure. They concluded that porosity was significantly reduced and compressive strength increased by up to 23% when mixed under the maximum reduced pressure (-86kPa) using a Mitab Optivac® system.

Research has shown that replacing pre-polymerized PMMA beads in the powder component with methylmethacrylate-styrene copolymer beads can increase compressive strength by up to 7%,[21] also omitting the $BaSO_4$ radiopacifier can lead to a small increase in compressive strength.[19] Changing powder to liquid ratio from 2/1 to 3/1 increases compressive strength[19] and correspondingly decreasing the powder ratio from 2/1 to 1.86/1 slightly decreases compressive strength.[48] Partial substitution of liquid methylmethacrylate with a higher molecular weight methacrylate decreases compressive and tensile strength[24] and increasing the molecular weight of the powder PMMA particles also decreases compressive strength.[22]

Shear Strength

Again, as bone cement is a brittle material it is weaker in shear than in compression, with ultimate shear strength values in the range of 41-49.3 MPa. Increasing barium sulphate levels above 10% can slightly reduce shear strength.[43]

2.3.1.1 Flexural/Bending Strength

When determining the breaking strength of many materials, a simple tensile test may be sufficient. However, for brittle materials (such as bone cement) the normal tensile test can be unreliable due to cracks forming where the grips of the tensile testing

machine hold the specimen and, according to Weber and Bargar,[41] "is minimally useful." One way to reduce these problems is by using the 3-point, or 4-point bending test which involves a combination of shear, tension and compression.[41] An example of a 3-point bending test is shown in Figure 2.3.

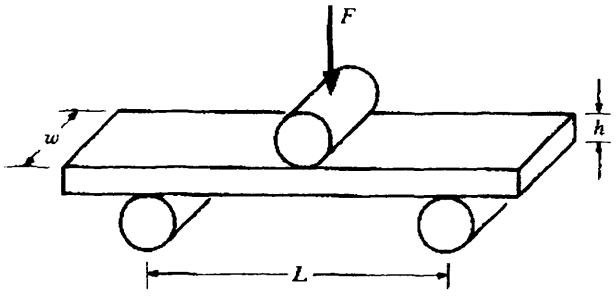

Figure 2.3: Schematic diagram of a 3-point bending test[33]

The load is applied at the centre, causing the specimen to bend, leading to a tensile stress at the mid-point of the lower face, resulting in fracture. The flexural strength using 3-point bending is then calculated using Equation 2.1,

$$\text{Flexural Strength (Nm}^{-2}) = \frac{3FL}{2wh^2} \qquad (2.1)$$

or, for 4-point bending, using Equation 2.2.

$$\text{Flexural Strength (Pa)} = \frac{3Fd}{wh^2} \qquad (2.2)$$

where F = applied force at failure

L = distance between the two outer loading points (span)

w = width of specimen

h = depth of specimen

d = distance between the inner and outer loading points

The flexural modulus under 3-point bending can be calculated using the following equation:-

$$\text{Flexural modulus} = \frac{L^3 F}{4wh^3\Delta} \qquad (2.3)$$

where Δ = deflection at loading point

The flexural properties of commercially available bone cements, hand mixed and cured in air at room temperature are shown in Table 2.3. The strengths and moduli range from 45.7-98.44 MPa and 1.95-2.68 GPa respectively and it can be that the flexural strengths determined by the 3-point bend test are higher than those determined by 4-point bending. This is due to the slightly different loading methods.[49]

Table 2.3: Flexural properties of bone cements hand mixed and stored in air at room temperature

Cement	Bending Test	Flexural Strength (MPa)	Flexural Modulus (GPa)
Palacos R	3-point	66[35]	2.5[35]
	3-point	54.67[32]	2.11[32]
	4-point	66.87[39]	
Zimmer	3-point	49.9[41]	1.95[41]
	4-point	56.1[41]	1.95[41]
	4-point	48.65[50]	2.92[50]
Zimmer LVC	3 point	52.3[41]	2.21[41]
	4 point	55.9[41]	2.21[41]
Simplex P	3 point	72.56[51]	2.29[41]
	3-point	60.2[41]	2.29[41]
	4 point	52.7[41]	
	biaxial	98.44[51]	
CMW 3	3 point	64.77[51]	
	4 point	57.67[50]	2.68[50]
	biaxial	89.39[51]	
Subiton	3 point	60.4[49]	
	3-point	54.5[52]	
	4 point	52.3[49]	
	4 point	45.7[52]	

The flexural properties can be improved by mixing the cements under vacuum to reduce the amount of porosity. A previous study has shown the flexural strength of Palacos R to increase from 54.67 MPa when hand mixed to 72.69 MPa when mixed under vacuum. The flexural modulus also increased from 2.11 GPa to 2.59 GPa.[32]

Other research on flexural properties has mainly focussed on the effect of the radiopacifier[52-54] and barium sulphate has been found to reduce flexural strength by 13%.[51] Lui *et al.*[54] examined a variety of commercial cements, including Palacos R and CMW 1, which had been stored in water at 37°C for 50 hours. They concluded that the presence of the radiopacifier, zirconium dioxide, in Palacos R resulted in a further reduction in flexural properties.

2.3.1.2 Fracture Toughness

One of the main problems associated with total joint replacements is aseptic loosening which can be caused by brittle fracture of the cement.[3] Brittle fracture is usually described in terms of fracture mechanics which is the study of unstable crack growth from a flaw or defect (e.g. a pore) either on the surface, or in the body of a material. The resistance of the material to rapid/unstable crack propagation is known as fracture toughness.[9]

The theory of brittle fracture was initially developed by Griffith in the 1920s.[55] Griffith related the stress for unstable crack growth (i.e. fracture) to the crack length of an existing flaw in a perfectly elastic brittle material under plane stress conditions, by the equation

$$\sigma_f = \left(\frac{2E\gamma}{\pi a}\right)^{1/2} \tag{2.4}$$

where σ_f = fracture stress

E = Young's Modulus

γ = surface energy of the material

a = half the length of a central crack or the full length of an edge crack

Griffith's equation assumes that the material behaves in a perfectly elastic manner and does not undergo any plastic deformation. However, even in very brittle materials there will be some plastic deformation around the crack tip leading to an increase in the amount of energy absorbed during crack propagation. Therefore, 2γ in Equation 2.4 is replaced with G_c, which represents the total work of fracture i.e. the fracture energy. Equation 2.4 then becomes

$$\sigma_f = \left(\frac{EG_c}{\pi a}\right)^{1/2} \tag{2.5}$$

and this equation can be used to predict the critical stress and crack length at which a crack will start to propagate spontaneously.[9, 56, 57]

By rearranging Equation 2.5, failure occurs when the term $\sigma_f \sqrt{\pi a}$ reaches the same value as $\sqrt{EG_c}$. This leads to the stress intensity factor, K, (for finite specimens) being defined as[9, 58]

$$K = Y\sigma\sqrt{\pi a} \tag{2.6}$$

where Y is a geometry factor, and

σ = applied stress.

For crack propagation to occur, K must reach a critical value, K_{1C}.

$$K_{1C} = Y\sigma_f\sqrt{\pi a} \tag{2.7}$$

which can also be written as

$$K_{1C} = \sqrt{EG_c} \qquad \text{for plane stress conditions} \tag{2.8}$$

$$K_{1C} = \sqrt{\frac{EG_c}{1-\upsilon^2}} \qquad \text{for plane strain conditions} \tag{2.9}$$

where υ is Poisson's ratio

The critical stress intensity factor, K_{IC}, is also referred to as the fracture toughness value as it characterizes the resistance of a material to crack propagation.[9]

The international standard for plastics (ISO 13586),[59] gives the following equation for determining fracture toughness (critical stress intensity factor K_Q) of a single edge notched beam in 3 point bending under plane strain conditions. This is the equation which many researchers have used to calculate the fracture toughness of bone cement.

$$K_Q = f(a/w)\frac{F_Q}{h\sqrt{w}} \tag{2.10}$$

where F_Q = load at crack growth initiation

a = original crack length

h = specimen depth

w = specimen width

$f(a/w)$ = geometry calibration factor, depending on the crack length a

The calibration factor, f, is given by

$$f = 6\alpha^{1/2}\left(\frac{1.99 - \alpha(1-\alpha)(2.15 - 3.93\alpha + 2.7\alpha^2)}{(1+2\alpha)(1-\alpha)^{3/2}}\right) \tag{2.11}$$

where $\alpha = a/w$

So far it has been assumed that the material will behave in a predominantly linear elastic manner. However, this is not always the case, and standards make some allowances for minor deviations from linearity. To determine if Equation 2.10 is valid for a specific material undergoing testing the following procedure is undertaken.[8, 59]

A best-fit line is drawn on the force/displacement curve (see Figure 2.4) obtained during testing to determine the initial compliance (C_0) of the material. A second line is drawn showing a 5% increase in compliance (C). If fracture occurs at a maximum load, F_{max}, which falls between these two lines then Equation 2.10 is valid and $F_{max} = F_Q$ (load at crack growth initiation). If F_{max} crosses the second line, then the load at crack growth initiation (F_Q) is taken at the point of intersection ($F_{5\%}$), and Equation 2.10 is still valid, providing F_{max} is less than $1.1F_{5\%}$. However, if F_{max} is greater than $1.1F_{5\%}$ the test is no longer valid.[8, 59]

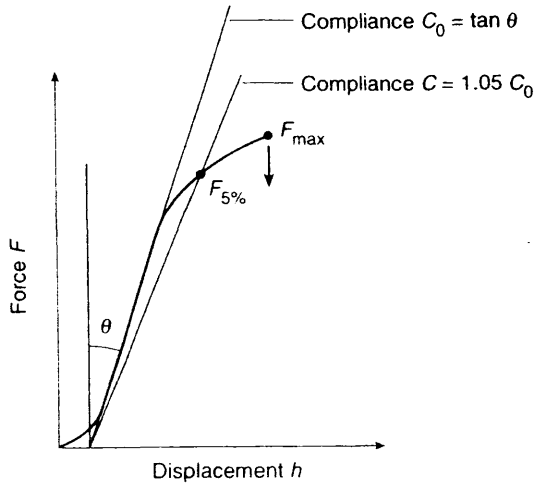

Figure 2.4: Procedure for determination of K_{1C} from a non-linear force-displacement curve[8]

The fracture toughness values of commercially available bone cements, stored in air at room temperature are shown in Table 2.4 and they range from 1.18 MPa.m$^{1/2}$ to 2.58 MPa.m$^{1/2}$. It is difficult to compare the results due to different test methods employed. However, the results show that the higher molecular weight cements, Palacos R and Osteopal, generally have a greater resistance to crack propagation than many of the other bone cements, and this is in agreement with research by Rimnac *et al*.[27] It is also thought that the radiopacifier, zirconium dioxide, present in Palacos contributes to increased fracture toughness.[60] In contrast with the previous static properties, barium sulphate has also been found to enhance fracture toughness by acting as a rigid filler.[60, 61] However, Beaumont considered barium sulphate to be detrimental to fracture toughness.[62]

Table 2.4: Fracture toughness values of bone cement stored in air at room temperature

Cement	Type of test specimen	K_{IC} (MPa.m$^{1/2}$)	Reference
Palacos R	SEN[i]	2.58	Lewis[63]
	CT[ii]	2.15	Lewis[63]
	Chevron notched short rod	2.11	Lewis[63]
	V-notch	1.78	Vallo *et al.*[61]
Simplex P	SEN	1.66	Higgs *et al.*[64]
	SEN	1.51	Robinson *et al.*[40]
	Charpy bar	1.21	Weber & Bargar[41]
	SEN	1.27	Gilbert *et al.*[65]
CMW 1	SEN	1.65	Alberts *et al.*[66]
CMW 3	CT	1.73	Lewis[67]
	CT	1.63	Lewis[67]
	CT	1.86	Lewis[67]
	-	2.26	Ishihara *et al.*[7]
Cemex	SEN	1.6	Taylor *et al.*[47]
Cemex XL	CT	1.81	Lewis & Bhattaram[68]
Zimmer	Charpy bar	1.18	Weber & Bargar[41]
	SEN	1.42	Robinson *et al.*[40]
	-	2.14	Ishihara *et al.*[7]
Zimmer LVC	Charpy bar	1.19	Weber & Bargar[41]
	SEN	1.23	Robinson *et al.*[40]
Osteopal	CT	2.33	Lewis[67]
	CT	2.37	Lewis[67]
	CT	2.36	Lewis[67]
Subiton			
radiopaque	V-notch	1.33	Vallo *et al.*[61]
low viscosity	V-notch	1.60	Vallo *et al.*[61]
radiolucent	V-notch	1.27	Vallo *et al.*[61]

[i]SEN = single-edge notched
[ii]CT = compact tension

2.4 DYNAMIC PROPERTIES

2.4.1 Fatigue

Given the cyclic nature of the human gait, and the fact that the average person loads his hip and knee joints approximately 1-2 million times per year, high cyclic fatigue strength is a critical mechanical property.[2] It has long been recognized that fatigue failure and fatigue crack propagation are primary cement failure mechanisms.[69-71]

Fatigue failure is caused by cracks initiating and propagating through the

material during cyclic loading. There are several possible crack initiation sites, such as pores introduced during the mixing of the cement and surface irregularities. Cracks can also be initiated as a result of residual stresses produced by thermal shrinkage during and after the polymerization process. Once cracks or micro-cracks have been initiated, high cyclic stresses lead to stable or unstable crack propagation resulting in the premature failure of the cement.[4-7] There are currently mixed reviews on whether the radiopacifier, barium sulphate, does or does not contribute to this type of failure.[62, 72, 73]

There are several approaches to determine the fatigue life of a brittle material. The first involves characterization of fatigue life in terms of the number of stress cycles needed to induce failure in an un-notched, defect free, specimen. The resulting curve, known as an S-N curve, (see Figure 2.5) incorporates the number of cycles to initiate a crack, the number of cycles to propagate this crack and the total number of cycles leading to catastrophic failure.[58, 74]

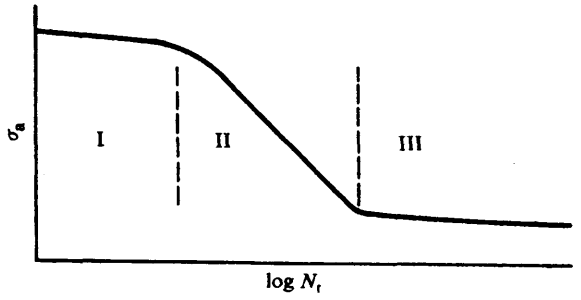

Figure 2.5: Schematic representation of the typical variation of stress amplitude, σ_a, with the number of cycles to failure, N_f, for polymeric materials[74]

From this curve the fatigue limit (i.e the maximum stress amplitude below which fatigue failure cannot occur) or endurance limit (i.e. the maximum stress amplitude which the specimen can support for at least 10^7 cycles) can be determined.[58, 74]

Figure 2.5 is a typical S-N curve for a polymer, such as Perspex, and shows three distinct regions. Region I is when crazes form at high values of stress amplitude. Crazes are not true cracks, but small crack-like entities which act as a localized form of plastic deformation. These crazes may eventually become true microscopic cracks. However, not all materials are capable of crazing at such high stress amplitudes, in which case region I is not so prominent. Region II shows the dependence of fatigue life on stress amplitude. At higher stress amplitudes the cracks initiate and propagate more rapidly than at lower stress amplitudes. Region III is essentially the endurance limit of the polymer.[74]

The second approach involves using facture mechanics to determine the crack propagation rate and ultimately the fatigue life of the material.

As bone cement is a brittle material which contains various crack initiation sites the rate at which a crack grows can be examined. During each loading cycle the crack will grow by a small amount until the crack reaches a critical size and brittle failure occurs. This can be monitored by measuring the amount of crack growth per cycle (da/dN), as a function of the applied stress. Paris and Erdogan showed that for many materials, the rate at which a crack propagates is related to the stress intensity factor range ΔK under mode 1 crack opening conditions, by the equation[9, 58, 74]

$$da/dN = C(\Delta K)^m \qquad (2.12)$$

where da/dN is the change in the length of the fatigue crack per load cycle

(a being the crack length and N the number of fatigue cycles)

ΔK is the stress intensity factor range defined by:-

$\Delta K = K_{max} - K_{min}$,

and by using Equation 2.6 defined in the fracture mechanics section

$$\Delta K = Y\Delta\sigma\sqrt{\pi a} \tag{2.13}$$

where $\Delta\sigma = \sigma_{max} - \sigma_{min}$

C and m are empirical constants which are dependent on the material properties and microstructure, fatigue frequency, load ratio, environment, loading mode, stress state and test temperature.[74]

To determine the fatigue crack propagation parameters in terms of the stress intensity factor range, da/dN can be plotted against ΔK on a logarithmic scale. Figure 2.6 shows the fatigue crack growth behaviour of several polymers, as well as two metal alloys for comparison.

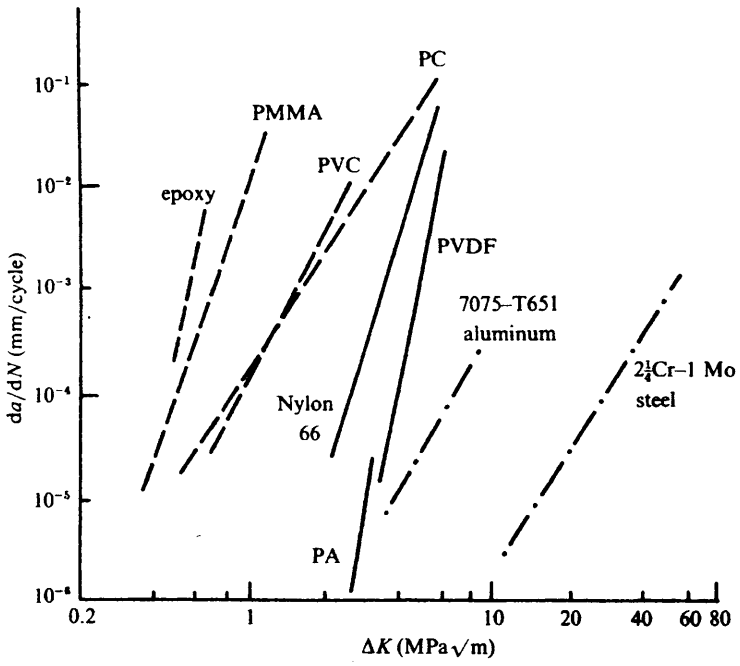

Figure 2.6: Fatigue crack growth characteristics of several polymers including two metal alloys[74]

The empirical constant C can then be determined as the crack propagation rate when ΔK = 1 MPa.m$^{1/2}$, and the empirical constant m is the gradient. m is usually found to be around 4 for metals, and between 4-6 for polymers but can reach as high as 12.[75] From Figure 2.6 it can be seen that the metal alloys have a superior resistance to fatigue crack propagation than the polymers. This is indicated by the crack propagating at a very high stress intensity factor range.

Research on the fatigue of bone cements has mainly focused on the number of fatigue cycles until failure.[69, 76-81] There has been a wide range of results, from 5938 cycles until failure (when testing a hand mixed cement, in air at 22°C, stress range 0.3-22 MPa, frequency 2 Hz)[77] to 2 628 680 cycles until failure (when testing a vacuum mixed cement, stored and tested in water at 37°C, stress range 0-13 MPa, frequency 10 Hz).[76] It is very difficult, or even inadvisable, to compare the extensive range of reported results due to differences in the types of cement, specimen configuration (i.e. notched and un-notched); preparation and storage; mode of loading, testing environment, frequency and sample size. However, various trends can be seen. Vacuum mixing and centrifuging the cement improves fatigue life.[69, 76-78] Increasing fabrication pressure also appears to improve fatigue life, but not significantly.[79] There have been mixed reviews on the effect of test frequency. Lewis *et al.*[78] concluded that increasing frequency does not have a statistically significant effect on fatigue life, however work produced by Johnson *et al.*[81] found that increasing frequency resulted in an increase in fatigue life. As expected increasing stress amplitude levels decreases fatigue life.[76, 80] From the results presented by various authors it is difficult to tell whether fatigue life is, or is not, improved when the cement is tested in saline or water at 37°C.[69, 76, 80] Nevertheless it is generally thought that the fluid, or elements present in the fluid, enhance crazing in the crack tip region. This results in an increased plastic

zone ahead of the crack tip, effectively increasing the ductility of the cement and so increasing its fatigue life.[12, 82]

Less work has been undertaken on the sub-critical crack propagation rate of bone cement. This is an important, more realistic area of research, as most of the working lifetime of the cement involves cracks growing at a sub-critical rate. Figure 2.7 shows the fatigue crack growth rate in terms of ΔK of the radiopaque cement, Simplex P, and the radiolucent cement, Simplex (stored and tested in deionized water at 37°C), obtained by Molino and Topoleski.[73] It can be seen that the stress intensity factor range, ΔK, over which the crack propagates is typical of many polymers (see Figure 2.6). The large scatter in the results is normal due to the complex effect of the residual stresses and microstructure,[74] as well as the sensitivity of fatigue behaviour to environmental conditions and temperature.[75]

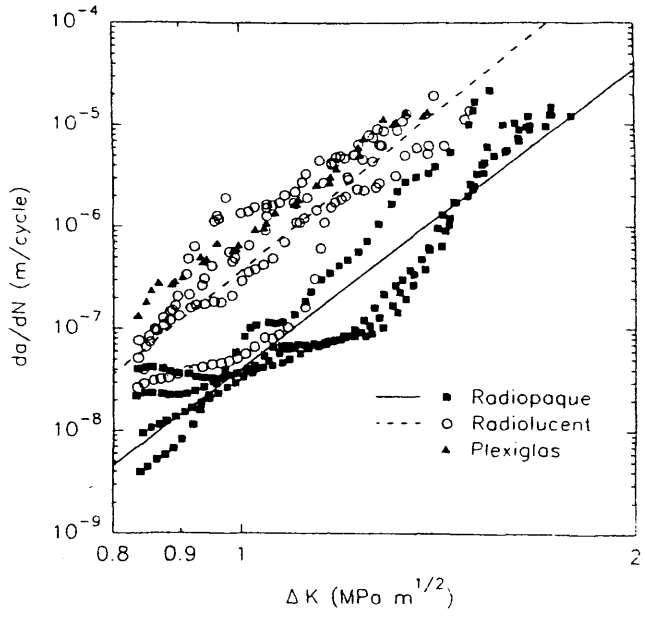

Figure 2.7: Fatigue crack growth rate behaviour of Simplex P (radiopaque) and Simplex (radiolucent)[73]

The crack growth rate of the radiolucent cement can be seen to be greater than the radiopaque cement, and the average calculated crack propagation rates. C when ΔK = 1 MPa.m$^{1/2}$, were 3.26 x 10^{-7} m/cycle for the radiolucent cement and 4.03 x 10^{-8} m/cycle for the radiopaque cement. Molino and Topoleski[73] concluded that void formation around the barium sulphate possibly acted to blunt the advancing crack. The calculated average m values for the radiolucent and radiopaque cement were 10.4 and 9.77 respectively. These m values seem higher than expected for most polymers, however this could be a consequence of the testing environment.[75]

The average crack propagation parameters of these two cements and different types of cements by other authors are shown in Table 2.5. Again a wide range of parameters have been determined, and crack propagation rates have been reported as high as 9.5 x 10^{-4} m/cycle[26] at ΔK=1 MPa.m$^{1/2}$. Interestingly, much lower m values have been obtained for cements undergoing testing in what appear to be very similar environmental conditions produced by Molino and Topoleski.[73] This is probably due to all the authors using different specimen geometries as well as different loading conditions and testing frequencies. This makes it very difficult to directly compare their results. However, it does appear that the crack growth rate decreases when tested in deionized water or Ringer's solution at 37°C, and again it is likely that the temperature, fluid, or elements present in the fluid, increase the size of the plastic zone ahead of the crack tip effectively blunting crack propagation.[12]

Table 2.5: Fatigue crack propagation parameters

Specimen	Testing environment	C m/cycles	m	Reference
Simplex P	deionized water at 37°C	4.03×10^{-8}	9.77	Molino & Topleski[73]
Radiolucent Simplex	deionized water at 37°C	3.62×10^{-7}	10.4	Molino & Topleski[73]
Simplex P	air at 25°C	4.6×10^{-7}	5.5	Nguyen *et al.*[82]
Simplex P	Ringers solution	3.3×10^{-9}	5.5	Nguyen *et al.*[82]
Simplex P	cured in water at 37°C	9.5×10^{-4}	4.98	Rimnac *et al.*[27]
CMW 3	Ringers solution at 37°C	7.6×10^{-8}	3.6	Ishihara *et al.*[7]
CMW 3	Ringers solution at 37°C	7.6×10^{-8}	3.6	Ishihara *et al.*[7]
Zimmer	Ringers solution at 37°C	7.6×10^{-8}	3.6	Ishihara *et al.*[7]
Zimmer	Ringers solution at 37°C	7.6×10^{-8}	3.6	Ishihara *et al.*[7]
Zimmer	air	8.46×10^{-7}	6.5	Wright & Robinson[83]
Zimmer	air at room temperature	12.9×10^{-7}	8.80	Askew *et al.*[84]
Zimmer LVC	air	1.22×10^{-6}	6.5	Wright & Robinson[83]
Palacos R	air at room temperature	1.30×10^{-7}	5.00	Askew *et al.*[84]
Palacos R	cured in water at 37°C	9.5×10^{-4}	4.98	Rimnac *et al.*[27]
Cemex	air	4.57×10^{-7}	6.05	Beleani *et al.*[85]

C represents crack growth rate when $\Delta K = 1$ MPa.m$^{1/2}$

Both m and C are dependent upon microstructure, fatigue frequency, load ratio, environment, loading mode, stress state and test temperature.[74]

2.4.2 Rheology

Understanding the rheology or flow characteristics of bone cement is important because the polymerization reaction causes the cement to change from a viscous liquid to a predominantly hard, elastic solid. During this polymerization reaction the handling/rheological properties exhibit three different phases. These phases are known as dough time, setting time and working/handling time and are shown and defined in Figure 2.2. This whole process takes approximately 10-15 minutes, allowing the surgeon only a few minutes of working/handling time to mix the cement and either inject it with a cement gun, or manually place into the body. Once in the body, the cement must still be fluid enough to be able to penetrate into the interstices of trabecular bone.[2]

Bone cement, like most polymers, is a viscoelastic material and so has both viscous and elastic components.[9] The viscous component follows Newton's Law i.e. the stress is proportional to strain-rate and independent of strain, and the elastic component follows Hooke's Law i.e. the stress is proportional to the strain and independent of loading rate. There are several different models combining these two components to describe the viscoelastic behaviour of these materials such as the Maxwell model and the Voigt model and these can be found in Young.[9] The mechanical response of polymers is therefore dependent on the rate and time period of loading as well as being affected by temperature. At low temperatures, polymers display mainly elastic behaviour, whereas at high temperatures their behaviour is mainly viscous.

Polymers are often subjected to variable loading at different frequencies. One way to examine how they behave under these conditions is by measuring the response of the material to deformation by periodic forces, e.g. during forced vibration or

small-amplitude oscillatory shear. The response obtained shows that stress and strain are not in phase, the strain lags behind the stress by a phase angle, δ, known as the loss angle.[9, 15, 86, 87]

If the oscillatory shear is sinusoidal, then

$$\tau = \tau_o \sin \omega t \tag{2.14}$$

where τ = shear stress

τ_o = stress amplitude

ω = angular frequency

t = time,

and

$$\gamma = \gamma_o \sin(\omega t - \delta) \tag{2.15}$$

where γ = shear strain

γ_o = strain amplitude

The equation for stress (Equation 2.14) can be expanded to give

$$\tau = \tau_o \sin \omega t \cos \delta + \tau_o \cos \omega t \sin \delta \tag{2.16}$$

This shows that the stress can be resolved into two components: $\tau_o \cos \delta$ which is in phase with the strain and $\tau_o \sin \delta$ which is $\pi/2$ out of phase with the strain. Therefore, two dynamic shear moduli (G) can be defined: G' which is in phase with the strain and G'', which is $\pi/2$ out of phase with the strain. As $G' = (\tau_o/\gamma_o)\cos \delta$ and $G'' = (\tau_o/\gamma_o)\sin \delta$, Equation 2.16 becomes

$$\tau = \gamma_o G' \sin \omega t + \gamma_o G'' \cos \omega t \tag{2.17}$$

This leads to the phase angle δ being

$$\tan \delta = G''/G' \tag{2.18}$$

Complex notation is often used and so the stress and strain become

$$\tau = \tau_o \exp i(\omega t + \delta), \quad \text{and} \tag{2.19}$$

$$\gamma = \gamma_o \exp i\omega t \tag{2.20}$$

where $i = \sqrt{-1}$

The overall complex modulus $G^* = \tau/\gamma$ is then given by

$$G^* = \frac{\tau_o}{\gamma_o} \exp i\delta = \frac{\tau_o}{\gamma_o}(\cos\delta + i\sin\delta) \tag{2.21}$$

Therefore by using the earlier definitions of G' and G''

$$G^* = G' + iG'' \tag{2.22}$$

G' and G'' are called the real and imaginary components of the modulus respectively. They are also known as the storage and loss moduli.

Different methods can be used to measure the dynamic viscoelastic behaviour of materials such as oscillatory strain, wave propagation and steady flow.[86] The oscillatory methods involve either free or forced oscillations either in tension or shear. A controlled shear stress rheometer applies a torque (forced oscillation) and measures the resultant displacement. The sample is subjected to a periodic deformation and its periodic response and phase lag (δ) are measured and recorded. From this, the phase angle, complex, elastic and viscous moduli, complex viscosity as well as shear stress and strain, can be calculated.

Far less work has been undertaken on the rheological properties of bone cement, unlike the extensive work and literature produced on their static and dynamic mechanical properties.[34, 45, 61] Previous work on rheological properties have included creep,[88-90] stress relaxation,[89, 91] temperature profiles of cements during curing,[92] and

cements characterized by rotational[93, 94] and capillary extrusion rheometers.[94] A comprehensive and extensive rheological study was produced by Farrar and Rose,[95] who used a parallel plate rheometer to characterize the initial rheological properties (i.e. during the dough phase) of a variety of low and high viscosity cements at a variety of temperatures (19, 21, 23 and 25°C). Measurements were made of viscosity, storage modulus, loss modulus and phase angle, δ, against time until the viscosity of the cement tested reached between 1000 – 1500 Pa s. Their results showed that the time taken to reach the desired viscosity decreased with increasing temperature as expected, and showed an Arrhenius dependence. Furthermore they showed that the increase in viscosity with time varied with each type of cement. Much of their work involved explaining the factors involved in the initial rise in viscosity such as phase volume of PMMA particles and swelling of the polymer beads. A more recent study was undertaken by Hernandez and co-workers,[96] who produced similar work to Farrar and Rose,[95] by studying the rheological properties of a variety of experimental bone cements during the dough and handling phases at 25°C. Their results also showed that the increase in viscosity with time varied with each formulation of cement.

2.5 REINFORCING BONE CEMENT

In order to improve the mechanical properties of bone cements, the effect of different types of inert reinforcing materials have been investigated. These include steel,[44, 97] graphite,[40, 98] aramid[99] and titanium[100, 101] in the form of wires, chopped fibres and particles. Even though researchers have reported increases in mechanical properties with these reinforcing materials, they are difficult to mix in with the bone cement in large quantities (> 7 wt.%)[99] and the bonding between fibre and matrix can be poor. Other reinforcing materials such as glass and glass-ceramic particles have also

improved mechanical properties.[102, 103] However the incorporation of hard particulate fillers can lead to a reduction in toughness.[104] To overcome the problems of reduced toughness organic rubber particles can be introduced. This is an effective method of toughening brittle polymers and is detailed in the following section.

2.5.1 Rubber Toughening

In order to make glassy or rigid polymers less brittle and more ductile, thereby reducing the risk of brittle fracture, a powdered rubber second phase can be introduced. This is known as rubber toughening and is widely used in engineering polymers.[8] The rubber second phase is usually a synthetic thermoplastic rubber, as natural rubber is susceptible to chemical degradation. Thermoplastic rubber consist of a rubbery homopolymer such as polybutadiene or polyisoprene, and a glassy (hard) homopolymer such as polystyrene, and generally have a Young's modulus lower than that of the glassy polymer they are reinforcing.[9] In the case of rubber toughened Perspex (PMMA) where transparency is an important criterion, the rubber particles usually consist of a rubber, poly[n-butyl acrylate)-co-styrene], core surrounded by an outer layer of grafted PMMA. The rubber toughened PMMA is then made by melt-blending the composite rubber particles with the PMMA.[105, 106]

The incorporation of a rubber phase decreases the modulus and allows the material to yield and deform plastically at a lower applied stress before eventually fracturing.[9, 10] This increased plastic deformation is not only due to the rubber particles extending and deforming under an applied stress, but also to the rubber particles inducing yielding throughout the matrix polymer. There are two mechanisms by which the rubber particles achieve this. The first is by crazing, whereby stress concentrations at the equators of the rubber particles initiate multiple crazing

throughout the glassy polymer. The subsequent growth of these crazes results in the polymer absorbing large amounts of energy during the deformation process and so increases the total energy required for fracture.

The second mechanism is the formation of dilatational shear bands. Instead of stress concentrations at the equators of the rubber particles initiating crazing, they induce planar shear bands in the matrix. The shear bands are similar to crazes as they absorb energy during deformation, but they do not involve the formation of new surfaces.

If the stress concentrations within the rubber particles become too great, the rubber particles may rupture internally, this is known as cavitation, and again leads to the formation of crazes or shear bands.[8, 106]

Whether crazes or shear bands are formed depends on the type of polymer, the size and internal structure of the rubber particles, the rate of deformation and environmental temperature. However, there is likely to be a complex combination of both mechanisms with one more dominent than the other.[8, 9, 105]

An extensive study was undertaken by Bucknall[105] to find the dominant mechanism of toughening of industrial rubber toughened PMMA. Crazing and other void forming processes produce an increase in the volume of the polymer, whereas there is no change in volume with the formation of shear bands. Bucknall measured the volume change of rubber toughened PMMA during creep in tension at 20°C, and found no significant increase in volume with time. This lead to the conclusion that the dominant mechanism was the formation of shear bands. However, there was stress whitening in the polymer thought to be due to voids forming within the rubber nucleus (cavitation), at the particle-matrix interface, or at the intersection of two shear bands in the matrix.

In order to understand deformation processes, fracture surfaces are usually examined using a scanning electron microscope (SEM). Unfortunately an SEM is not sufficient to examine crazing or shear bands as this information usually lies below the fracture surface. Therefore crazes and shear bands are more likely to be detected using a transmission electron microscope (TEM).[105, 106] Researchers who have used this method to examine fracture surfaces of rubber toughened PMMA have reported different findings. Lovell[106] and Todo[107] found evidence of crazing whereas Young stated there is none.[9] Todo[107] reported that although microcrazing was present in the immediate vicinity of the rubber particles, shear yielding had occurred in the surrounding matrix along the crack path.

It is likely that both mechanisms play a role in the toughening of PMMA,[8] but given the lack of volumetric change, the formation of shear bands may be the dominant mechanism.

To reduce the risk of rubber particles becoming debonded and initiating crack growth and/or voids forming at the rubber particle-polymer matrix, the rubber particles must be well-bonded to the matrix.[8, 9, 105, 106] This also increases the efficiency of the rubber particles in acting as stress concentrators. Creating a strong interface can be achieved by pre-treating the surface of the rubber particles with a suitable cross-linking agent (silane) capable of reacting/bonding with the PMMA matrix during the polymerization process.[10]

2.5.2 Silane coupling/cross-linking agents

Silane coupling agents are bi-functional organosilane compounds capable of forming stable bonds between two dissimilar materials. They are mainly used as coupling agents to bond inorganic filler materials to an organic matrix,[10] but can also be used to

cross-link plastics, such as polyethylene with an acrylic.[108] The structure of an organosilane compound is shown in Figure 2.8, where R is a non-hydrolysable organic radical able to bond with the organic matrix phase during the matrix polymerization process, and X are hydrolysable groups which react with -OH groups on the surface of an inorganic (or hydroxyl functional polymer) secondary phase.

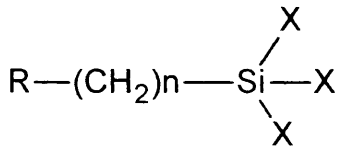

Figure 2.8: Structure of an organosilane

A commonly used silane coupling agent for acrylics is methacryloxy propyltrimethoxy-silane,[109] where

X = methoxy group (OCH_3)

R = methacrylate radical ($CH_2C(CH_3)COOCH_2$)

The organosilane is initially applied to the secondary phase and the reaction between the silane and the filler particles take place as follows:-[109, 110]

1. With the addition of water, two of the three methoxy (X) groups hydrolyse forming a highly reactive silanol group, $R\text{-}Si(OH)_3$
2. These silanol groups then condense with other silanol groups to form a stable three dimensional siloxane structure (-O-Si-O-) around the filler particles
3. Simultaneously the third methoxy group forms hydrogen bonds with hydroxyl sites present on the surface of the filler
4. Finally during drying, a covalent bond is formed between the filler particles and silane with the loss of water.

The reaction between the silane and plastic fillers with no hydroxyl sites present on its surface can only take place as far as stage 2 and is sometimes referred to as cross-linking.[108] For coupling to take place, and hence a covalent bond to be formed between the filler particles and silane, all four stages need to take place.

The methacrylate radical (R) part of the organosilane is then able to react with the PMMA during the free-radical polymerization process forming strong covalent C-C bonds between the silane and the matrix.

2.5.3 Previous Work on Rubber Toughened Bone Cements

Previous work examining rubber toughened bone cements has mainly focused on the incorporation of either acrylonitrile-butadiene-styrene (ABS) particles, or commercially available rubber toughened PMMA particles, such as Plexiglas DRG.

The most comprehensive studies were carried out by Vila *et al.*[111, 112] They investigated various mechanical properties of experimental cements containing different quantities of ABS particles. Initially the tensile and compressive strengths/moduli of cements containing 5, 10, 15, 20 and 25 volume (vol.) % ABS were examined. These properties were found to decrease with increasing ABS content until the cement contained 20 vol. % ABS. Increasing the quantity of ABS yet further had no additional effect on the tensile properties which remained the same, however, the compressive properties continued to decrease. During the tensile testing there was also a corresponding increase in strain to fracture i.e. elongation, with increasing ABS content, again until the cement contained 20 vol. % ABS. This is to be expected as the introduction of the ABS particles has increased yielding and therefore ductility in the matrix material.

The tensile and compressive strengths and moduli are shown in Table 2.6 and will be used as a reference when examining the results obtained in this current research.

Table 2.6: Change in compressive/tensile properties with increasing quantites of ABS

ABS (vol. %)	Compressive modulus (GPa)	Compressive strength (MPa)	Tensile modulus (GPa)	Tensile strength (MPa)
0	1.78	87.9	2.6	44
5	1.74	82.2	2.5	42
10	1.51	78.3	2.3	39
15	1.36	76.3	1.75	34
20	1.29	49.9	1.25	29
25	1.10	41.8	1.25	29

N.B 10 volume % is approximately equivalent to 8 weight %

Vila *et al.* also examined the effect of the ABS particles on fracture toughness of bone cement. Testing was carried out using CT (compact tension) specimens in tensile opening mode and their results are shown in Table 2.7 to be used as a comparison with the work undertaken during this study.

Table 2.7: Fracture toughness of an experimental cement containing ABS

ABS (vol. %)	K_{1max} (MPa.m$^{1/2}$)	Increase in toughness
0	1.39 ± 0.13	-
5	1.70 ± 0.06	22.3%
10	1.89 ± 0.21	36.0%
15	2.17 ± 0.07	56.1%
20	2.24 ± 0.15	61.2%
25	2.15 ± 0.09	54.7%

Their results clearly show a dramatic increase in fracture toughness with increasing ABS content, reaching a peak of 2.24 MPa.m$^{1/2}$ with 20 vol. % ABS. Following this there is a small decrease in fracture toughness with 25 vol. % ABS. According to Vila *et al.* the ABS particles have increased the resistance of the material to crack

propagation by acting as a partial barrier to microcrack growth as well as promoting energy absorbing mechanisms during fracture (see Section 2.5.1). Visual inspection of the fracture toughness specimens during testing showed stress whitening ahead of the crack tip, leading to the conclusion that crazing was the mechanism of toughening, however, Young[9] reports that stress whitening in PMMA is caused by the rubber particles voiding as opposed to crazing.

Continuing with this work Vila *et al.*[112] studied the fatigue crack propagation of cement containing 10 vol. % ABS. Testing was undertaken by cyclically loading a CT specimen in tension-tension at a load ratio of 0.5 and at a frequency of 2 Hz. The crack propagation was measured per fatigue cycle, da/dN, and plotted graphically against the stress intensity factor range, ΔK. Their results showed that the incorporation of ABS particles reduced the calculated crack propagation rate, C, from 2.827 mm/cycle (no ABS present) to 0.004 mm/cycle (10 volume % ABS present) when ΔK = 1 MPa.m$^{1/2}$. The corresponding m values were found to be 10.95 and 9.64 respectively. Both m values are slightly high but are in agreement with the m values obtained by Molino and Topoleski.[73] Interestingly, the presence of the ABS particles appeared to have very little effect on the stress intensity factor range, and both types of cement fractured when ΔK was approximately 0.9 MPa.m$^{1/2}$.

Several studies have investigated the mechanical properties of experimental cements containing rubber toughened Plexiglas DRG powder. Puckett *et al.*[113] examined the properties of experimental cements containing 25%, 50% and 100% Plexiglas DRG and compared them to Simplex bone cement, and Moseley *et al.*[114] examined the properties of experimental cements containing 0% and 100% Plexiglas DRG.

Moseley *et al.* found that the compressive strength and modulus decreased from 90 MPa and 2.1 GPa respectively, to 55 MPa and 1.4 GPa when the cement was made using 100% rubber toughened Plexiglas DRG powder.[114] Puckett *et al.* also showed that incorporating the Plexiglas DRG powder resulted in an overall decrease in compressive strength. There was a reduction from 72.0 MPa when containing 25% Plexiglas DRG to 62.2 MPa with 100% Plexiglas DRG.[113] Correspondingly, there was an increase in fracture toughness with K_{IC} values more than doubling from 0.8 MPa.m$^{1/2}$ to 1.9 MPa.m$^{1/2}$ with 100% Plexiglas DRG showing that this material has an increased resistance to crack propagation.[114]

Other studies have involved adding rubber toughened PMMA powder to commercial bone cements. Murakami *et al.*[115] examined the effect of incorporating a rubber toughened PMMA powder (TD542) into CMW bone cement. The tensile properties of CMW containing increasing quantities of TD542, i.e. 33.3, 50.0, 66.6% TD542 were investigated. Again there was an overall decrease in tensile properties with increasing rubber content along with a marked increase in elongation. The fracture toughness of the CMW cement with 50% rubber toughened PMMA powder was also determined and compared to CMW with no rubber particles present. Again there was an increase in fracture toughness from 1.94 MPa.m$^{1/2}$ for the original CMW cement to 2.26 MPa.m$^{1/2}$ for the rubber toughened CMW cement. Unlike previous studies Murakami also monitored the setting time of some of the CMW cements and found that the incorporation of the rubber particles reduced the overall setting time.

Perek and Pilliar[116] investigated the fracture toughness of Zimmer low viscosity cement modified with rubber toughened Plexiglas DR100 powder. Zimmer cements containing 10, 20, 30 and 40% Plexiglas DR100 powder were fabricated and their fracture toughness values determined. All the cements showed a greater

resistance to crack propagation than the original Zimmer cement, and the fracture toughness continually increased with increasing Plexiglas content. Eventually the fracture toughness of the initial plain Zimmer bone cement almost doubled from 1.07 MPa.$m^{1/2}$ to 2.08 MPa.$m^{1/2}$ with 40% Plexiglas DR100. In contrast to the work by Murakami *et al.*,[115] Perek and Pilliar found that the setting time of the Zimmer cements increased with the incorporation of rubber particles.

During testing both Murakami *et al.*[115] and Perek and Pilliar[116] observed stress whitening just before fracture on all the modified cements. Examination of the fracture surfaces by SEM revealed either holes generated by particle-matrix debonding[115] or ruptured DR100 particles[116]. Murakami *et al.* also examined a fracture surface using a TEM and discovered lines which could indicate crazing, but considered more research was required in this area.

All of the above workers demonstrated that adding rubber particles increases the fracture resistance of the matrix material along with a corresponding reduction in the tensile and compressive properties. However, there are some differences over their effect on the setting time of the cement. Most researchers have concluded that the rubber toughening mechanism is crazing, and there has been no mention of the formation of dilatational shear bands. It is clear that far more work needs to be undertaken examining a variety of fracture surfaces using a TEM to understand the contribution of both crazing and dilatational shear yielding mechanisms.

Following on from the work by Villa *et al.*[111, 112] this study investigated the fracture behaviour and rheological properties of an experimental cement containing a much wider range of ABS content. The main objectives were to:-

1. determine the quantity of ABS particles required to maximize the fracture toughness of the experimental cements.
2. establish what quantity of ABS particles is most likely to substantially reduce sub-critical fatigue crack propagation.
3. examine any changes the ABS particles may have on the rheological properties including setting time.
4. create a bond between the ABS particles and the cement matrix by coating the ABS particles with a silane coupling agent.
5. repeat stages 1-3 using ABS particles coated with a silane coupling agent.
6. quantify the ultimate quantity of non-coated or silane coated ABS particles which maximizes the resistance of the cement to crack propagation without dramatically changing its rheological properties in comparison with commercial cements.

CHAPTER 3

ANALYSIS OF COMMERCIAL BONE CEMENTS

3.1 INTRODUCTION

The overall object of this study was to examine the effect of adding rubber particles to experimental bone cements in order to improve their resistance to fracture. The addition of rubber particles could also adversely affect the flexural and rheological properties of the cements. It was important, therefore, to first determine these properties in currently available bone cements which would then be used as a baseline. Consequently, the mechanical properties requiring investigation were; fracture toughness, sub-critical crack growth behaviour under fatigue as well as flexural strength and flexural modulus.

Fracture toughness is a critical parameter as it characterizes the resistance of a brittle material to catastrophic failure by unstable crack growth. Cracks in bone cement can be generated from pores, surface irregularities and residual stresses.[5] Previous work examining the fracture toughness of cements stored in air at room temperature, have given values between 1.18 and 2.58 MPa.m$^{1/2}$.[7, 40, 41, 47, 61, 63-68]

Fatigue fracture is also a major failure mechanism of bone cement.[69-71] A large amount of research has been carried out on the number of stress cycles to induce failure,[69, 76-81] however, far less work has been produced on sub-critical crack propagation during fatigue.[7, 27, 73, 82, 83] This is an important area of research because under cyclic loading, sub-critical cracks will eventually propagate to a critical size leading to the eventual failure of an implant. So far crack propagation rates, when ΔK

= 1 MPa.m$^{1/2}$, have ranged from 3.3 x 10^{-9} m/cycle[82] to 9.5 x 10^{-4} m/cycle.[27] The extensive variation in rates is due to different, mixing, storing and testing conditions

Flexural strength and modulus are also important properties as the cement is subjected to both tensile and compressive forces in situ. A review of the literature reveals a large variation in values, with flexural strengths and moduli ranging from 45.7-98.44 MPa and 1.95-2.6 GPa respectively.[32, 35, 39, 41, 50-52]

Finally, the rheological behaviour, and therefore the handling/curing properties as well as the setting time, was also examined for each commercial cement throughout the entire curing process both at room temperature (25°C) and body temperature (37°C).[20] This would characterize the currently acceptable range of rheological properties.

By assessing the resultant data from each test, a range of values were determined which would be used as a baseline. The results obtained from the experimental cements developed in the consequent chapters would then be compared with this data.

3.2 MATERIALS AND METHODS

3.2.1 Materials

Three different types of bone cement were tested; the traditional CMW 1 and Palacos R, and the more recently developed Cemex ISOPLASTIC. All are high viscosity cements and their composition and manufacturer's details are given in Table 2.1 Both CMW 1 and Palacos R are mixed in the usual 2/1 powder to liquid ratio, but Cemex ISOPLASTIC has a reduced proportion of monomer and so is mixed in a 3/1 powder to liquid ratio. As Cemex ISOPLASTIC is a relatively new cement there is very little published data on the following tests carried out in air at room temperature.

3.2.2 SEM Examination of PMMA Powders and Fracture Surfaces

To determine the particle sizes of the three different PMMA powders, they were prepared and examined using an SEM. Preparation involved gold sputter coating the powders using a Palaron E5400 sputter coater, and mounting the powders on stubs with Mikrostick adhesive (Agar Scientific Ltd, Essex, U.K). The powders were viewed on an EBT 1 SEM (S.E.M. TECH Ltd, Derbyshire, U.K) at 20 kV. Measurements of particle sizes were taken using Scion Image measuring package (Scion Corporation, N.I.H. U.S.A.).

When examining fracture surfaces the above method was followed, except Leit-c plast adhesive (Agar Scientific Ltd, Essex, U.K) was used instead of Mikrostick adhesive.

3.2.3 Flexural Properties

Preparation

40g of each cement (i.e. an entire packet as supplied) was mixed by hand, in air, at room temperature following the manufacturers' instructions. When the cement had reached the required doughy stage, it was manually placed into five open ultra high molecular weight polyethylene (UHMWPE) moulds, each measuring 80mm by 10mm by 5mm.[117] An UHMWPE plate was placed on top of the moulds and weighted down with a 5kg mass. This ensured that the cement cured under a similar pressure to the handling pressure which the cement is subjected to during clinical operations.[118] The cement was allowed to cure in these moulds for 24 hours, and any samples with visible porosity greater than 1mm in diameter were discarded. A total of 10 acceptable samples were prepared for each type of cement.

Experimental

Three-point bending tests were carried out on the 10 samples using a Lloyds Instruments LRX tensile testing machine with a load cell of 1kN. The crosshead speed (load rate) was set at 5 mm/min and the span, L, at 60mm (see Figure 2.3, Chapter 2, Section 2.3.1.1). The width and height of each specimen was measured using a micrometer for input into "Lloyd Windap," a computer programme which recorded the change in load and deformation during testing as well as calculating the flexural strength of each specimen. The flexural modulus was calculated using Equation 2.3, Chapter 2, Section 2.3.1.1. All tests were performed at room temperature, 21 ± 1°C.

3.2.4 Fracture Toughness

Preparation

Fracture toughness values were determined for 10 samples of each type of cement. These samples were the fractured test pieces obtained from the three-point bending tests, and so their dimensions were 10mm by 5mm by approximately 40mm. A small (1-2mm) notch was made in the side of each sample half-way along its length using a hacksaw and a crack was introduced into the tip of the notch by using a disposable Stanley knife blade (see Figure 3.1). As bone cement is brittle, each sample was examined under a microscope to check that the crack introduced had not propagated through the whole sample. The crack length was then measured using a travelling microscope and the width and depth of each sample was measured using a micrometer.

Experimental

Tests were performed at room temperature (21 ± 1°C) using a Lloyd Instruments LRX tensile testing machine, with a 1 kN load cell. The applied loading configuration was the same as for three-point bending, except the span, L, was set at 30mm and the crosshead speed was 2.5 mm/min. The load at which each sample broke was recorded, and fracture toughness values were calculated using Equations 2.10 and 2.11 given in Chapter 2, Section 2.3.1.2.

Following testing the fracture surfaces were prepared and examined using an SEM as described in Section 3.2.2.

3.2.5 Fatigue

Preparation

Two Compact Tension (CT) specimens (Figure 3.2) were made of each of the three different types of bone cement in the following way:-

For each specimen, a whole packet of bone cement (40g powder) was mixed by hand in a fume cupboard at room temperature following the manufacturer's instructions. The cement was manually placed in an open UHMWPE mould measuring 62.5mm x 60mm x 10mm. A UHMWPE plate was placed on top of the mould and weighted down with a 5 kg mass. The cement was left to cure and remained in the mould for 24 hours.

To produce the notched CT configuration, two 12.5mm diameter holes were drilled through the specimen and a notch was made using a hacksaw. A crack was introduced by tapping a scalpel blade at the tip of the notch. The length of the notch plus crack was measured using a travelling microscope.

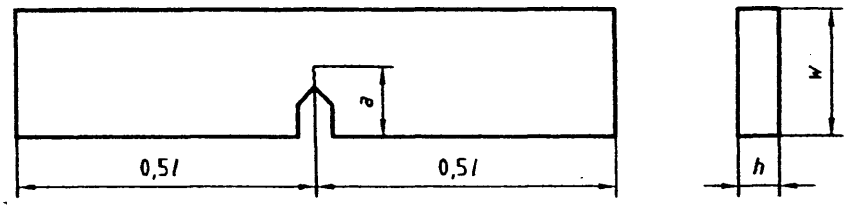

Figure 3.1: Diagram of a single-edged notched specimen[59]

where a = original crack length
h = height of specimen
w = width of specimen
l = length of specimen

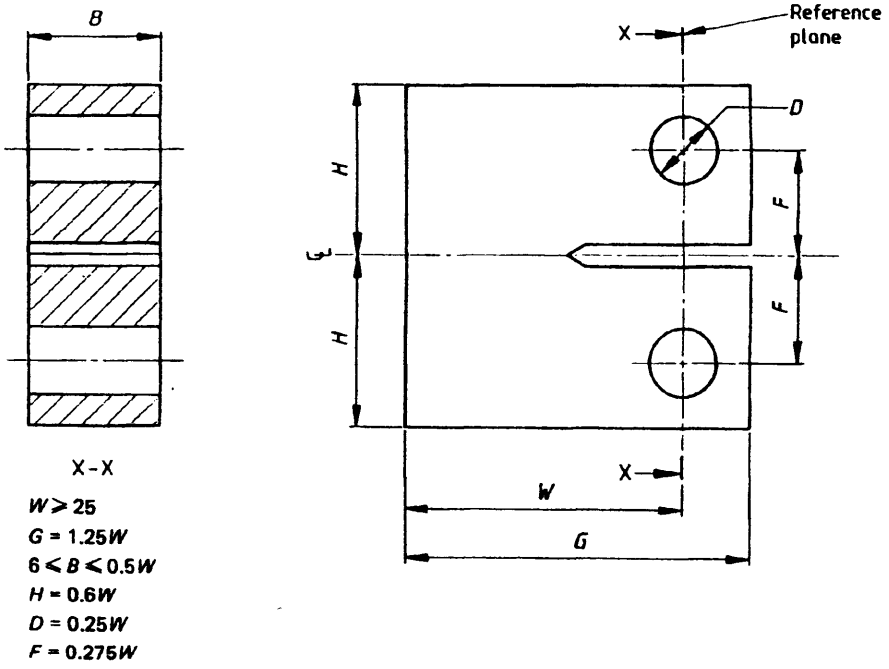

Figure 3.2: Compact tension specimen[119]

Monitoring crack growth

To monitor the increase in crack length during testing, a metal foil Krak-Gage® (model B20, Russenburger Prufmaschinen AG, Neuhausen-am-Rheinfall, Switzerland) was bonded to the surface of the sample. This gauge comprises of a thin resistive foil on a brittle plastic backing and measures indirect potential drop, i.e. when a constant current passes across the gauge, the longer the crack gets the further the current has to travel, resulting in an increase in voltage. A constant current was applied to the gauge using a precision constant current supply and amplifier system specifically designed for the purpose. This system uses a very accurate voltage reference, a precision resistor and an ultra-low offset drift operational amplifier to control the current through the gauge. The resultant potential drop/voltage drop across the gauge was amplified using a precision instrumentation amplifier and recorded every 10 seconds using a Pico Technology ADC16 data logging recording programme (Pico Technology Ltd).

Experimental

Sinusoidal loading was applied to the sample, using a servo-hydraulic testing machine (Dartec 9500), at a load ratio R (ratio of minimum to maximum load) of 0.1 and a frequency of 10 Hz. The initial load applied was based on preliminary tests to obtain initial crack growth rates of approximately 10^{-9}m and typically the maximum load was 190N. All tests were performed in air at room temperature (23 ± 1°C).

To determine the crack propagation parameters C and m of the Paris Erdogan relationship (see Equation 2.12, Chapter 2, Section 2.4.1), the increase in crack length per cycle (da/dN) and the stress intensity factor range, ΔK, were calculated, then plotted on log-log graphs. First, the increase in crack length was calculated using the initial crack length measurement and the corresponding initial voltage reading.

Previous calibration of the Krak-Gages had shown that a change in the output voltage of 1mV corresponded to an increase in crack length of 11.59μm. By converting the output voltage into crack length measurements and knowing that output voltage was recorded every 10 seconds and testing frequency was 10 Hz, the number of cycles and the corresponding crack length could be determined. da/dN was then calculated at every 115.9μm intervals by numerical differentiation of crack length as a function of the number of cycles.

The stress intensity factor range, ΔK, was calculated using the crack length, sample dimensions and applied load at the same 115.9μm intervals as above following Equations 3.1 and 3.2.[119]

where
$$K = \frac{P}{BW^{1/2}} f(a/W) \tag{3.1}$$

and

$$f(a/W) = \frac{[2+(a/W)][0.866+4.64(a/W)-13.32(a/W)^2+14.72(a/W)^3-5.6(a/W)^4]}{[1-(a/W)^{1.5}]} \tag{3.2}$$

P = load

a = crack length

B, W = specimen dimensions defined in Figure 3.2

Having plotted da/dN on a log-log scale as a function of ΔK, linear regression was used to determine m, the slope of the graph, and C, the intercept for each type of cement.

After testing, the fracture surfaces were prepared and examined using an SEM at 15 kV as described in Section 3.2.2.

3.2.6 Rheology

The change in rheological properties of ten samples of each of the three cements were measured using a Bohlin Instruments CVOR 200 rheometer (Malvern Instruments Ltd, Malvern, Worcestershire, U.K.) with a parallel plates measuring system. The diameter of the upper parallel plate measured 40mm and the gap between the two plates was set at 2mm. Approximately 4g of each cement was mixed by hand and placed between the plates of the rheometer. The top plate was lowered and the excess cement carefully removed.

The rheometer was used in continuous oscillation mode with a frequency of 5 Hz. Readings were taken, by the rheometer, every 6 seconds and continued until the bone cement became so solid that the top parallel plate was no longer able to oscillate at a frequency of 5 Hz. A time of 90 seconds elapsed from the onset of mixing each cement until the first rheometer reading.

As the rheometer has isothermal temperature options allowing the temperature of the bottom plate of the measuring system to be set to a desired temperature, the cements were tested at both room temperature (25°C) and body temperature (37°C).

3.2.7 Statistical Analysis

Results were statistically analysed using One Way Analysis of Variance (one way ANOVA) with a significance level of 0.05, followed by Tukey's HSD post hoc test. [ANOVA is used to test for significant differences between means when there are more than two groups to be compared. A post hoc test is performed when there has been no specific hypothesis made before experimentation.[120]]

3.3 RESULTS AND DISCUSSION

3.3.1 SEM Analysis of PMMA Powders

SEM micrographs of the powder component of Palacos R, CMW 1 and Cemex ISOPLASTIC, are shown in Figures 3.3 - 3.5. The morphology of all the PMMA powders is very similar. They all contain both spherical and irregular shaped beads with CMW 1 having the largest proportion of irregular shaped beads.

The range of bead sizes, however, is different for each type of cement. Palacos R has the largest range of bead sizes, approximately <5 - 70μm, followed by CMW 1, <5 - 50μm. Cemex ISOPLASTIC has the smallest range of bead sizes, approximately <5 - 40μm.

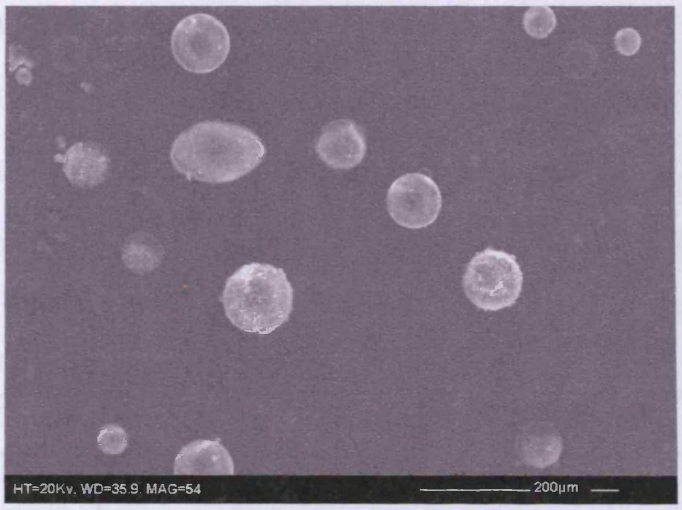

Particle diameter range approximately <5 - 70µm

Figure 3.3: Palacos R powder, magnification x 54

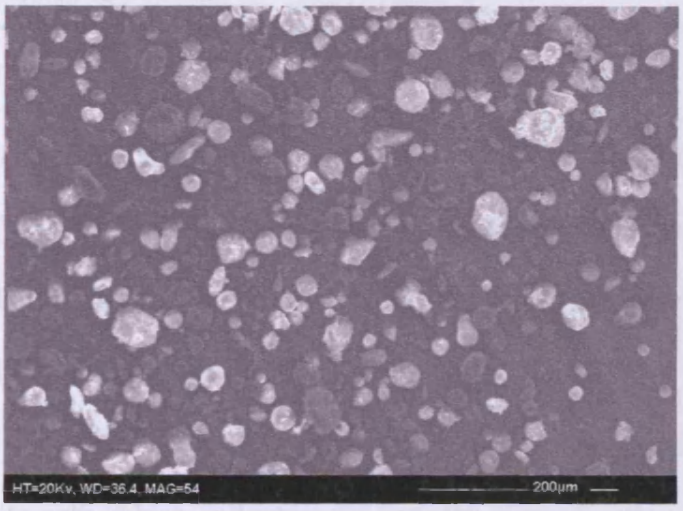

Particle diameter range approximately <5 - 50µm

Figure 3.4: CMW 1 powder, magnification x 54

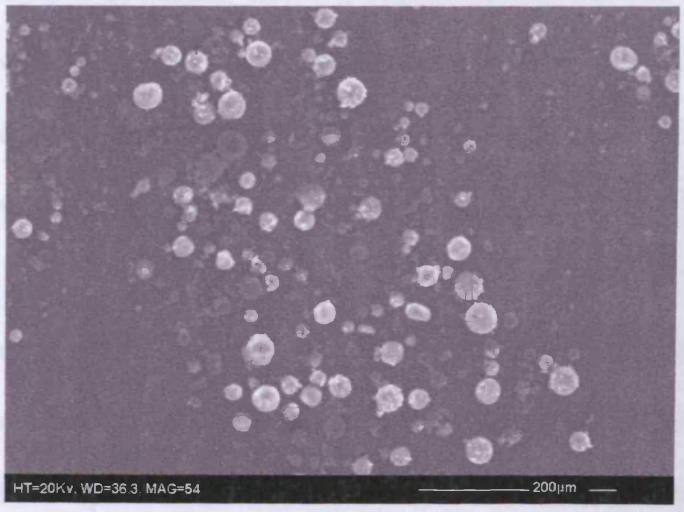

Particle diameter range approximately <5 - 40µm

Figure 3.5: Cemex ISOPLASTIC powder, magnification x 54

3.3.2 Flexural Properties

The average flexural strength and flexural modulus of each cement are shown in Table 3.1. Graphs showing the change in load and displacement during testing for one representative sample of each type of cement are found in Figures 3.6 - 3.8.

Table 3.1: Flexural properties of bone cement

Cement	Flexural Strength (MPa)	Flexural Modulus (GPa)
Palacos R	63.47 ± 4.66	2.26 ± 0.11
CMW 1	49.53 ± 4.11	2.61 ± 0.12
Cemex ISOPLASTIC	55.63 ± 4.48	2.39 ± 0.16

The flexural strength of Palacos R is significantly greater than both CMW 1 ($p<0.0005$) and Cemex ISOPLASTIC ($p<0.005$). However, the flexural modulus of Palacos R at 2.26 GPa is significantly lower than both CMW 1 ($p<0.0005$) and Cemex ISOPLASTIC ($p<0.005$).

The three cements exhibit a wide range of statistically different flexural strength values, reflecting the breadth of results obtained by other authors (Table 2.3, Chapter 2, Section 2.3.1.1). The strength of Palacos R compares favourably with the work by Puska[35] and Dunne and Orr[32] under similar conditions. The strengths of CMW 1 and Cemex ISOPLASTIC also lie well within the range reported by other workers, and appear to have values similar to Zimmer[41] and Subiton[49, 52] cements.

The flexural moduli of the three cements are also significantly different from each other, but again fall within the range of results found in the literature. The moduli of CMW 1 is very similar to the modulus of CMW 3 obtained using four point bending[50] and the modulus of Palacos R lies in between the results produced by Puska[35] and Dunne and Orr.[32]

Effect of porosity and composition on flexural properties

The flexural strengths and moduli of Palacos R, CMW 1 and Cemex ISOPLASTIC reveal that different types of cements can produce very different flexural properties. The most obvious explanation is the different composition of the cements (Table 2.1, Chapter 2, Section 2.2.1) and the extent of the internal porosity.

There have been extensive studies on reducing porosity[26-28] and vacuum mixing appears the most promising.[28] However, reducing porosity may lead to other problems such as increased shrinkage, resulting in the loosening of an implant.[5, 29] Dunne and Orr[32] examined the effect of different levels of porosity on the flexural properties of Palacos R. Interestingly, they showed that reducing porosity levels beyond a certain point did not always correspond with an increase in flexural strength/modulus or decrease in standard deviation.

Work undertaken on the composition of commercial cements and flexural properties have mainly been concerned with the effect of the radiopacifier.[52-54] It is generally considered that barium sulphate reduces flexural properties[52] and Lui *et al.*[54] concluded that zirconium dioxide reduces these properties yet further. There are less reports on the effect of the different particle sizes or reduced monomer of the commercial cements on flexural properties. Lui *et al.*[54] stated that the larger particle sizes of Palacos R results in decreased flexural strength/modulus. However, other researchers have found that particles sizes have little effect on flexural properties.[22, 53] There has been little published work on the flexural properties of the reduced monomer Cemex cements, stored and tested in air at room temperature. Kuhn[39] studied a variety of commercial cements having been stored in water at 37°C including Cemex cements, and found these cements to have lower flexural strengths, whereas Lewis and Bhattaram[68] showed that their flexural strengths were not affected.

Given the complex nature of the effect of the composition of bone cement and internal porosity it is difficult to isolate the influence of one factor on the results of the flexural testing. Nevertheless, the results clearly show that Palacos R has the greatest flexural strength and CMW 1, the poorest, whereas Cemex ISOPLASTIC has the highest flexural modulus and Palacos R, the lowest.

Load/displacement curves of the commercial cements

Typical load/displacement curves of each type of cement, obtained during testing are shown in Figures 3.6-3.8 (for clarity they are each presented on individual graphs). They each show the maximum load occurring at the point of failure indicating the brittle nature of bone cement. Interestingly, they also show a very slight curve (this is more pronounced in the case of Palacos R). This implies that the cements are undergoing a very small amount of yielding. Yielding is important, because only materials which are capable of some degree of yielding can be effectively rubber toughened.[106]

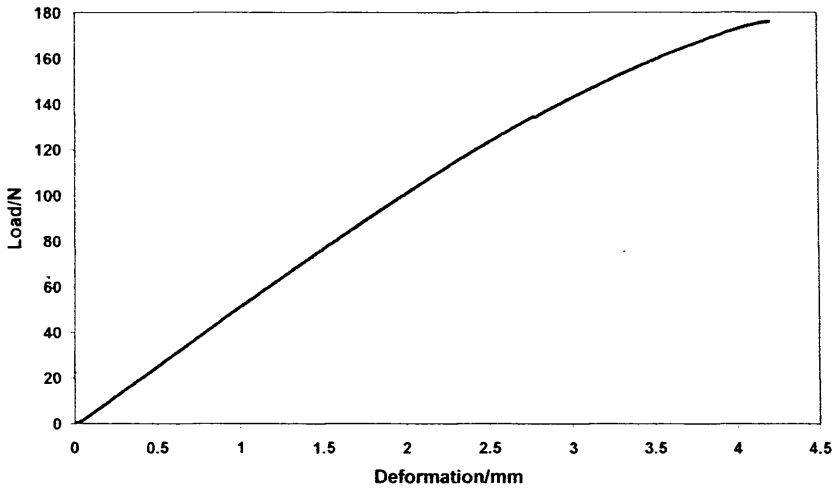

Figure 3.6: Load/displacement graph of Palacos R

Figure 3.7: Load/displacement graph of CMW 1

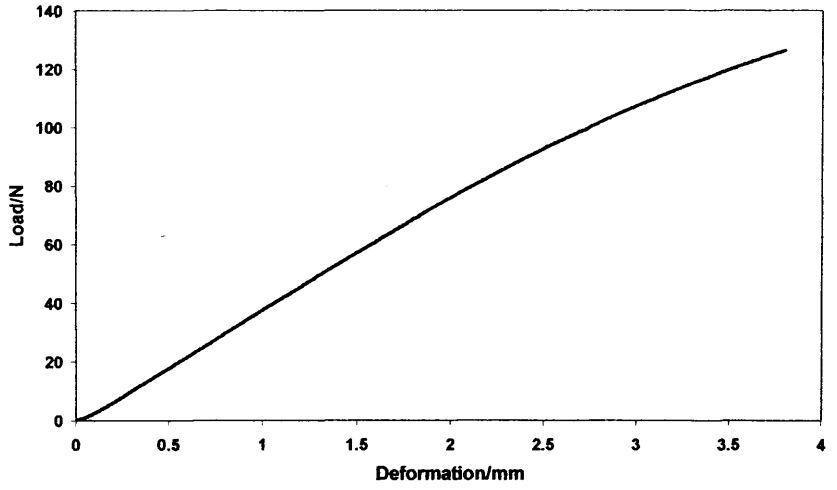

Figure 3.8: Load/displacement graph of Cemex ISOPLASTIC

3.3.3 Fracture Toughness

The fracture toughness values i.e. the resistance of the material to fast crack propagation, are shown in Table 3.2.

Table 3.2: Fracture toughness values of bone cement

Cement	Fracture Toughness, K_{IC} (MPa.m$^{1/2}$)
Palacos R	2.42 ± 0.20
CMW 1	2.17 ± 0.10
Cemex ISOPLASTIC	1.87 ± 0.12

Palacos R has a significantly higher fracture toughness than both CMW 1 ($p<0.05$) and Cemex ISOPLASTIC ($p<0.0005$) with CMW 1 having a significantly higher fracture toughness than Cemex ISOPLASTIC ($p<0.01$). All three cements exhibit very different fracture toughness values and this is reflected in the literature (see Table 2.4, Chapter 2, Section 2.3.1.2). The fracture toughness of CMW 1 is notably higher than the value for CMW 1 reported by Alberts,[66] whereas the fracture toughness of Palacos R is slightly lower than Lewis[63] obtained under similar testing conditions. Even though Cemex ISOPLASTIC has the lowest fracture toughness of the three tested cements, it is still greater than some of commercially available cements such as Zimmer[7, 40, 41] and Subiton.[6] It also corresponds with the fracture toughness value obtained by Lewis and Bhattaram[68] for Cemex XL and has a higher value than the Cemex (type unknown) investigated by Taylor *et al.*[47]

Effect of composition on fracture toughness

The differences in fracture toughness values are again probably due to the different composition, PMMA bead sizes and bead size distribution of these cements, as well as internal porosity. There has been very little research focusing on the effect of PMMA bead sizes on the mechanical properties of commercial cements, and so far results have shown that bead sizes have little influence on fracture toughness,[53, 68] however it is clear that far more research needs to be undertaken in this area.

An explanation for Palacos R having a higher resistance to rapid crack propagation, therefore, is probably because it contains ZrO_2 as a radiopacifier instead of $BaSO_4$. Ginebra[60] studied the effect of different radiopacifiers on the fracture toughness of bone cement and found that cements containing ZrO_2 had greater fracture toughness values than those containing $BaSO_4$. It was suggested that the ZrO_2 particles, having a different surface morphology from the $BaSO_4$, could mechanically anchor onto, and therefore become structurally part of the polymeric matrix.

Both CMW 1 and Cemex ISOPLASTIC contain $BaSO_4$ which may account for their lower K_{IC} values in comparison with Palacos R. Cemex ISOPLASTIC also contains a larger proportion of $BaSO_4$, and less liquid monomer than CMW 1 and both these factors may have a further detrimental effect on fracture toughness.

SEM examination of fracture surfaces following fracture toughness testing

Scanning electron microscopy is a useful way of examining surface features, and may provide details about the deformation processes occurring during fracture. This in turn should give a better understanding about why there are differences in toughness between the cements.

Figure 3.9 shows the fracture surface of Cemex ISOPLASTIC. This cement had the poorest resistance to crack propagation and some of the reasons for this can be seen by looking at the fracture surface. The surface is predominantly smooth with cleaved PMMA beads, which shows that the crack encountered little resistance during propagation, and has, therefore, taken the most direct route through the cement. The PMMA beads have 'river lines' radiating through them mainly in a fan shape and these are seen more clearly in Figure 3.10. The true meaning of these river lines remains unclear but they possibly indicate that the crack is propagating on slightly different planes through the beads. There are a few areas where the surface is rough and display what is termed 'ductile tears', the most obvious area being around the hole in the centre of the micrograph. This is probably due to the hole acting as a stress concentrator resulting in plastic deformation. Given the depth of this hole, it is likely that it was created during fabrication of the specimen, introduced either by mixing, or by monomer evaporation. The lighter circle towards the bottom of the micrograph is also a hole. The barium sulphate opacifier can be seen as small, light particles in the polymer matrix around the PMMA beads and is fairly evenly distributed throughout the matrix.

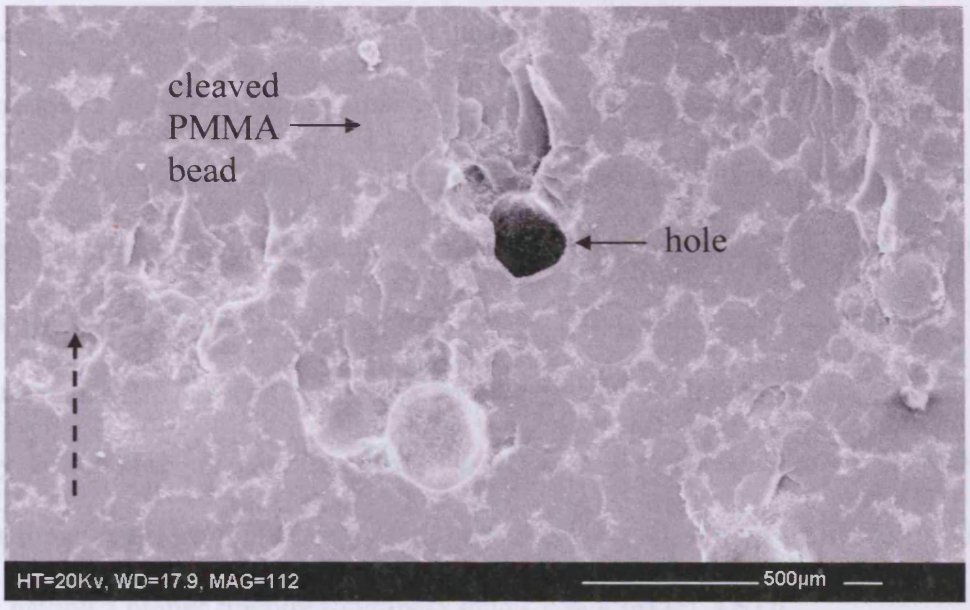

Figure 3.9: SEM micrograph of the fracture surface of Cemex ISOPLASTIC magnification x 112. Direction of crack propagation is shown by the dashed arrow

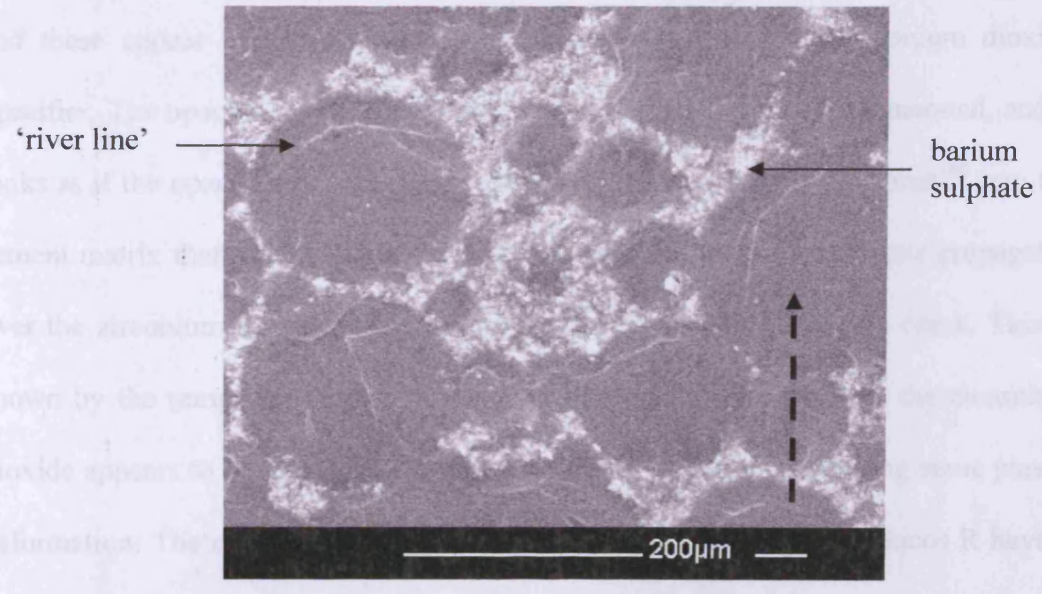

Figure 3.10: SEM micrograph of the fracture surface of Cemex ISOPLASTIC magnification x 285

The fracture surface of CMW 1 (Figure 3.11) is not quite as smooth as Cemex ISOPLASTIC. Again the PMMA beads have been cleaved and show river lines, but there are also a number of rough areas which suggest that the crack is propagating in a slightly convoluted manner through the cement. A particularly prominent rough area, displaying a large number of ductile tears, can be seen around the hole on the bottom left hand side of the micrograph, and there is also a micro-crack propagating from this hole. Internal PMMA beads can clearly be seen protruding in the two other holes. The slightly convoluted manner in which the crack has propagated has increased its surface area, therefore more energy was required for propagation, which corresponds with it having a higher fracture toughness than Cemex ISOPLASTIC.

The fracture surface of Palacos R (Figure 3.12) is very different from CMW 1 and Cemex ISOPLASTIC. There are no distinct cleaved PMMA beads visible, however they are there but are difficult to see due to the contrast available on the SEM, though some river lines remain visible. There are a number of rough regions and these appear to be either generated from, or around, the zirconium dioxide opacifier. The opacifier is not finely distributed but has become agglomerated, and it looks as if the opacifier is sufficiently attached or 'mechanically anchored'[60] into the cement matrix that microcracks ahead of the main advancing crack have propagated over the zirconium dioxide opacifier before being joined by the main crack. This is shown by the ramp-like surfaces in front of the opacifier. Therefore, the zirconium dioxide appears to be acting as a reinforcing agent as well as promoting some plastic deformation. The combination of both these factors has resulted in Palacos R having the highest fracture toughness of the three cements tested.

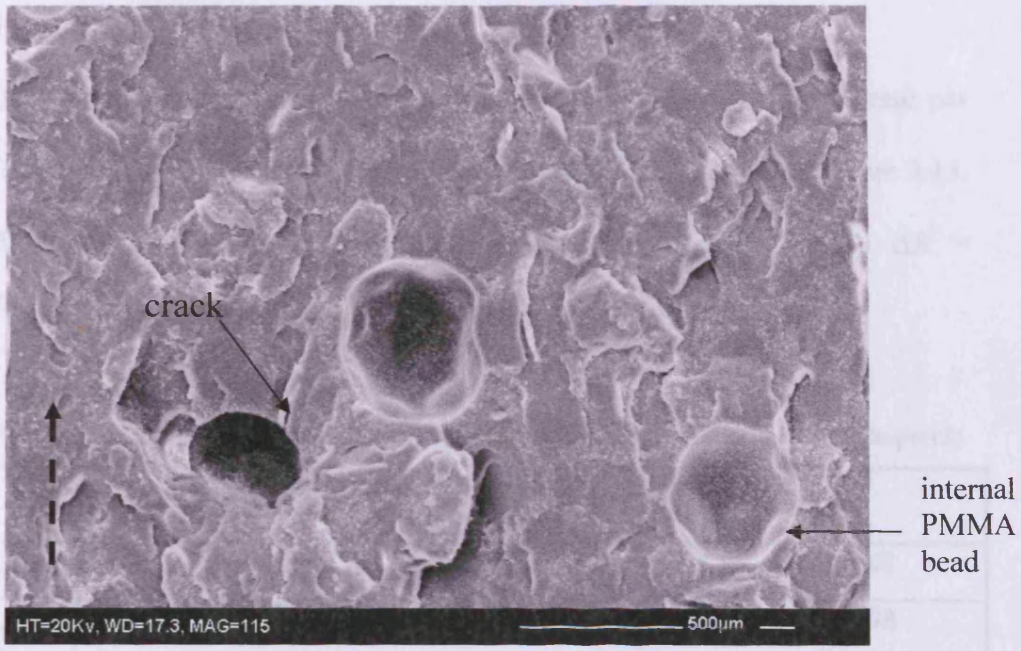

Figure 3.11: SEM micrograph of the fracture surface of CMW 1 magnification x 115

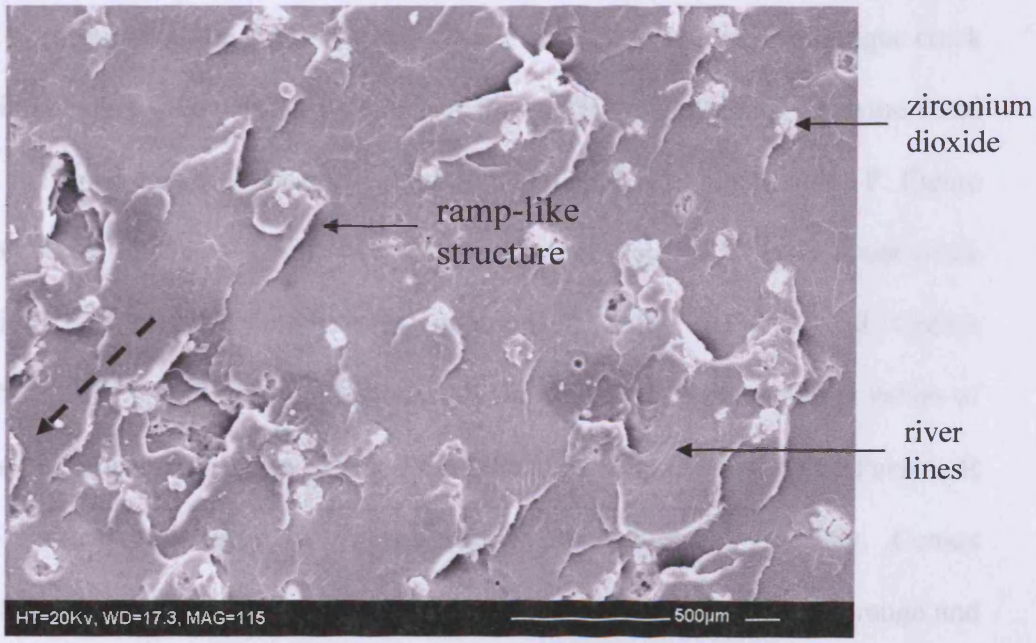

Figure 3.12: SEM micrograph of the fracture surface of Palacos R magnification x 115

3.3.4 Fatigue

The results of the fatigue crack propagation behaviour in terms of growth rate per cycle, da/dN, as a function of the stress intensity range, ΔK, are shown in Figure 3.13. The resultant calculated crack growth rate parameters, m and C when ΔK = 1 MPa.m$^{1/2}$, along with the correlation coefficient, R^2 are found in Table 3.3.

Table 3.3:Fatigue crack propagation rate parameters (calculated using Equation 2.12, Chapter2)

Cement	Crack growth rate, C, m/cycle (MPa m$^{1/2}$)$^{-m}$	m	R^2
Palacos R (a)	2.48 x 10^{-7}	6.55	0.98
Palacos R (b)	4.97 x 10^{-7}	6.90	0.98
CMW1 (a)	2.46 x 10^{-6}	7.74	0.94
CMW1 (b)	1.40 x 10^{-6}	7.45	0.98
Cemex ISOPLASTIC (a)	1.21 x 10^{-5}	7.63	0.92
Cemex ISOPLASTIC (b)	5.70 x 10^{-6}	7.22	0.99

Figure 3.13 reveals that the stress intensity factor range, ΔK, required for fatigue crack propagation lies between 0.3 and 1.68 MPa.m$^{1/2}$. This is typical of many polymers and is within the same range observed by Molino and Topoleski[73] for Simplex P. Figure 3.13 also shows that for a given stress intensity range Palacos R has a lower crack propagation rate and acceleration in comparison with CMW 1 and Cemex ISOPLASTIC. Palacos R also continues stable crack growth to much higher values of the stress intensity factor range, ΔK = 1.68 MPa.m$^{1/2}$. This illustrates that Palacos R has the greatest resistance to fatigue crack propagation. Conversely, Cemex ISOPLASTIC has the fastest crack propagation for a given stress intensity range and only continues stable crack growth to ΔK = 0.93 MPa.m$^{1/2}$ therefore showing the least resistance to crack propagation. This is clearly shown in the resultant calculated

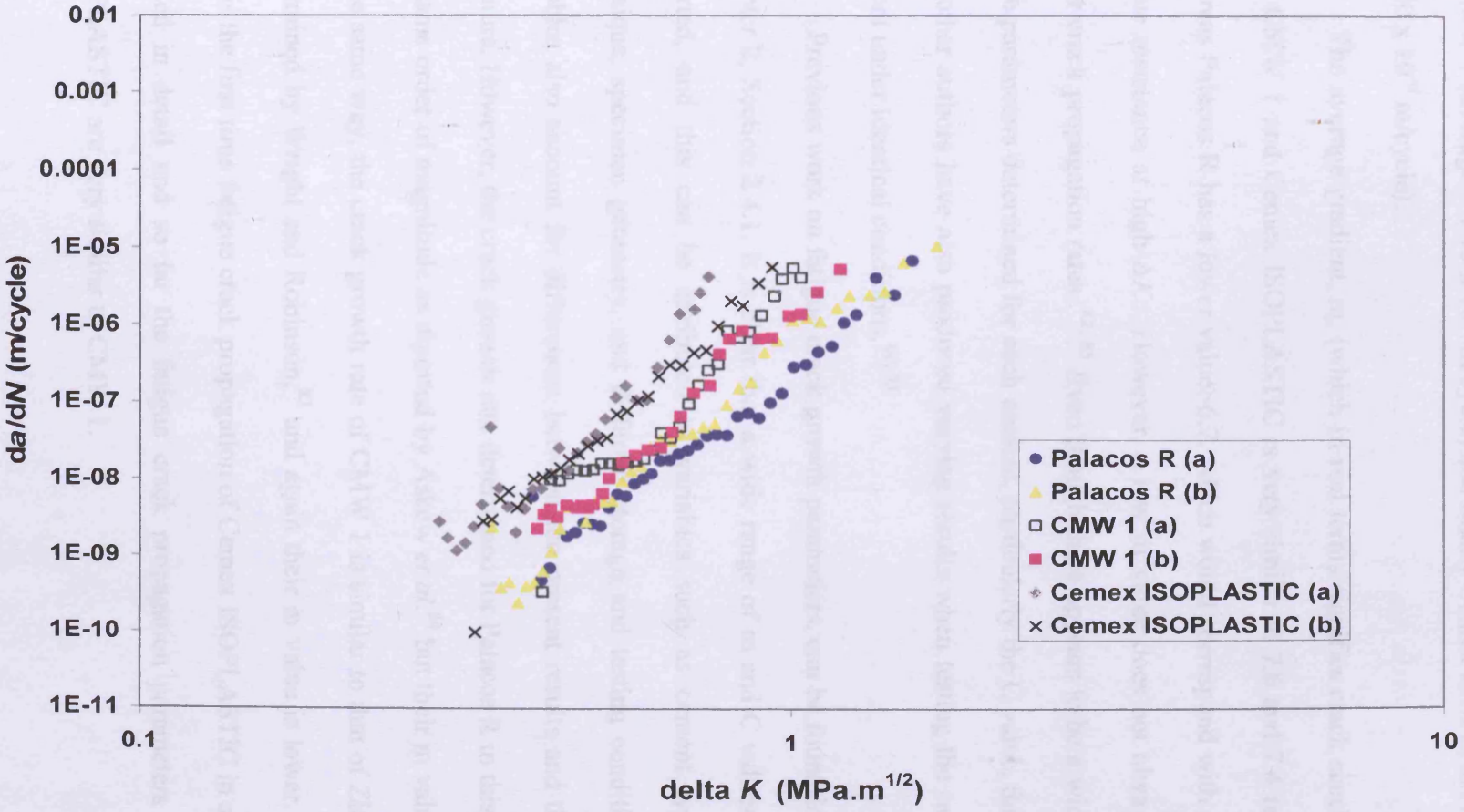

Figure 3.13: Fatigue crack growth rate, d*a*/d*N*, plotted against the stress intensity range, delta *K*, for Palacos R, CMW1 and Cemex ISOPLASTIC

fatigue parameters, C and m (Table 3.3) where Palacos R has the slowest crack propagation rate, C, (average = 3.72 x 10^{-7} m/cycle when ΔK = 1 MPa.$m^{1/2}$) followed by CMW 1 (average = 1.93 x 10^{-6} m/cycle) and finally Cemex ISOPLASTIC (average = 8.90 x 10^{-6} m/cycle).

The average gradient, m, (which in real terms signifies crack acceleration) of both CMW 1 and Cemex ISOPLASTIC is very similar at 7.6 and 7.4 respectively. Whereas Palacos R has a lower value, 6.7, which would correspond with its superior fatigue resistance at high ΔK. However, a low m value does not always result in lower crack propagation rates .[82, 83] Even though there appears to be a wide variation in the parameters determined for each cement, particularly the C value, this is normal and other authors have also produced varying results when testing the same type of cement under identical conditions.[60, 73]

Previous work on fatigue crack growth parameters, can be found in Table 2.5, Chapter 2, Section 2.4.1. It is clear that a wide range of m and C values have been reported, and this can be attributed to variables such as cement type, mixing technique, specimen geometry, and different storage and testing conditions. These variables also account for differences between the present results and those in the literature. However, the crack growth rate determined for Palacos R in this study is of the same order of magnitude as reported by Askew *et al.*[84] but their m value is lower. In the same way, the crack growth rate of CMW 1 is similar to that of Zimmer LVC determined by Wright and Robinson,[83] and again their m value is lower. It is likely this is the first time fatigue crack propagation of Cemex ISOPLASTIC in air has been studied in detail and so far the fatigue crack propagation parameters of Cemex ISOPLASTIC are very similar to CMW 1.

Effect of composition on fatigue crack growth behaviour

Overall the results reveal that Palacos R has the greatest resistance to slow crack propagation under sinusoidal loading with CMW 1 and Cemex ISOPLASTIC performing less well and this corresponds with the results obtained by rapid fracture (Fracture Toughness, Section 3.3). As with fracture toughness, the differences in the fatigue crack propagation parameters are probably due to differences in composition, bead sizes and volume of liquid monomer.

In contrast with the work on fracture toughness, it has been found that differences in particle size do affect the fatigue crack growth behaviour. Ginebra *et al.*[121] and Lewis and Bhattaram,[68] showed that cements with larger bead sizes had a significantly greater resistance to fatigue crack propagation. Ginebra *et al.*[60] also studied the fatigue behaviour of cements containing different radiopacifiers and unlike their research on fracture toughness they discovered that the radiopacifier $BaSO_4$ had a more beneficial effect on fatigue resistance than ZrO_2.

The results of this present study appear to correspond with the work on particle sizes produced by Ginebra[121]. There is some possibility that the larger average PMMA bead size and size distribution of Palacos R may outweigh the detrimental effect of the ZrO_2 but obviously more research needs to be undertaken in this area.

SEM examination of fracture surfaces following fatigue testing

The fatigue fracture surface of Palacos R (Figure 3.14) is very different from the smooth fracture surface obtained following fracture toughness testing (Figure 3.12). The fatigue fracture surface is very rough and highly irregular showing that the crack has propagated in a very convoluted way indicative of a slower rate of fracture. The PMMA beads are visible and whole beads can clearly be seen on the right hand side of the micrograph. According to Nguyen *et al.*[82] at such a low crack growth rates (10^{-7} m/cycle when ΔK = 1 MPa.m$^{1/2}$), the crack is able to find the easiest path through the microstructure, and as such can propagate around the PMMA beads. Again, the zirconium dioxide is clearly visible and is not evenly distributed, but has agglomerated at localised sites. It is possible that the zirconium dioxide has promoted plastic deformation which has resulted in the uneven fracture surface. There is also some void formation possibly caused by separation of zirconium dioxide particles with the surrounding matrix .[83]

The fatigue fracture surface of CMW 1 (Figure 3.15) is much smoother than the fatigue fracture surface of Palacos R. The crack has propagated in a less tortuous manner which corresponds with the faster crack growth rate (10^{-6} m/cycle when ΔK = 1 MPa.m$^{1/2}$). The PMMA beads can still be seen and appear to be cleaved, however, the surface is not as smooth as the surface produced by rapid fracture (see Figure 3.11).

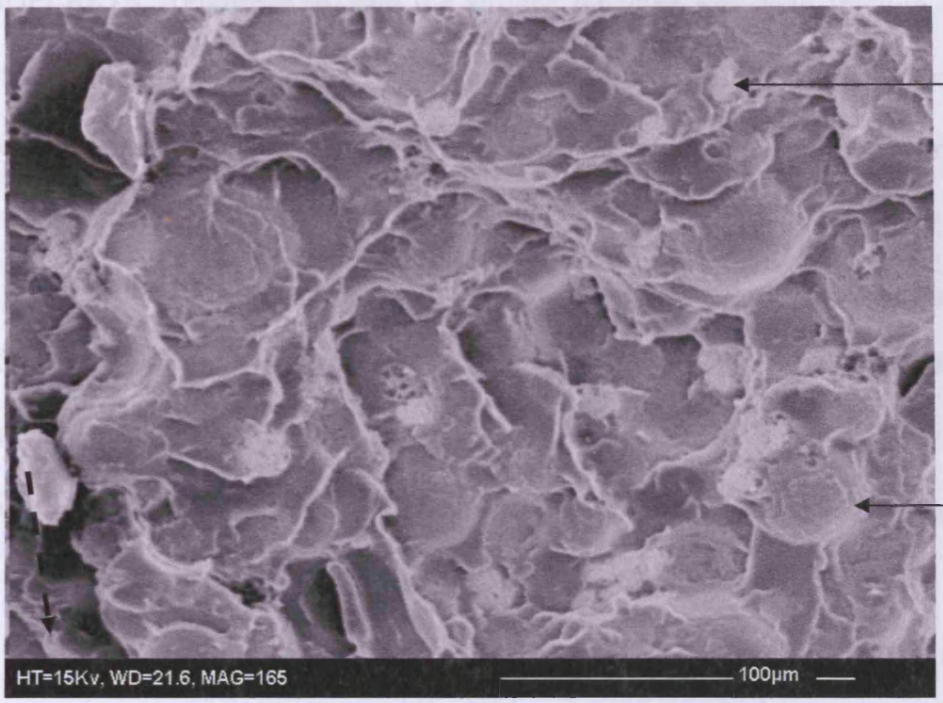

Figure 3.14: Fatigue fracture surface of Palacos R, magnification x 165.
Direction of crack propagation is indicated by the dashed arrow

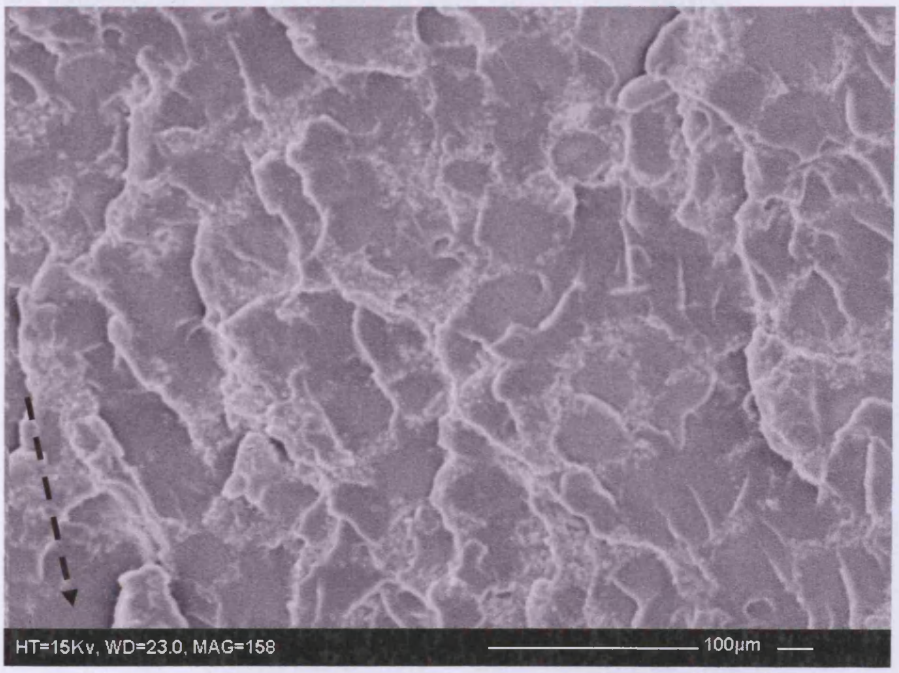

Figure 3.15: Fatigue fracture surface of CMW 1, magnification x 158

Again, there is a large contrast between the fatigue fracture surface of Cemex ISOPLASTIC (Figure 3.16) and the surface obtained following fracture toughness testing (Figure 3.9). The fatigue fracture surface is much more irregular signifying the slower rate of fracture and although cleaved PMMA beads can still be seen, they are not so dominant.

The fatigue fracture surface is almost identical to the fatigue fracture surface of CMW 1, although there is more barium sulphate present in Cemex ISOPLASTIC. In comparison with the fatigue fracture surface of Palacos R, the surface of Cemex ISOPLASTIC is not as rough and irregular indicating the faster crack propagation rate (10^{-6} m/cycle when $\Delta K = 1$ MPa.m$^{1/2}$) through Cemex ISOPLASTIC.

At the higher magnification (see Figure 3.17), striations can be seen on the left hand side of the micrograph, and these are thought to be caused by crack blunting during the loading portion of the fatigue cycle and resharpening during the unloading part of the cycle.[73, 83] There is also some void formation, possibly caused by the barium sulphate particles debonding from the PMMA matrix.

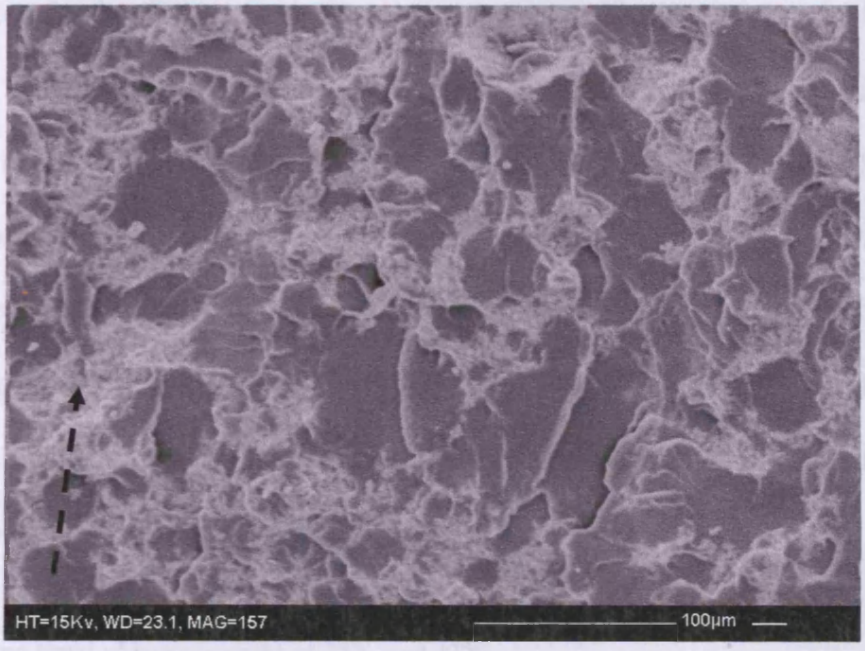

Figure 3.16: Fatigue fracture surface of Cemex ISOPLASTIC magnification x 157

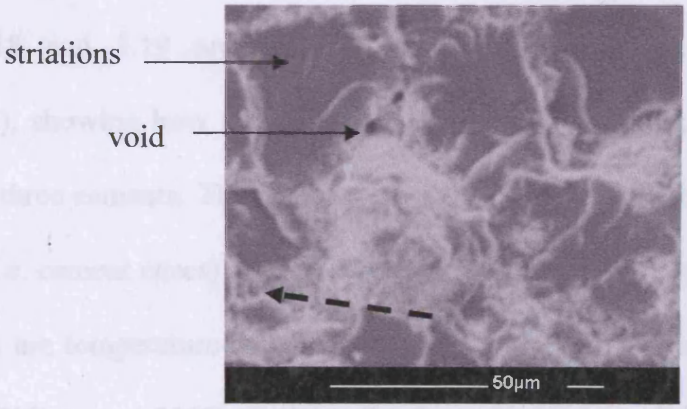

Figure 3.17: Fatigue fracture surface of Cemex ISOPLASTIC magnification x 234

3.3.5 Rheology

The times taken for the different bone cements to cure, signified by a constant elastic modulus, are shown in Table 3.4. The results show that at 25°C, CMW 1 cured at a significantly faster rate than both Palacos R ($p<0.0005$) and Cemex ISOPLASTIC ($p<0.0005$) bone cements. Both Palacos R and Cemex ISOPLASTIC took a similar length of time to cure, and as such there is no significant difference ($p>0.05$) between their curing rates. At 37°C (body temperature) all the cements cured at a much faster rate ($p<0.0005$) than at room temperature, with CMW 1 curing at a significantly faster rate than both Palacos R ($p<0.0005$) and Cemex ISOPLASTIC ($p<0.01$).

Table 3.4: Curing times of bone cements at 25°C and 37°C

Material	Curing Time at 25°C (minutes)	Curing Time at 37°C (minutes)
Palacos R	12.8 ± 0.1	6.6 ± 0.1
CMW 1	8.7 ± 0.4	4.1 ± 0.5
Cemex ISOPLASTIC	12.9 ± 0.2	5.1 ± 0.2

Figures 3.18 and 3.19 are graphs (using one representative sample at each temperature), showing how the viscosity increases with time at 25°C and 37°C, for each of the three cements. They clearly show how much faster the viscosity increases with time (i.e. cement cures) at 37°C than at 25°C, which is to be expected given that curing rates are temperature-dependent. Cemex ISOPLASTIC cures 2.5 times more rapidly at 37°C than at 25°C, CMW 1, 2.1 times, and Palacos R 1.9 times. For all the cements, the viscosity reached a maximum at approximately 75 x 10^3 Pa.s. This is the point at which the cement is no longer a viscous liquid but an elastic solid. Again these graphs also show that at both temperatures CMW 1 cures much faster than either Palacos R or Cemex ISOPLASTIC. However, Palacos R and Cemex

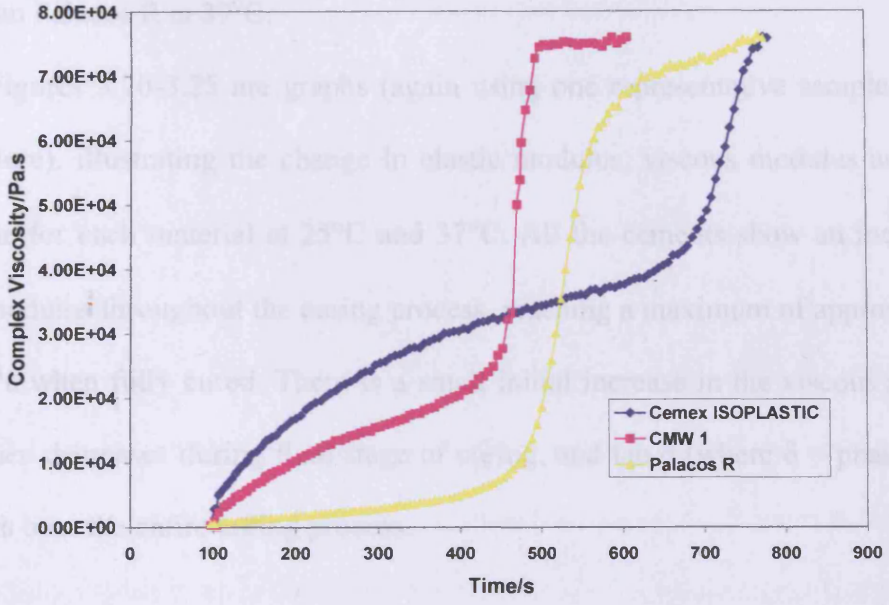

Figure 3.18: Change in complex viscosity during curing at 25°C

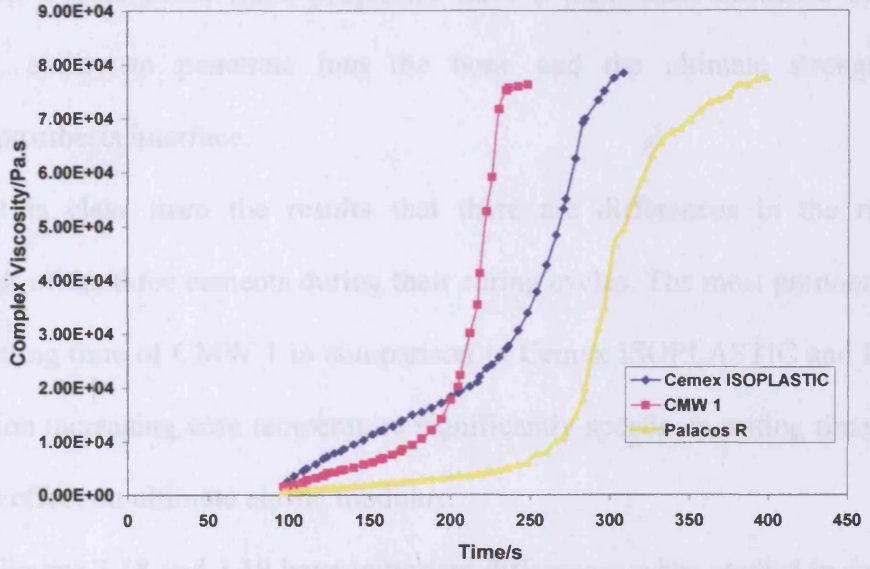

Figure 3.19: Change in complex viscosity during curing at 37°C

ISOPLASTIC both take similar times to cure at 25°C, but Cemex ISOPLASTIC cures faster than Palacos R at 37°C.

Figures 3.20-3.25 are graphs (again using one representative sample at each temperature), illustrating the change in elastic modulus, viscous modulus and tan δ with time for each material at 25°C and 37°C. All the cements show an increase in elastic modulus throughout the curing process, reaching a maximum of approximately 2.35 MPa when fully cured. There is a small initial increase in the viscous modulus which then decreases during final stage of curing, and tan δ (where δ = phase angle) decreases over the entire curing process.

Analysis of changes in rheological properties

The rheological properties of bone cements during their curing phase are very important in determining their mixing/handling characteristics and viscoelastic properties. Furthermore, these properties have a significant influence on material porosity, ability to penetrate into the bone and the ultimate strength of the cement/prosthesis interface.

It is clear from the results that there are differences in the rheological properties of the three cements during their curing cycles. The most pronounced is the faster setting time of CMW 1 in comparison to Cemex ISOPLASTIC and Palacos R. In addition increasing cure temperature significantly speeds up setting time, however has little effect on ultimate elastic modulus.

Figures 3.18 and 3.19 have important differences when studied in detail. They both show 3 different phases, (1) an initial increase in viscosity followed by (2) a plateau (where the viscosity increases slightly), and then (3) a final rapid increase in viscosity. According to Farrar and Rose[95] there are two different processes which

account for these different increases in viscosity. The first is when the PMMA beads are added to the methylmethacrylate monomer, the beads themselves absorb some of the monomer and swell. This leads to the initial increase in viscosity. The second (final) rise in viscosity is then due to the polymerization reaction.

A comparison of the cements at the three different viscosity phases is given below:-

1. *Initial increase*. Cemex ISOPLASTIC bone cement at both temperatures showed the largest/most rapid increase in viscosity, and its viscosity at this stage was much higher than the other two bone cements. Palacos R showed the least increase, and had the lowest viscosity of all the cements at this point. For Palacos R there appeared to be no differentiation between this stage and the plateau stage. CMW 1 lies in between the two.
2. *Plateau*. The viscosity of Cemex ISOPLASTIC is again much greater than the other two, and showed a gradual increase with time. The average viscosity was approximately 30 x 10^3 Pa.s. (at 25°C). Palacos R had the lowest viscosity (ave. 3.0 x 10^3 Pa.s at 25°C), and CMW 1 again lay between the two (15 x 10^3 Pa.s).
3. *Final increase*. In the latter stages of curing, the viscosity suddenly increased reaching a maximum (approximately 75 x 10^3 Pa.s) when the cement finally became a solid. CMW 1 was found to cure/polymerize the fastest at this point followed by Palacos R then Cemex ISOPLASTIC.

At 25°C, Palacos R showed a further final plateau, unlike the other cements. This may be unique to Palacos R or may be due to the other cements becoming so stiff that the rheometer was unable to oscillate at 5 Hz (and so unable to take more readings) leading to this stage being unmeasured. Recent work by Hernandez *et al.*[96]

also showed differing viscosity profiles for the different formulations of experimental cements, with viscosities reaching a maximum of 80 x 10^4 Pa.s.

At 37°C all the graphs are similar, but have a much shorter initial and plateau region, especially Cemex ISOPLASTIC. Essentially the increase in temperature has lead to the polymer beads absorbing the monomer and swelling more rapidly, and also increasing the rate of polymerization.

Examination of Figures 3.20-3.25, (where the elastic modulus = real modulus, G', the viscous modulus = imaginary modulus, G'', and δ = phase/loss angle) reveals that initially both the viscous and elastic moduli increase, with the elastic modulus increasing much more rapidly as the cement changes from being a viscous liquid to an elastic solid. In the early stages of polymerization tan δ was very large due to the ratio between the viscous and elastic modulus being large, but as the cement cured, this ratio became much smaller, leading to tan δ becoming almost zero.

For all of the cements tested there was a peak in the viscous modulus. This occurs during the transition of the cement, i.e., when it changes from being a viscous liquid to an elastic solid. It is interesting to note that this peak does not always occur at the same point on all the graphs. In CMW1 it occurred at the very end of curing as expected, with Palacos it was very near the end but the cement still appeared to carry on curing. With Cemex ISOPLASTIC there was not a sudden peak, but a gradual build up over the whole curing process. The peaks in G'' (viscous modulus) and tan δ (see Figures 3.12-3.17) occur when there is some kind of molecular motion, such as rotation of side groups, in the polymer structure.[9] The peaks are a damping effect i.e. energy is not stored but is dissipated mainly as heat.[15] This causes an increase in free volume which allows space for the molecules to move. Previous work on commercial

cements by Farrar and Rose[95] missed these peaks in viscous modulus and tan δ, due to viscosity measurements being stopped at 1000-1500 Pa.s.

The point at which the cement has cured can clearly be seen when the elastic modulus reaches a maximum and both viscous modulus and tan δ reach a minimum. The elastic modulus increases in a very similar way to the complex viscosity, but only showing two distinct phases: a slow gradual increase followed by a final rapid increase. This final rapid increase in elastic modulus occurs during polymerization, reaching a maximum when the cement is fully cured. Only Cemex ISOPLASTIC at 25°C shows an initial increase in elasticity followed by a plateau region before finally curing.

Overall, the three high viscosity cements tested showed distinct differences in curing rate, with CMW 1 curing in 8.7 min at 25°C and both Cemex ISOPLASTIC and Palacos R curing in 13 min at 25°C. The curing time was also approximately halved when the testing temperature was increased to 37°C, with CMW 1 taking 4.1 min, Cemex ISOPLASTIC, 5.1 min and Palacos R, 6.6 min.

The viscosity during the early stages of curing was also very different for each cement, with Cemex ISOPLASTIC being the most viscous and Palacos R the least.

The handling times were also very different, with CMW 1 having the shortest handling time at both temperatures, and Cemex ISOPLASTIC the longest at 25°C and Palacos R at 37°C.

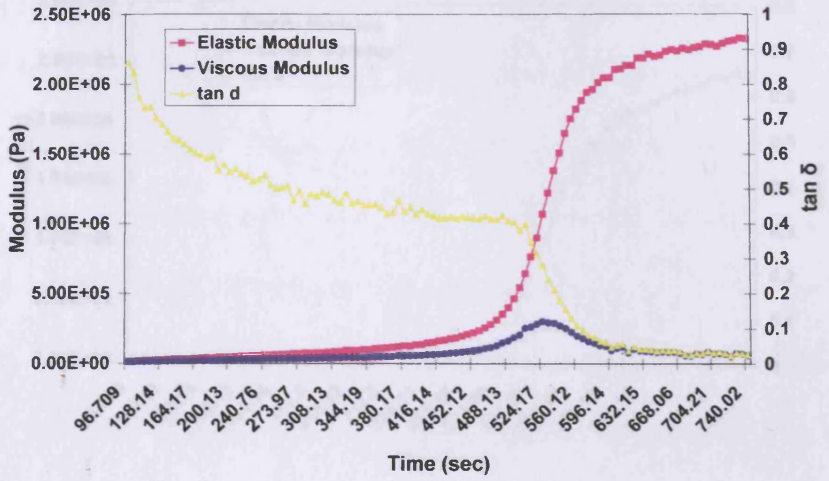

Figure 3.20: Change in elastic/viscous modulus and tan δ of Palacos R at 25°C

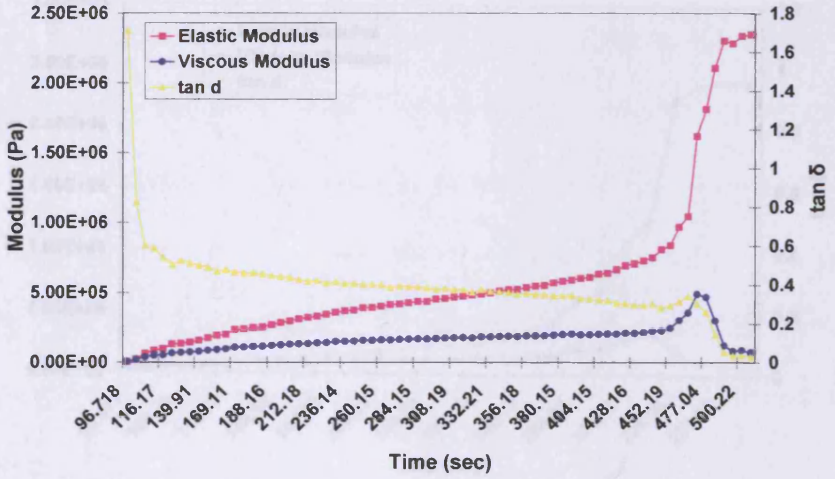

Figure 3.21: Change in elastic/viscous modulus and tan δ of CMW 1 at 25°C

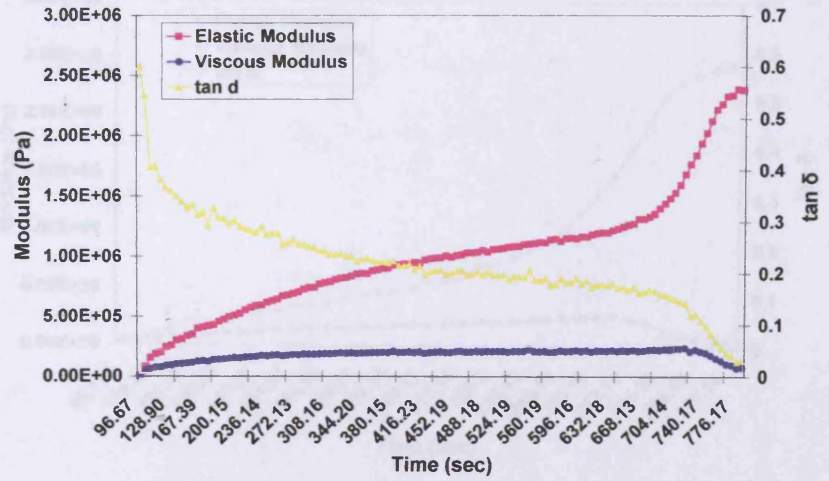

Figure 3.22: Change in elastic/viscous modulus and tan δ of Cemex ISOPLASTIC at 25°C

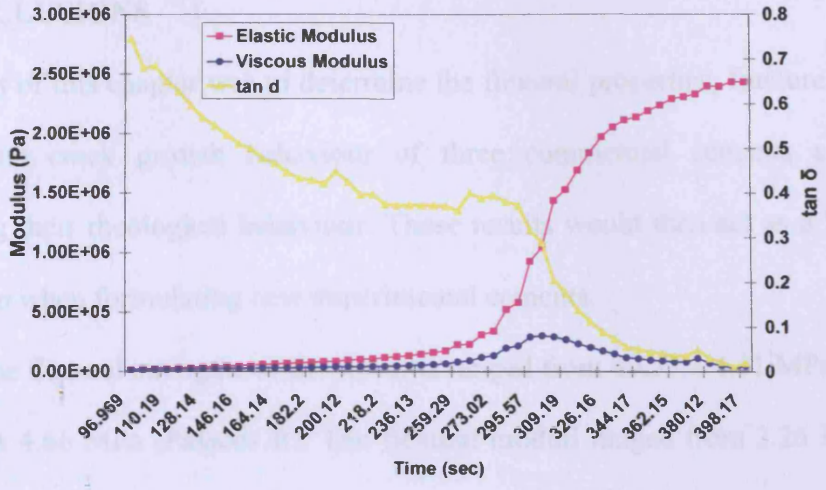

Figure 3.23: Change in elastic/viscous modulus and tan δ of Palacos R at 37°C

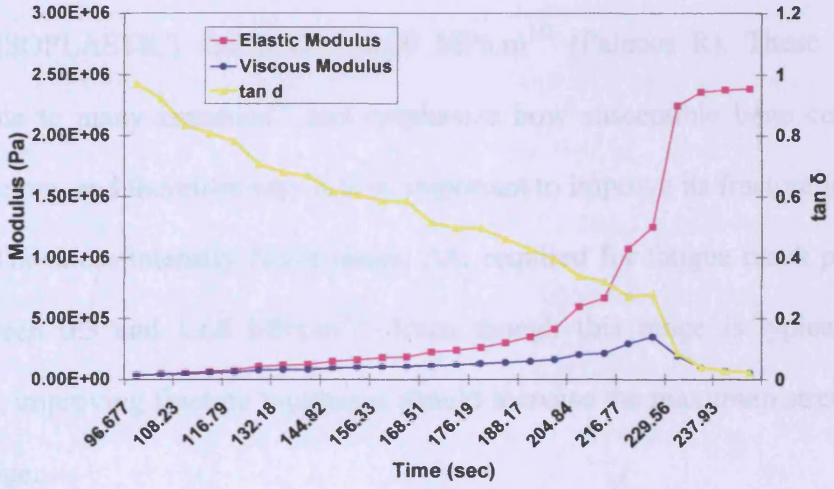

Figure 3.24: Change in elastic/viscous modulus and tan δ of CMW 1 at 37°C

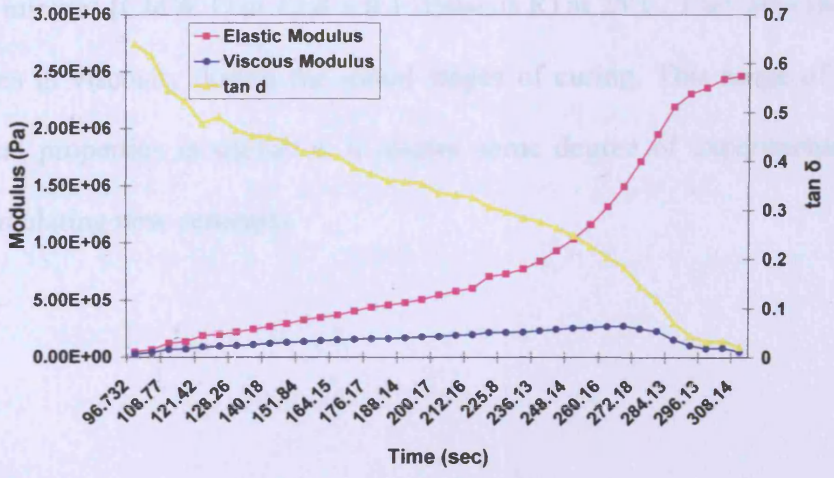

Figure 3.25: Change in elastic/viscous modulus and tan δ of Cemex ISOPLASTIC at 37°C

3.4 CONCLUSIONS

The object of this chapter was to determine the flexural properties, fracture toughness and fatigue crack growth behaviour of three commercial cements as well as examining their rheological behaviour. These results would then act as a baseline to build upon when formulating new experimental cements.

The flexural strengths of the cements ranged from 49.53 ± 4.11 MPa (CMW 1) to 63.47 ± 4.66 MPa (Palacos R). The flexural moduli ranged from 2.26 ± 0.11 GPa (Palacos R) to 2.62 ± 0.12 GPa (CMW 1).

The fracture toughness values were found to be between 1.87 ± 0.12 MPa.m$^{1/2}$ (Cemex ISOPLASTIC) and 2.42 ± 0.20 MPa.m$^{1/2}$ (Palacos R). These values are comparable to many ceramics[33] and emphasize how susceptible bone cement is to brittle fracture, and therefore why it is so important to improve its fracture toughness.

The stress intensity factor range, ΔK, required for fatigue crack propagation lies between 0.3 and 1.68 MPa.m$^{1/2}$. Even though this range is typical of many polymers, improving fracture toughness should increase the maximum stress intensity factor range.

The three different cements also exhibited a wide range of curing times from 8.7 ± 0.4 minutes (CMW 1) to 12.8 ± 0.1 (Palacos R) at 25°C. They also showed large differences in viscosity during the initial stages of curing. This range of acceptable rheological properties is useful as it allows some degree of experimental freedom when formulating new cements.

CHAPTER 4

DEVELOPMENT AND TESTING OF NEW ACRYLIC BONE CEMENTS

4.1 INTRODUCTION

In the previous chapter, the mechanical and rheological parameters of three different commercial cements; Palacos R, CMW 1 and Cemex ISOPLASTIC, were determined to give a baseline of properties. In the present chapter a set of experimental cements were formulated because the intention of this research was to incorporate ABS particles into an acrylic cement by replacing substantial portions of the PMMA powder w/w with ABS. This cannot be achieved by simply removing some of the powder from a commercial cement as the commercial powder contains other important ingredients such as benzoyl peroxide. In addition, although the chemical constituents of the commercial cements are listed in the instructions for use, not all manufacturers fully list all chemical components.[39] Therefore it was important to formulate experimental cements from the individual constituents to allow the composition to be fully controlled.

The set of experimental cement formulations underwent the same mechanical and rheological testing as the commercial cements to establish two experimental cements which performed in a similar manner. These two experimental cement formulations were then rubber toughened.

The experimental cements were initially based on the commercial bone cement CMW 1. This was to keep to the traditional 2/1 powder to liquid ratio and so minimize any effect of reduced monomer, as well as using the more commonly

utilized radiopacifier, $BaSO_4$. Therefore the liquid component consisted of 99.2% methylmethacrylate stabilized with 10-100 ppm monomethyl ether hydroquinone to prevent it from polymerizing whilst in storage and 0.82% N, N-dimethyl-p-toluidine. The N, N-dimethyl-p-toluidine is required to accelerate the polymerization reaction. Both chemicals were obtained from Sigma-Aldrich Company Ltd, Dorset, U.K.

The powder component consisted of 88.85% PMMA powder, 2.05% benzoyl peroxide to initiate the polymerization reaction and 9.1% barium sulphate to act as radiopacifier. Both benzoyl peroxide and barium sulphate were also supplied from Sigma-Aldrich Company Ltd. To produce different experimental cement formulations two medical grade PMMA powders, Colacryl® B866 and Colacryl® TS1881, and one medical grade PMMA co-polymer, Colacryl® TS1713, were provided by Lucite International, County Durham, U.K. Co-polymers are mainly used in the commercial cement Palacos R.

From these three grades of PMMA powders a set of 21 different cements were formulated. All 21 cement formulations underwent flexural testing and from these results the most appropriate 4-6 formulations were selected to continue with the remaining mechanical and rheological tests. This would ultimately lead to the two most desirable cement formulations to undergo rubber toughening.

4.2 MATERIALS AND METHODS

4.2.1 Materials

The materials used in the development of the experimental cement formulations are shown in Tables 4.1 - 4.2.

Table 4.1: Materials used in the powder component

Materials	Mean particle size*	Manufacturer
PMMA powder Colacryl® B866	38μ	Lucite International, County Durham, U.K.
PMMA powder Colacryl® TS1881	35μ	Lucite International, County Durham, U.K.
PMMA co-polymer# powder Colacryl® TS1713	38 - 54μ	Lucite International, County Durham, U.K.
Benzoyl Peroxide	-	Sigma-Aldrich Company Ltd, Dorset, U.K.
Barium Sulphate	-	Sigma-Aldrich Company Ltd, Dorset, U.K.

*Mean particle size given by manufacturer

#Co-polymer consisting of poly(methylmethacrylate/methylacrylate) [PMMA/MA]

Table 4.2: Materials used in the liquid component

Materials	Manufacturer
Methylmethacrylate stabilised with 10-100 ppm monomethyl ether hydroquinone	Sigma-Aldrich Company Ltd, Dorset, U.K.
N, N-dimethyl-p-toluidine	Sigma-Aldrich Company Ltd, Dorset, U.K.

4.2.2 SEM Examination of PMMA Powders

In order to determine the size distribution and surface morphology of each of the three different PMMA powders; Colacryl®B866, Colacryl®TS1881 and Colacryl®TS1713, they were prepared and examined using an SEM as described in Chapter 3, Section 3.2.2. Measurements of particle sizes were also carried out as described in Section 3.2.2.

4.2.3 Preparation of experimental cement formulations for flexural testing

Five experimental cements were formulated using the following PMMA powder:-

(1) 100% Colacryl®B866

(2) 100% Colacryl®TS1881

(3) 100% Colacryl®TS1713

(4) Colacryl®B866 + Colacryl®TS1713, and

(5) Colacryl®TS1881 + Colacryl®TS1713.

All the cements were made using a 2/1 ratio with 40g of the powder component (35.54g PMMA powder, 0.82g benzoyl peroxide and 3.64g barium sulphate) and 20g of the liquid component (19.84g methylmethacrylate and 0.16g N, N-dimethyl-p-toluidine).

Cements (1), (2) and (3) contained the PMMA powder Colacryl®B866, Colacryl®TS1881, and Colacryl®TS1713 respectively

For cement (4) nine different formulations were produced all based on the PMMA powder Colacryl®B866, with 10, 20, 30, 40, 50, 60, 70, 80, and 90% Colacryl®B866 being replaced w/w with the co-polymer Colacryl®TS1713.

For cement (5) nine different formulations were made, this time based on the PMMA powder Colacryl®TS1881, with 10, 20, 30, 40, 50, 60, 70, 80, and 90% Colacryl®TS1881 being replaced w/w with Colacryl®TS1713.

10 acceptable samples were prepared of each formulation by adding the liquid component to the powder component, hand mixing, and manually placing the cement in the moulds as described in Chapter 3, Section 3.2.3.

4.2.4 Flexural Properties

All cement formulations underwent three-point bending as described in Chapter 3, Section 3.2.3.

4.2.5 Fracture Toughness

Fracture toughness values were determined for selected cement formulations containing the PMMA powder stated in Table 4.3

Table 4.3: Selected PMMA powder formulations, including abbreviated names

PMMA powder	Abbreviated name
100% Colacryl®B866	100% B866
100% Colacryl®TS1881	100% TS1881
100% Colacryl®TS1713	100% TS1713
50% Colacryl®B866 - 50% Colacryl®TS1713	50% B866
50% Colacryl®TS1881 - 50% Colacryl®TS1713	50% TS1881

Ten samples of each type of cement were tested as described in Chapter 3, Section 3.2.4. The samples were again the fractured pieces obtained from the three-point bending tests, and so measured 10mm by 5mm by approximately 40mm. Following testing the fracture surfaces were examined using an SEM using the method described in Chapter 3, Section 3.2.2.

4.2.6 Fatigue

The fatigue crack growth rate parameters, m and C, were determined for each of the five aforementioned cement formulations.

CT specimens were produced of each type of cement using 40g powder component and 20g liquid component (see Section 4.2.3 for detailed composition). The liquid was added to the powder, hand mixed, and manually placed in the mould as described in Chapter 3, Section 3.2.5. Testing was also carried out as described in Section 3.2.6 and the resultant fracture surfaces were prepared and examined using an SEM following the method given in Chapter 3, Section 3.2.2.

4.2.7 Rheology

In order to determine the setting time of 100% TS1713, 100% B866, 100% TS1881, 50% B866 and 50% TS1881 and to examine their rheological behaviour whilst curing, the changes in complex viscosity, elastic and viscous modulus with time were investigated using a rheometer.

Ten samples of each type of cement were tested following the same method as given in Chapter 3, Section 3.2.6. However, this time 12g of powder (10.65g PMMA, 0.24g benzoyl peroxide and 1.08g barium sulphate) was mixed with 6g of liquid (5.94g methyl methacrylate and 0.06g N, N-dimethyl-p-toluidine). These larger amounts were chosen because they could be accurately measured. As the experimental cements were easier to mix than the commercial varieties due to their lower viscosity, only 70s elapsed between start of mixing and the first rheometer reading.

4.2.7 Statistical Analysis

The same statistical analysis was used as mentioned in Chapter 3, Section 3.2.7.

4.3 RESULTS AND DISCUSSION

4.3.1 SEM Analysis of PMMA Powders

The SEM micrographs of the three PMMA powders/beads; Colacryl®B866, Colacryl® TS1881 and Colacryl®TS1713, are shown in Figures 4.1 - 4.3.

The Colacryl®B866 PMMA beads are all spherical with a very smooth surface morphology. The bead size distribution ranges from approximately <5μm to 44μm with the bulk of the beads being 35μm or less.

The Colacryl®TS1881 PMMA beads have a very different surface morphology. The majority of these beads have surface indentations and some of the beads appear almost 'squashed'. This powder exhibits the widest range of bead sizes with a maximum bead size of approximately 80μm, and the smallest approximately 1μm.

The surface morphology of the Colacryl®TS1713 PMMA beads is very similar to Colacryl®B866 i.e. the beads are all spherical with a smooth surface. However, the Colacryl®TS1713 polymer beads have a very different size distribution. The beads, instead of having continuous size distribution, have a more bimodal size distribution, with the larger beads ranging between 50-80μm and the smaller beads ranging between <5μ-20μm.

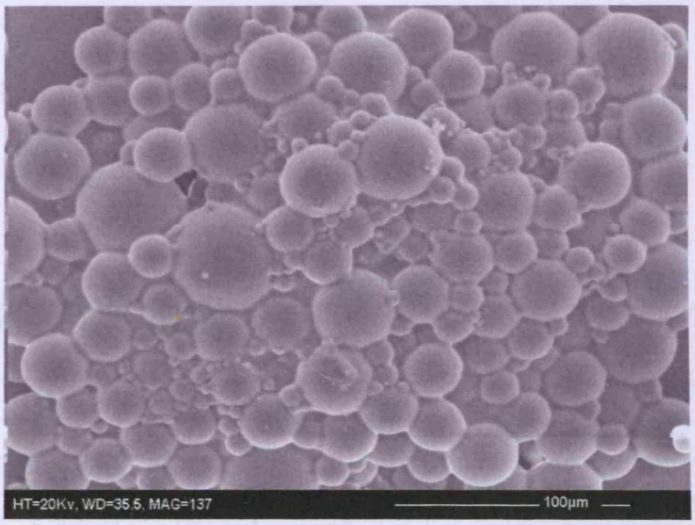

Mean particle size, stated by manufacturer, 38µm.

Figure 4.1: Colacryl®B866 powder, magnification x137

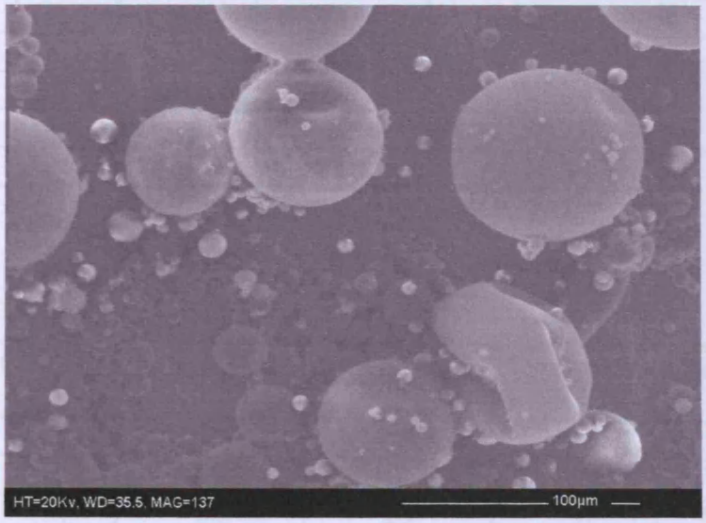

Mean particle size, stated by manufacturer, 35µm.

Figure 4.2: Colacryl®TS1881 powder, magnification x 137

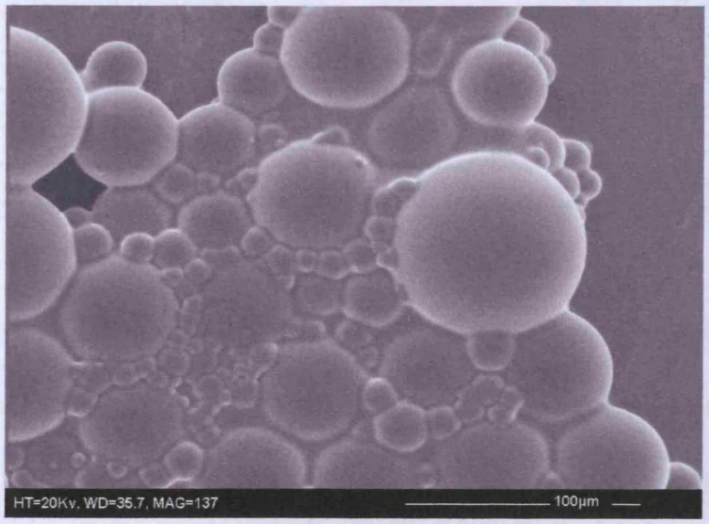

Mean particle size, stated by manufacturer, 38-54µm.

Figure 4.3: Colacryl®TS1713 powder, magnification x 137

4.3.2 Flexural properties

The average flexural strength and modulus of each type of cement are shown in Tables 4.4 and 4.5.

Table 4.4: Flexural properties of cements containing B866

Cement	% B866	% TS1713	Flexural Strength MPa	Flexural Modulus GPa
(1)	100	-	52.00 ± 3.17	2.75 ± 0.12
(4)	90	10	55.46 ± 4.43	2.71 ± 0.17
(4)	80	20	57.74 ± 4.86	2.70 ± 0.08
(4)	70	30	55.63 ± 5.32	2.66 ± 0.19
(4)	60	40	57.36 ± 4.48	2.40 ± 0.14
(4)	50	50	55.24 ± 5.16	2.46 ± 0.10
(4)	40	60	55.55 ± 4.36	2.30 ± 0.13
(4)	30	70	54.28 ± 3.63	2.47 ± 0.07
(4)	20	80	57.55 ± 2.21	2.53 ± 0.12
(4)	10	90	56.28 ± 4.56	2.49 ± 0.11
(3)	-	100	58.80 ± 4.26	2.44 ± 0.09

Table 4.5: Flexural properties of cements containing TS1881

Cement	% TS1881	% TS1713	Flexural Strength MPa	Flexural Modulus GPa
(2)	100	-	48.90 ± 4.70	2.39 ± 0.09
(5)	90	10	49.74 ± 5.71	2.38 ± 0.06
(5)	80	20	51.28 ± 3.44	2.46 ± 0.04
(5)	70	30	50.70 ± 5.58	2.49 ± 0.08
(5)	60	40	50.39 ± 5.07	2.15 ± 0.26
(5)	50	50	50.95 ± 6.27	2.30 ± 0.07
(5)	40	60	52.11 ± 5.69	2.38 ± 0.15
(5)	30	70	53.95 ± 4.47	2.38 ± 0.07
(5)	20	80	56.22 ± 5.10	2.54 ± 0.07
(5)	10	90	53.35 ± 6.79	2.53 ± 0.07
(3)	-	100	58.80 ± 4.26	2.44 ± 0.09

The results show that cement (3), i.e. 100% TS1713, has the greatest flexural strength, 58.80 MPa, of all the cement formulations and cement (2), i.e. 100% TS1881, has the lowest, 48.90 MPa. However, cement (1), i.e. 100% B866 has the greatest flexural modulus, 2.75 GPa.

Combining the PMMA powders B866 and TS1713 (cement 4) results in an increase in flexural strength when compared to 100% B866 (cement 1), but none of these formulations significantly increase strength ($p<0.05$). In addition, there appears to be no strong/direct link between the proportion of TS1713 and the increase in flexural strength. Combining the PMMA powders TS1881 and TS1713 (cement 5) also increases the flexural strength when compared with 100% TS1881 (cement 2), but there is only a significant increase in strength with the cement containing 20% TS1881, $p<0.05$. However, there does appear to be a slight increase in strength with increasing amount of TS1713. Overall, the flexural strengths of the cement formulations containing the PMMA powder B866 are slightly higher than those containing TS1881.

When comparing the strengths of all the different cement formulations with cement (5), i.e. with cement containing 100% TS1713, only 100% TS1881 ($p<0.005$), 90% TS1881 ($p<0.05$) and 60% TS1881 ($p<0.05$) have significantly lower flexural strength values.

Cement (1) i.e. 100% B866 has the greatest flexural modulus of all the cement formulations. Therefore combining the PMMA powder B866 with TS1713 (cement 4), reduces the modulus. This reduction is only significant with the 60%B866 ($p<0.05$) and 40% B866 ($p<0.005$) cement formulations. It loosely appears as if the modulus decreases with increasing proportion of TS1713 until the cement contains 60%TS1713-40%B866, following this, there is a slight, but not significant increase in modulus ($p>0.05$).

100% TS1881 (cement 2) has a significantly lower modulus than 100% B866 (cement 1), $p<0.05$, and combining the PMMA powders, TS1881 with TS1713 (cement 5) does not significantly increase or decrease the flexural modulus (with the

exception of the cement containing 60% TS1881 where $p<0.05$). There does not appear to be a correlation between the amount of TS1713 powder present and any changes in flexural modulus. However, the majority of the cements containing TS1881 have lower flexural moduli than the cements based on the powder B866 with the equivalent quantity of TS1713, with the following formulations having significantly lower moduli ($p<0.05$); 90% TS1881, 80% TS1881 and 60% TS1881.

Again, when comparing the moduli of all the cement formulations with cement (5) i.e. 100% TS1713, only 60% TS1881 has a significantly lower flexural modulus value ($p<0.05$).

Effect of composition, particle size and morphology on flexural properties

Previously mentioned in Chapter 3, Sections 3.3.2 and 3.3.3, was the minimal effect of PMMA bead sizes on the static mechanical properties of commercial bone cements.[53, 68] However, very little research has been undertaken in this area,[22, 53] therefore it is important to fully examine the influence of PMMA bead sizes, bead size distribution and surface morphology on flexural properties.

From the results it is clear that the cement containing 100% TS1881, i.e. cements (2), has slightly poorer flexural properties than the cement containing the 100% B866 although their chemical composition is the same. The TS1881 polymer beads have a wide range of particle sizes (approximately 1-80μm) with an irregular surface morphology (Figure 4.2), whereas the B866 polymer beads have a smaller range of particle sizes (approximately 5-44μm) with a regular surface morphology (Figure 4.1).

The irregular surface morphology of the TS1881 beads, as well as the larger proportion of smaller beads in comparison with B866, effectively increases surface

area resulting in the beads absorbing more monomer. This leaves less available monomer for the polymerization reaction, thereby affecting the curing process which appears to affect the final mechanical properties of the cured cement, and this is discussed further in the fracture toughness and rheology sections, Sections 4.3.3 and 4.3.5.

Conversely, the smooth surface morphology of the B866 polymer beads, as well as the reduced range of smaller particles, decreases the surface area for monomer absorption leaving more available monomer for the polymerization reaction which may lead to an increase in the final mechanical properties of the cured cement.

The addition of the co-polymer TS1713 to TS1881 (cement 5) has, on the whole, increased flexural properties, but there is a tenuous link between increased proportion of TS1713 and increased flexural properties. Given the bimodal distribution of the spherical TS1713 polymer beads (Figure 4.3) this increase could possibly be a result of the increased proportion of larger bead sizes (50 - 80μm) and their regular spherical shape, as well as its co-polymer formulation.

The addition of TS1713 to B866 (cement 4) has increased flexural strength, but decreased flexural modulus, and there is no direct correlation between the quantity of TS1713 and the changes in these properties. Therefore, it does not seem that the presence of the co-polymer has a substantial effect on strength/modulus It is also difficult to draw meaningful conclusions about the effect of the PMMA particle sizes on flexural properties.

Selecting cement formulations for further testing

The object of the flexural testing was not only to examine the flexural properties of the cements, but also to facilitate the selection of the most suitable cement formulations for further testing. As all the cement formulations had flexural strengths

and moduli which lay in the same range as the commercial cements it was not clear which should be selected. Therefore five experimental cements were selected which would be representative of the whole range. These were 100% B866, 100% TS1881, 100% TS1713, 50% B866-50% TS1713 and 50% TS1881-50% TS1713.

The flexural strengths and moduli of the five selected cement formulations including those obtained for the three commercial cements; Palacos R, CMW 1 and Cemex ISOPLASTIC are shown in Figures 4.4 - 4.5. The extensive range of flexural strengths/moduli of the commercial cements has already been discussed in Chapter 3.

The flexural strengths of all the experimental cements (Figure 4.4) lie within the range obtained for the three commercial cements. They are comparable with, if not greater than, CMW 1 (strength = 49.53 MPa), with 100% TS1713 having a significantly higher flexural strength ($p<0.005$). However, none of the experimental formulations has a flexural strength as high as Palacos R. The strength of Palacos R, at 63.47 MPa, is significantly greater than four the experimental cements (100% B866 $p<0.005$, 100% TS1881 $p<0.001$, 50% B866 $p<0.05$, 50% TS1881 $p<0.001$) but not significantly greater than 100% TS1713 ($p>0.05$).

The flexural moduli are shown in Figure 4.5. The cement containing 100% B866 has the highest modulus of all the cements and is significantly greater than the commercial cements Palacos R and Cemex ISOPLASTIC ($p<0.05$). The four remaining experimental cements, i.e. 100% TS1881, 100% TS1713, 50% B866 and 50% TS1881, all have similar moduli to Palacos R and Cemex ISOPLASTIC and as such there is no statistical difference ($p>0.05$) between these four experimental cements and Palacos R and Cemex ISOPLASTIC. However, 100% TS1881 and 50% TS1881 have significantly lower moduli ($p<0.05$) than CMW 1.

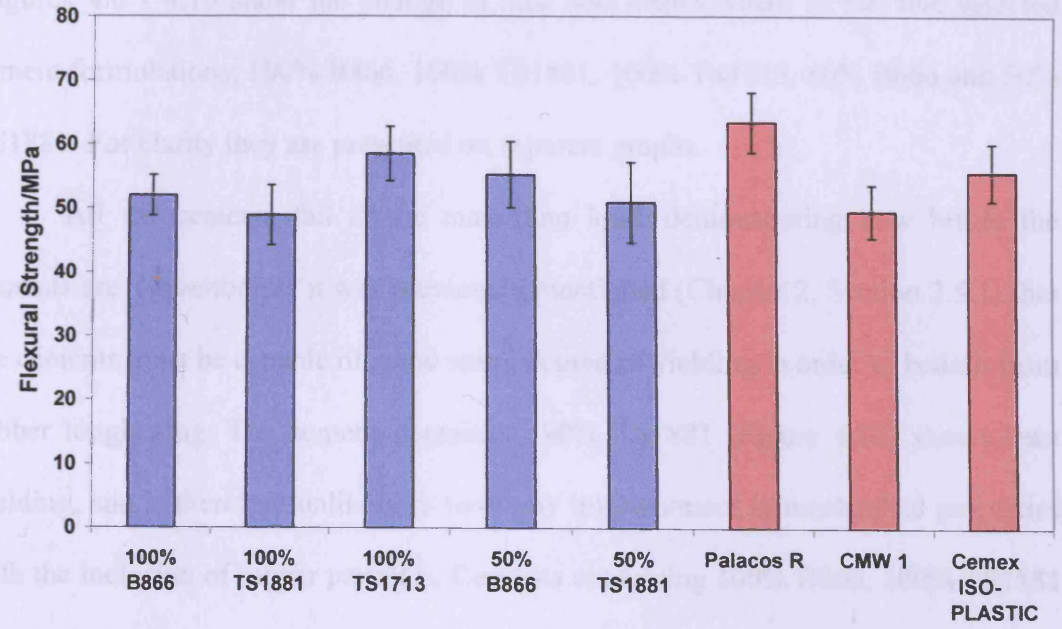

Figure 4.4: Flexural strengths of the selected experimental cements and commercial cements

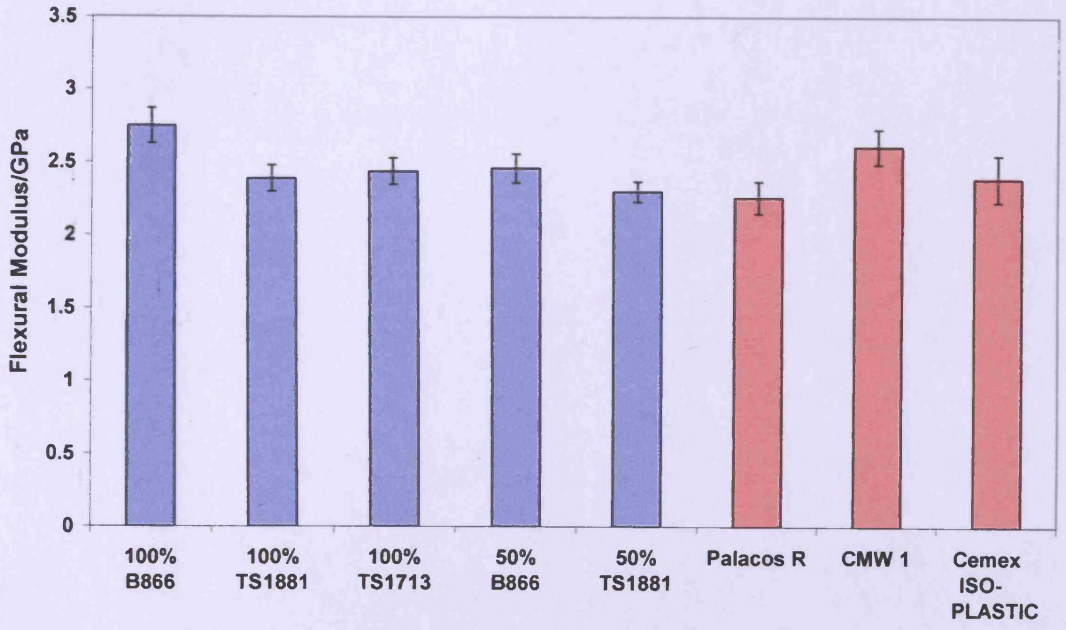

Figure 4.5: Flexural moduli of the selected experimental cements and commercial cements

Load/displacement curves of selected cements

Figures 4.6 - 4.10 show the change in load and displacement of the five selected cement formulations; 100% B866, 100% TS1881, 100% TS1713, 50% B866 and 50% TS1881. For clarity they are presented on separate graphs.

All the cements fail at the maximum load, demonstrating how brittle the cements are. Nevertheless it was previously mentioned (Chapter 2, Section 2.5.1) that the cements must be capable of some small degree of yielding in order to benefit from rubber toughening. The cement containing 50% TS1881 (Figure 4.10) shows least yielding, and is therefore unlikely to have any improvement in mechanical properties with the inclusion of rubber particles. Cements containing 100% B866, 100% TS1881 and 50% B866 (Figures 4.6, 4.7 and 4.9) all show a very small amount of yielding towards the latter stage of testing. Of all the experimental cements, 100% TS1713 (Figure 4.8) shows the greatest yielding, and is the most comparable to the three commercial cements.

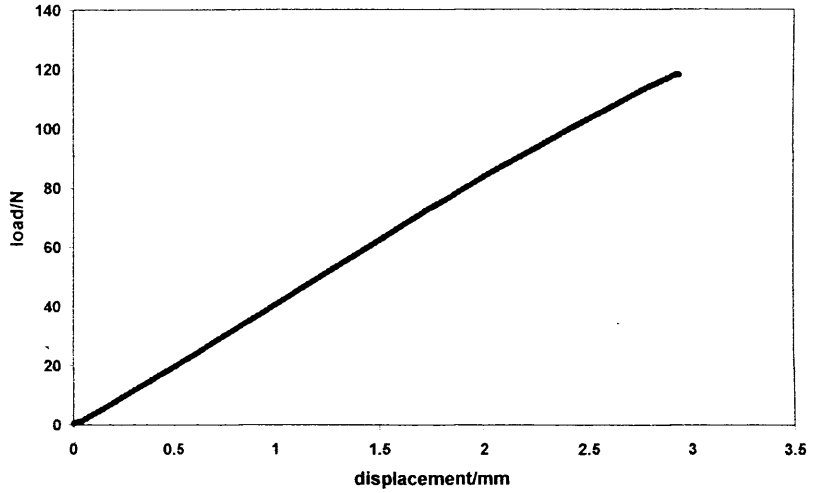

Figure 4.6: Load/displacement graph of 100% B866

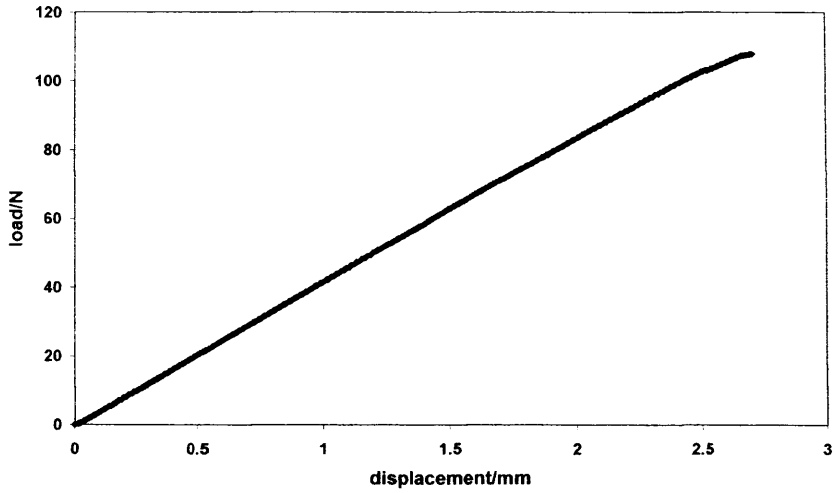

Figure 4.7: Load/displacement graph of 100% TS1881

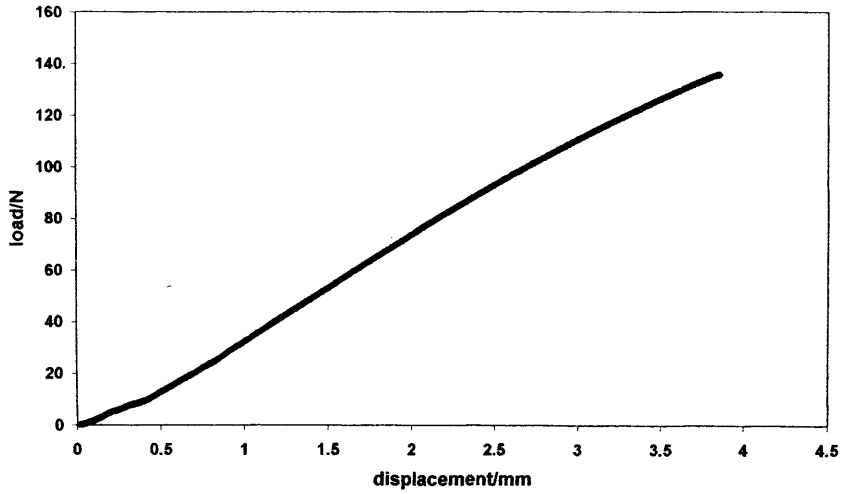

Figure 4.8: Load/displacement graph of 100% TS1713

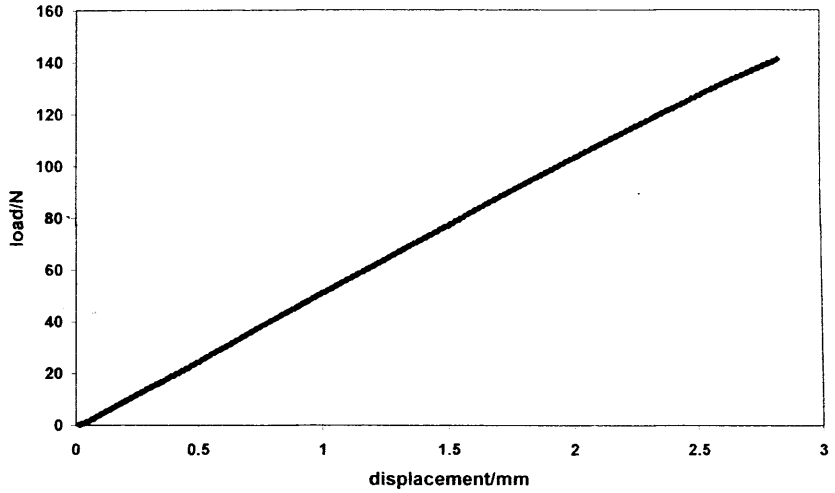

Figure 4.9: Load/displacement graph of 50% B866

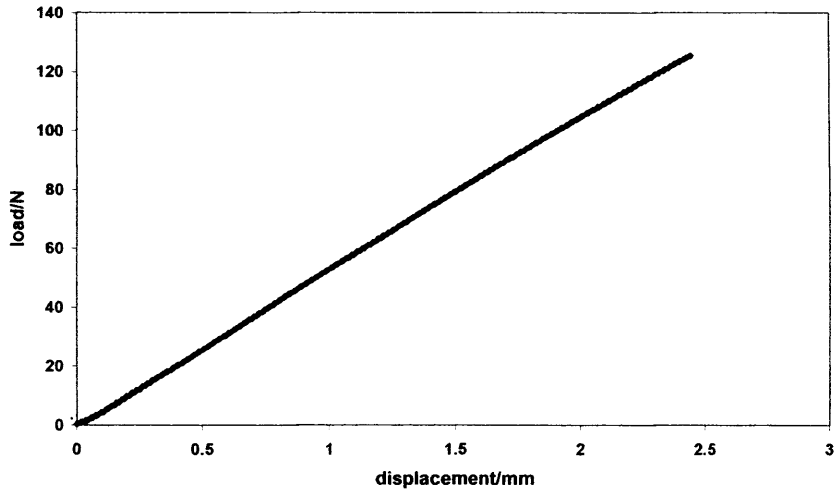

Figure 4.10: Load/displacement graph of 50% TS1881

4.3.3 Fracture Toughness

The average fracture toughness values of the five selected cements i.e. their resistance to fast crack propagation are shown in Table 4.6. SEM micrographs of the fracture surfaces are shown in Figures 4.12 - 4.21.

Cement 100% B866 shows the greatest resistance to rapid crack propagation with a K_{IC} value of 2.40 MPa.m$^{1/2}$, and 100% TS1881 has the least resistance with a K_{IC} value of 2.12 MPa.m$^{1/2}$. Both 100% TS1713 and 50%B866 have the same fracture toughness, 2.30 MPa.m$^{1/2}$, and 50%TS1881 has a K_{IC} value of 2.24 MPa.m$^{1/2}$. There is no statistically significant difference ($p>0.05$) in fracture toughness between the five cements.

Table 4.6: Fracture toughness values of experimental cements

Cement	Fracture Toughness, K_{IC} (MPa.m$^{1/2}$)
100% B866	2.40 ± 0.13
100% TS1881	2.12 ± 0.12
100% TS1713	2.30 ± 0.12
50% B866 – 50% TS1713	2.30 ± 0.13
50% TS1881 – 50% TS1713	2.24 ± 0.12

Effect of composition on fracture toughness

In the previous chapter, the largest effect on fracture toughness of bone cement was thought to be caused by the different radiopacifiers utilized in the commercial cements. In these experimental cements the same radiopacifier, barium sulphate, was used and as a result the different experimental cements have fairly similar fracture toughness values. Even though the results are fairly similar, the cements containing the PMMA powder TS1881 have the lowest fracture toughness values and this again

is probably caused by the irregular surface morphology and larger proportion of smaller bead sizes of this powder in comparison with the two other PMMA powders.

The effect of the different surface morphologies of the initial polymer powders have on the fully cured cement is shown in the SEM micrographs of the fracture surfaces at low magnification, x25, (Figures 4.12 - 4.16). Both the cements containing the PMMA powder TS1881, i.e. 100% TS1713 and 50% TS1713, have extensive porosity. This porosity will have contributed not only towards their lower fracture toughness, but also to their lower flexural strengths/moduli obtained in Section 4.3.2. It was mentioned in Chapter 2, Section 2.2.3, that porosity is introduced during the mixing stage of producing the cement, either by air bubbles becoming entrapped while mixing, or by monomer evaporation as a result of the exothermic curing reaction. Both 100% TS1881 and 50% TS1881 cements were very easy to mix because of their low viscosity, so it is more likely that the porosity was caused by monomer evaporation. This increased level of monomer evaporation in comparison with the cements 100% TS1713, 100% B866 and 50% B866 was probably caused by the irregular surface morphology of the TS1881 PMMA beads or, according to Pascual,[22] the greater proportion of small diameter beads. Both these factors increase the surface area available for monomer absorption, resulting in less available monomer for the polymerization reaction. This effectively increases the concentration of benzoyl peroxide (initiator) and N, N-dimethyl-p-toluidine (accelerator) reacting with the monomer, thereby increasing the polymerization temperature.[21, 23]

It appears that the increased surface area of the PMMA beads as a result of irregular surface morphology and/or bead size has a significant effect on the curing behaviour of cement, which ultimately affects the extent of porosity in the final cured cement. This in turn affects the cements' static mechanical properties. This is in

contrast with previous authors' findings that bead sizes and bead size distributions have little influence on static mechanical properties.[53, 90]

Comparison with commercial cements

Figure 4.11 shows the different fracture toughness values of the experimental cements and the three commercial cements; Palacos R, CMW 1 and Cemex ISOPLASTIC.

The fracture toughness of all the experimental cements lie within the range obtained for the three commercial cements. Four of the experimental cements have a significantly greater resistance to rapid crack propagation than Cemex ISOPLASTIC (K_{1C} = 1.87 MPa.m$^{1/2}$); 100% B866 ($p<0.0005$), 100% TS1713 ($p<0.0005$), 50% B866 ($p<0.001$) and 50% TS1881 ($p<0.005$). The same four cements have higher fracture toughness values than CMW 1 (K_{1C} = 2.17 MPa.m$^{1/2}$), but not significantly ($p>0.05$). However, none of the cements have a greater fracture toughness than Palacos R (K_{1C} = 2.42 MPa.m$^{1/2}$), but 100% B866 has a very similar value (K_{1C} = 2.40 MPa.m$^{1/2}$).

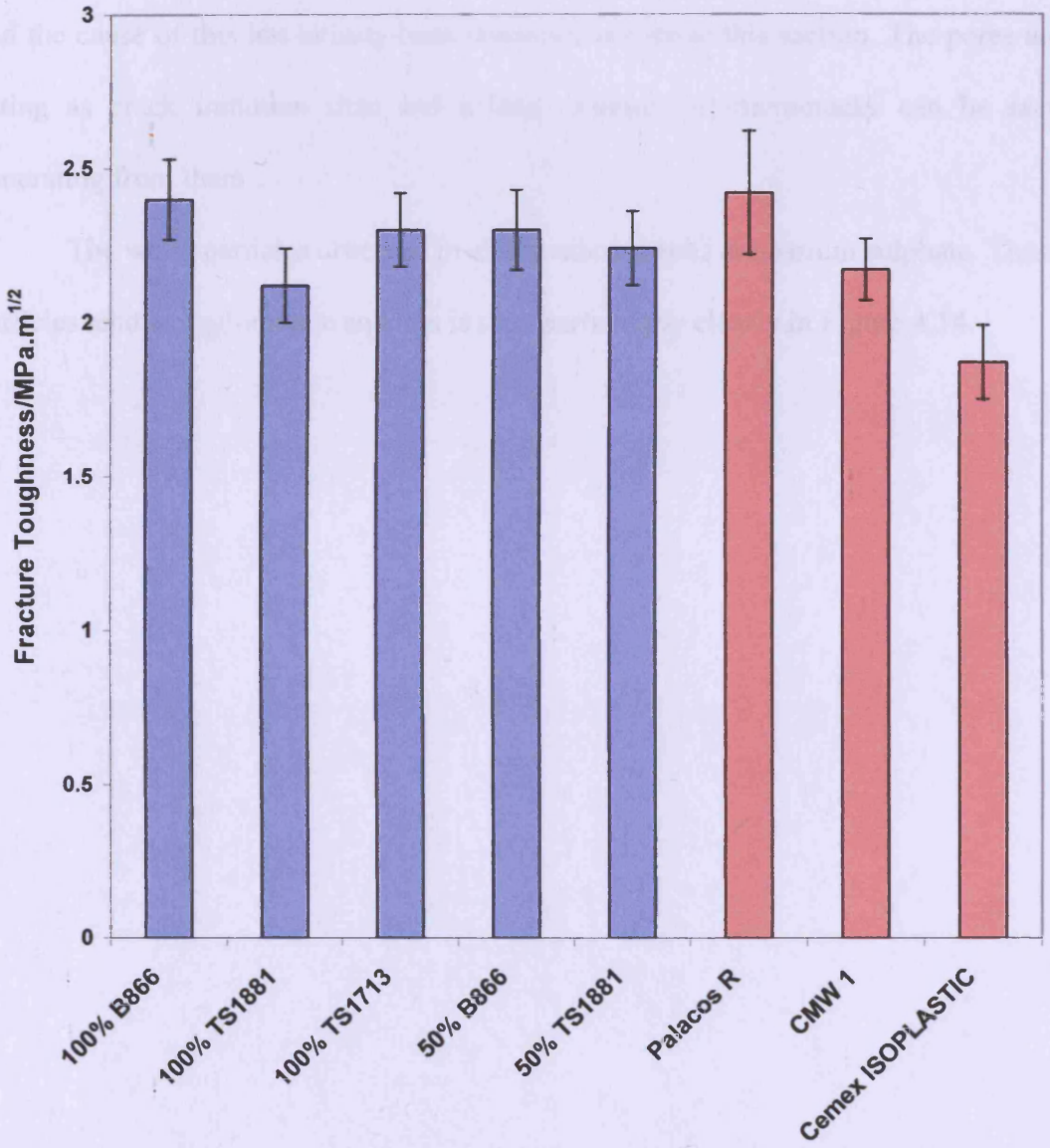

Figure 4.11: Fracture toughness of experimental cements and commercial cements

SEM examination of fracture surfaces following fracture toughness testing

The SEM micrographs of the fracture surfaces are shown in Figures 4.12 - 4. 21. Examination of these fracture surfaces at low magnification, x25, (Figures 4.12 - 4.16) reveals the extensive porosity in the cements 100% TS1881 and 50% TS1881 and the cause of this has already been discussed earlier in this section. The pores are acting as crack initiation sites and a large number of microcracks can be seen generating from them.

The white particles observed in all the micrographs are barium sulphate. These particles tend to agglomerate and this is seen particularly clearly in Figure 4.14.

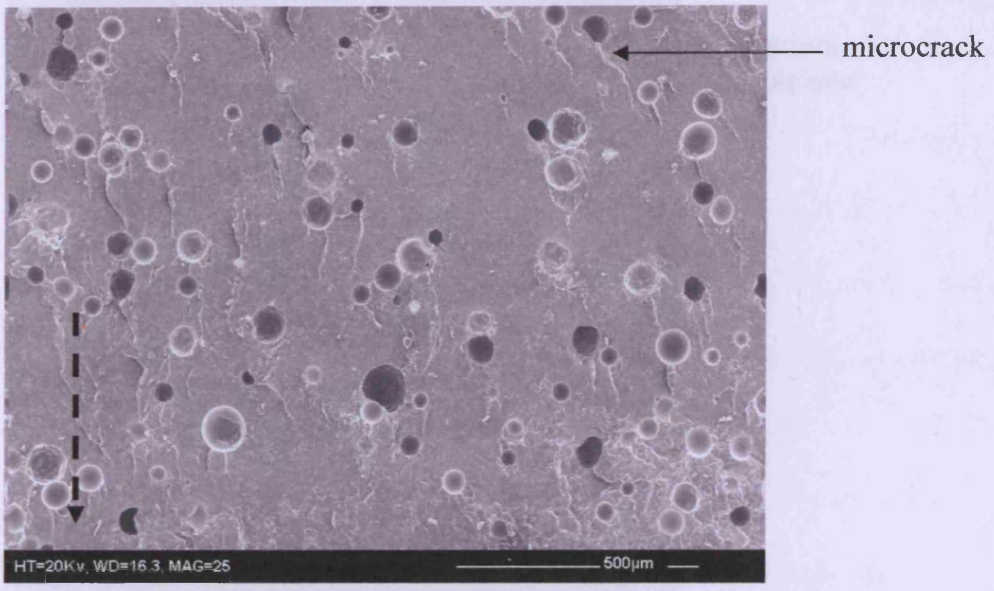

Figure 4.12: Fracture surface of 100% TS1881, magnification x 25
Direction of crack propagation is indicated by the dashed arrow

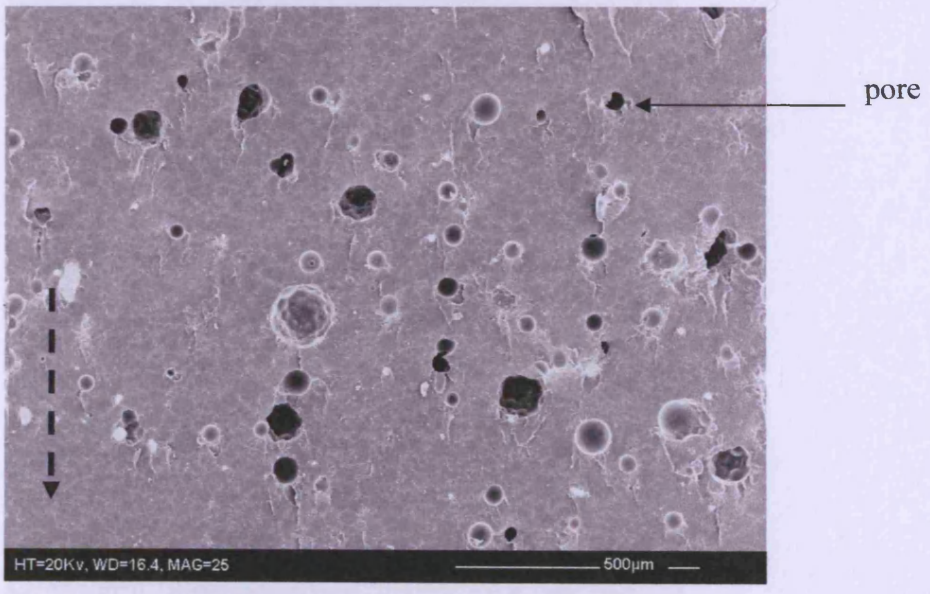

Figure 4.13: Fracture surface of 50% TS1881, magnification x 25

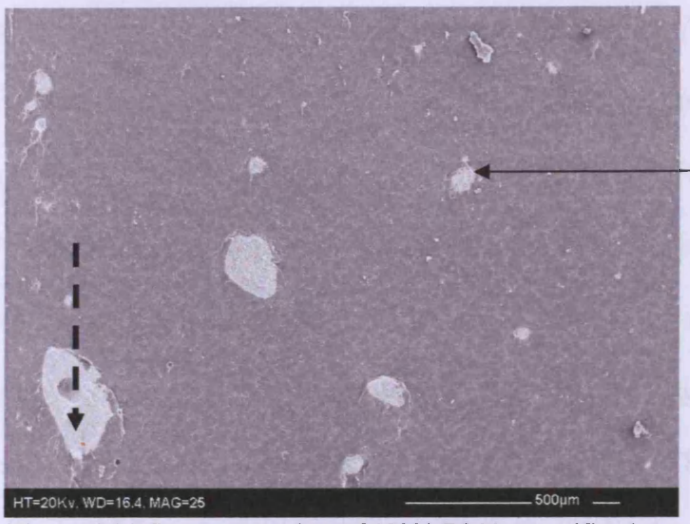

Figure 4.14: Fracture surface of 100% B866, magnification x 25

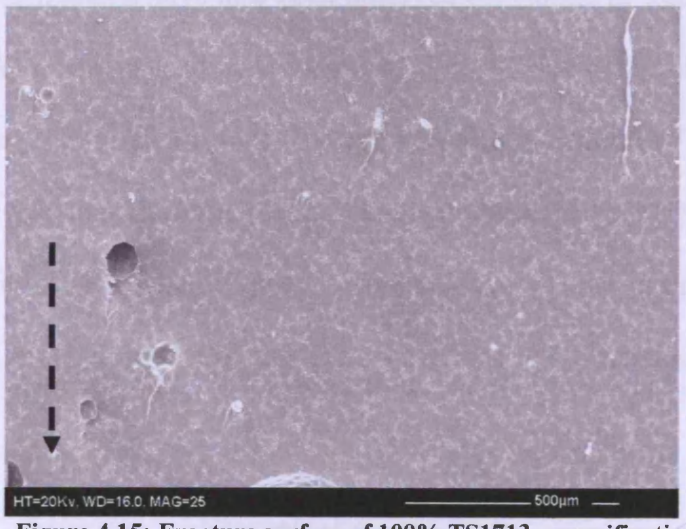

Figure 4.15: Fracture surface of 100% TS1713, magnification x 25

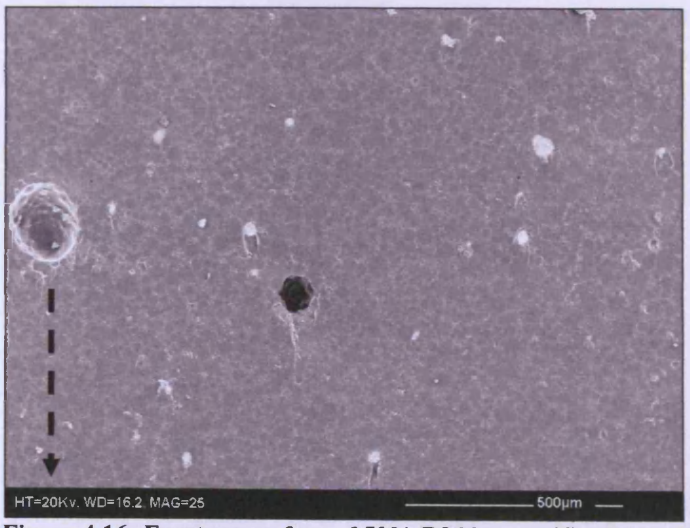

Figure 4.16: Fracture surface of 50% B866, magnification x 25

At higher magnification (x115) and avoiding areas of porosity, the fracture surfaces of all the five cement formulations are very similar. Therefore, only the fracture surfaces of 100% B866, 100% TS1881 and 100% TS1713 are shown (Figures 4.17 - 4.19).

All the fracture surfaces are predominantly smooth and all the PMMA beads have been cleaved indicating the fast rate of fracture. Again river lines can be seen radiating through some of the PMMA beads and circular ridges or indentations can also be seen towards the outer edge of some of the beads. These particular features have been magnified further (x289) and are shown in Figures 4.20 - 4.21. The ridges/indentations have also been observed by Molino & Topoleski[73] when studying radiolucent cement, and they concluded this was due to the absence of radiopacifier. However, this is clearly not the case. The magnification of the river lines (Figure 4.21) reveal that the crack has propagated through the PMMA beads on different planes, creating a slightly uneven surface. Overall, the morphology of the fracture surfaces most closely resemble the fracture surface of Cemex ISOPLASTIC (Figure 3.9).

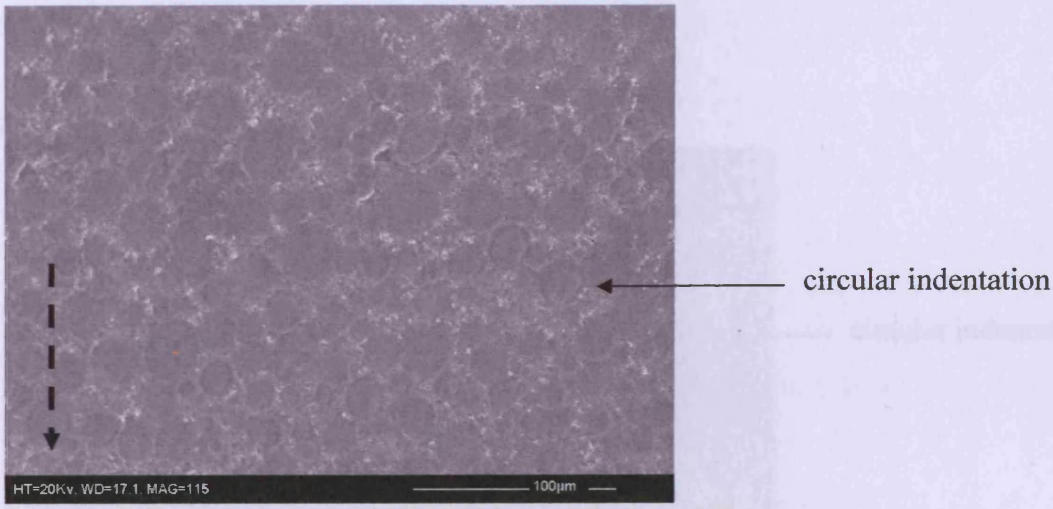

Figure 4.17: Fracture surface of 100% B866, magnification x 115

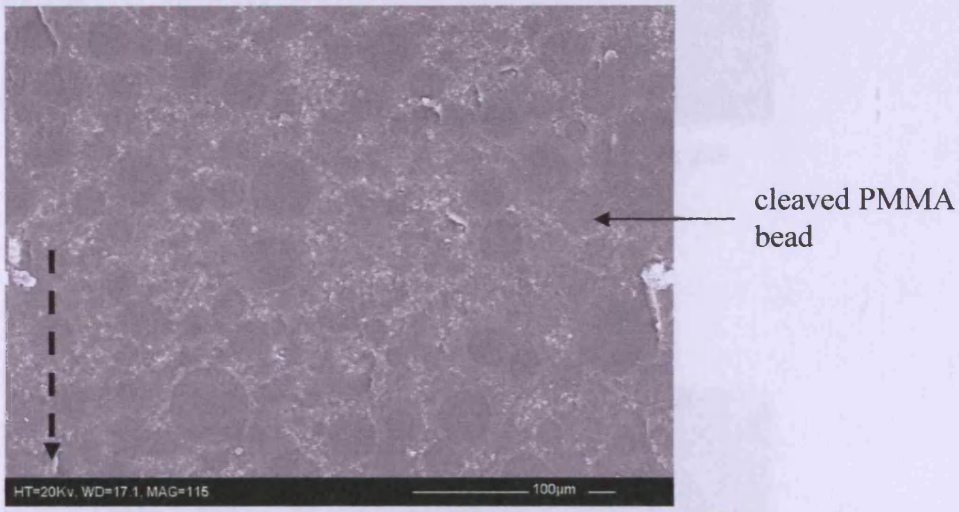

Figure 4.18: Fracture surface of 100% TS1881, magnification x 115

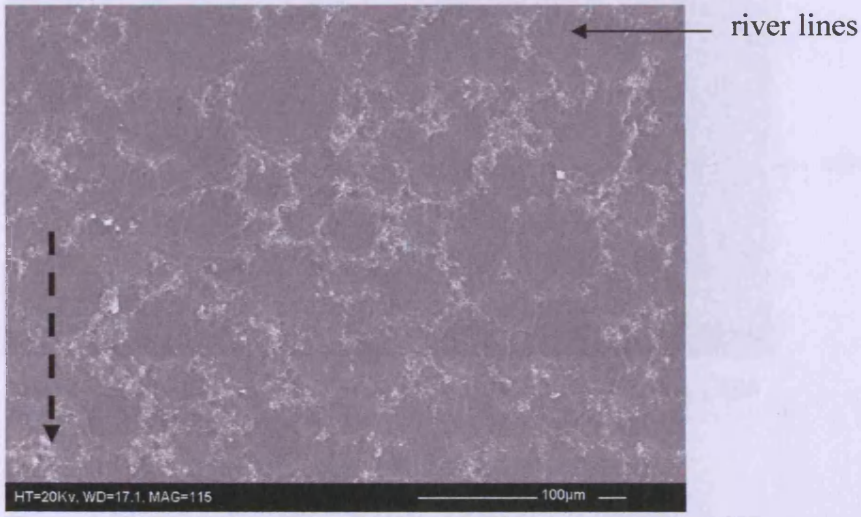

Figure 4.19: Fracture surface of 100% TS1713, magnification x 115

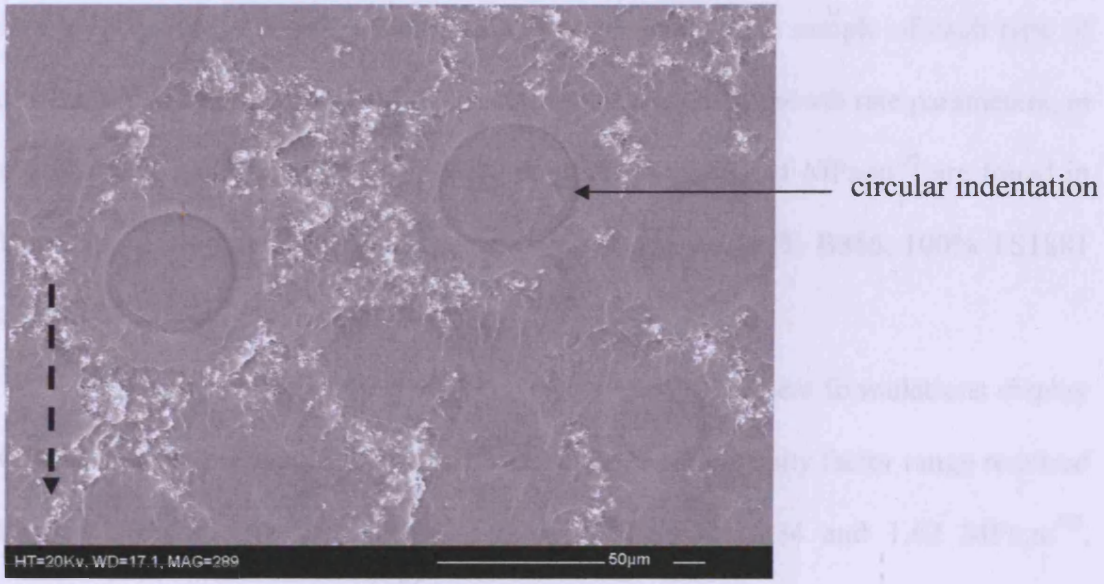

Figure 4.20: Fracture surface of 100% B866, magnification x 289

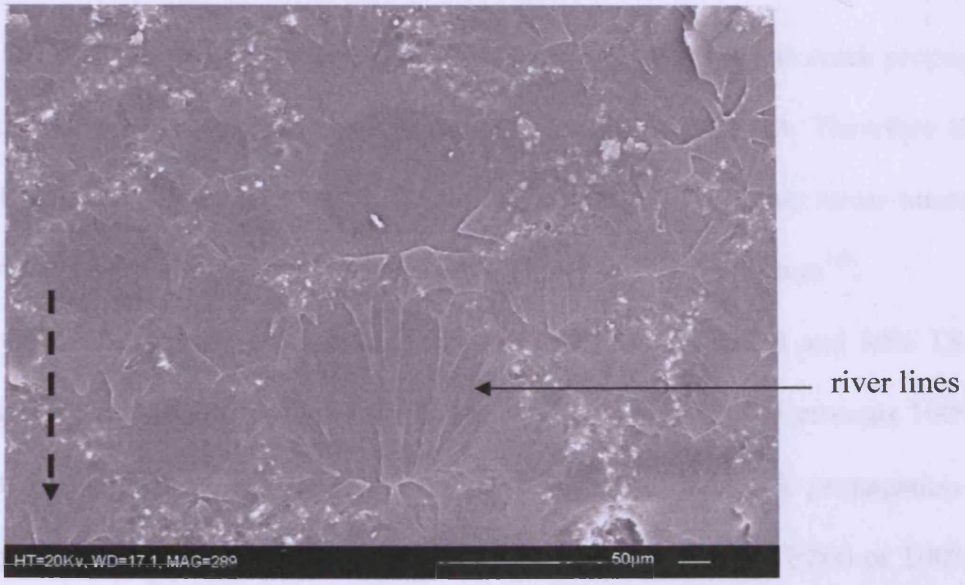

Figure 4.21: Fracture surface of 100% TS1713, magnification x 289

4.3.4 Fatigue

The results of the fatigue crack propagation in terms of growth rate per cycle, da/dN, as a function of the stress intensity factor range, ΔK, of one sample of each type of cement, are shown in Figure 4.22. The corresponding crack growth rate parameters, m and C, along with the correlation coefficient R^2 when ΔK = 1 MPa.m$^{1/2}$ are found in Table 4.4. SEM micrographs of the fracture surfaces of 100% B866, 100% TS1881 and 100% TS1713 are shown in Figures 4.23 - 4.26.

From Figure 4.22 it can be seen that all the five cement formulations display very similar fatigue crack growth behaviour. The stress intensity factor range required for crack propagation for all the cements is between 0.34 and 1.62 MPa.m$^{1/2}$. Although their crack propagation behaviour, and hence resistance to crack growth closely matches each other, on closer inspection there are some differences.

In general, for a given stress intensity range, both 100% TS1713 and 100% B866 have lower crack propagation rates than 100% TS1881, 50% B866 and 50% TS1881. Towards the latter stages of propagation, however, the crack propagation rate of 100% B866 accelerates more rapidly than 100% TS1713. Therefore the cement 100% TS1713 continues more stable crack growth to a higher stress intensity factor range (ΔK = 1.52 MPa.m$^{1/2}$) than 100% B866 (ΔK = 1.34 MPa.m$^{1/2}$).

The fatigue crack growth rates of both 100% TS1881 and 50% TS1881, at a given stress intensity range, are on the whole faster than the cements 100% TS1713 and 100% B866. However, during the final stages of crack propagation the crack propagation rate of 50% TS1881 is lower than either 100% B866 or 100% TS1713. The cement containing 100% TS1881 only continues stable crack growth until ΔK = 1.14 MPa.m$^{1/2}$ and as such shows the lowest resistance to fatigue crack propagation of all the experimental cements.

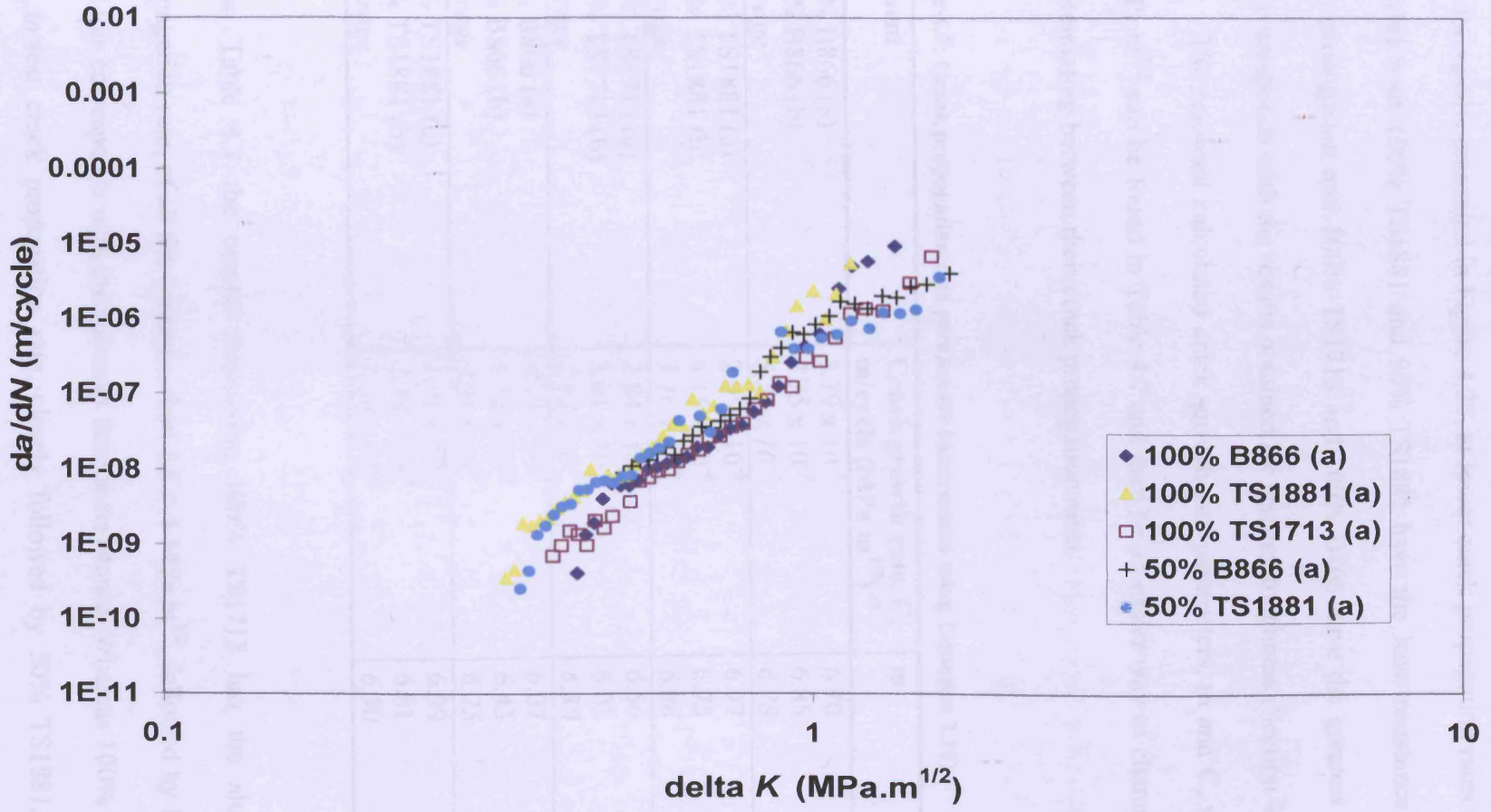

Figure 4.22: Fatigue crack growth rate, da/dN, plotted against the stress intensity range, delta K, for 100% B866, 100% TS1881, 100% TS1713, 50% B866 and 50% TS1881

The fatigue crack growth behaviour of 50% B866 is superior than 100% TS1881 and 50% TS1881, but less desirable than either 100% TS1713 or 100% B866. Therefore from the results presented in Figure 4.22, at lower crack propagation rates (10^{-8} - 10^{-7} m/cycle) both 100% TS1881 and 50% TS1881 have the least resistance to fatigue crack propagation and 100% TS1713 and 100% B866 have the greatest resistance. This corresponds with the results obtained for fracture toughness (Section 4.3.3).

The resultant calculated crack growth rate parameters, m and C, when ΔK = 1 MPa.m$^{1/2}$ can be found in Table 4.7 and may be an easier way of characterizing or differentiating between their crack propagation rates.

Table 4.7: Crack propagation rate parameters (determined using Equation 2.12)

Cement	Crack growth rate, C, m/cycle (MPa m$^{1/2}$)$^{-m}$	m	R^2
100% B866 (a)	3.79 x 10^{-7}	6.70	0.93
100% B866 (b)	2.75 x 10^{-7}	6.85	0.98
Average	*3.27 x 10^{-7}*	*6.78*	
100% TS1881 (a)	2.05 x 10^{-6}	6.97	0.96
100% TS1881 (b)	4.15 x 10^{-6}	6.75	0.97
Average	*3.10 x 10^{-6}*	*6.86*	
100% TS1713 (a)	2.84 x 10^{-7}	6.56	0.99
100% TS1713 (b)	3.01 x 10^{-7}	6.03	0.96
Average	*2.92 x 10^{-7}*	*6.30*	
50% B866 (a)	4.15 x 10^{-7}	6.07	0.97
50% B866 (b)	5.76 x 10^{-7}	6.43	0.98
Average	*4.96 x 10^{-7}*	*6.25*	
50% TS1881 (a)	1.01 x 10^{-6}	6.99	0.91
50% TS1881 (b)	3.76 x 10^{-6}	6.81	0.96
Average	*3.38 x 10^{-6}*	*6.90*	

From Table 4.7 the cement containing 100% TS1713 has the slowest crack propagation rate, of all the cements when ΔK = 1 MPa.m$^{1/2}$, followed by 100% B866, and this corresponds with their greater fatigue resistance. Whereas 100% TS1881 has the fastest crack propagation rate, closely followed by 50% TS1881. The crack

propagation rates of 100% TS1881 and 50% TS1881 are an order of magnitude greater than 100% TS1713, 100% B866 and 50% B866 and this is also correspond with their reduced fatigue resistance. The m values (crack acceleration) of all the cements are fairly similar and typical of polymers. Both 100% TS1881 and 50% TS1881 have the highest m values and this is in keeping with their poorer fatigue resistance.

Effect of composition on fatigue crack growth rate parameters

The composition of the five cement formulations is fairly similar including the type of radiopacifier employed, any differences in the fatigue crack growth rate parameters are likely to be caused by the methylacrylate co-polymer, porosity and/or the different sizes and morphologies of the PMMA beads as well as the inhomogeneous microstructure. Initial examination of the fracture surfaces (Figures 4.23 - 4.26) shows no porosity in the crack growth region of the samples, therefore the co-polymer (TS1713), or the bead sizes and their surface morphology must have an influence on the fatigue parameters. However, in real terms the differences in fatigue crack growth behaviour between the different cement formulations is small, therefore it is difficult to make any definite conclusions.

Again there has been very little research examining the influence of bead sizes and bead size distributions on fatigue crack propagation. Previous work has mainly focused on the effect of different radiopacifiers[60, 73] antibiotics[85] and environmental conditions.[82] Ginebra *et al.*[121] studied the influence of bead sizes on fatigue crack propagation and concluded that larger PMMA bead sizes resulted in increased resistance to crack propagation, but it is clear that far more work is required in this area.

Comparison with commercial cements

By comparing the fatigue crack growth behaviour of the experimental cements with the commercial cements, Figures 4.22 and 3.13, it can be seen that the crack growth behaviour of all the experimental cements most closely resembles Palacos R, i.e. the fatigue crack propagates over the same stress intensity factor range (0.34 - 1.62 $MPa.m^{1/2}$). Of the three commercial cements tested, Palacos R, CMW 1 and Cemex ISOPLASTIC, Palacos R had the greatest resistance to fatigue crack propagation. Put simply, for a fatigue crack to propagate through Palacos R at a stable rate a much greater stress intensity factor range was required in comparison with the two other commercial cements. The experimental cements, therefore, all showed a similar resistance to fatigue as Palacos R.

In terms of calculated crack propagation rates, C when ΔK = 1 $MPa.m^{1/2}$, all the experimental cements have slower, more favourable crack propagation rates than Cemex ISOPLASTIC (C = 8.90 x 10^{-6} m/cycle). The crack propagation rates of 100% TS1881 and 50% TS1881 are comparable to CMW 1 (C = 1.93 x 10^{-6} m/cycle) and the three remaining cements; 100% B866, 100% TS1713 and 50% B866 are comparable to Palacos R (C = 3.72 x 10^{-7} m/cycle).

Overall, the sub-critical crack propagation behaviour of all the experimental cements has been found to be comparable to the commercial cements.

SEM examination of fracture surfaces following fatigue testing

The fatigue fracture surfaces of the five different cement formulations are all very similar, therefore only the fracture surfaces of 100% B866, 100% TS1881 and 100% TS1713 will be shown. Again, direction of crack propagation is shown by a dashed arrow.

Examination of the fatigue fracture surfaces (Figures 4.23 - 4.26) show that these surfaces are very different from those obtained under fast fracture, i.e. as a result of fracture toughness testing (Figures 4.12 - 4.21). The fatigue surfaces are not as smooth and 'ductile tears' are present indicating the slower rate of fracture. The PMMA beads are visible but are not so distinct, and some of the beads show river lines. The ridges/indentations towards the edge of the beads observed in the fast fracture surfaces can no longer be seen but the barium sulphate is clearly visible and fairly evenly distributed throughout the matrix. Generally the fracture surfaces of the experimental cements most closely resemble the fatigue fracture surfaces of CMW 1 and Cemex ISOPLASTIC (Figures 3.14 and 3.15).

Very little additional information could be gained at higher magnification (x239), with the exception of 100% TS1881 (Figure 4.26). There are possibly fine striation markings indicating the cyclic loading and unloading process during testing. Therefore, this is the only micrograph shown at the higher magnification.

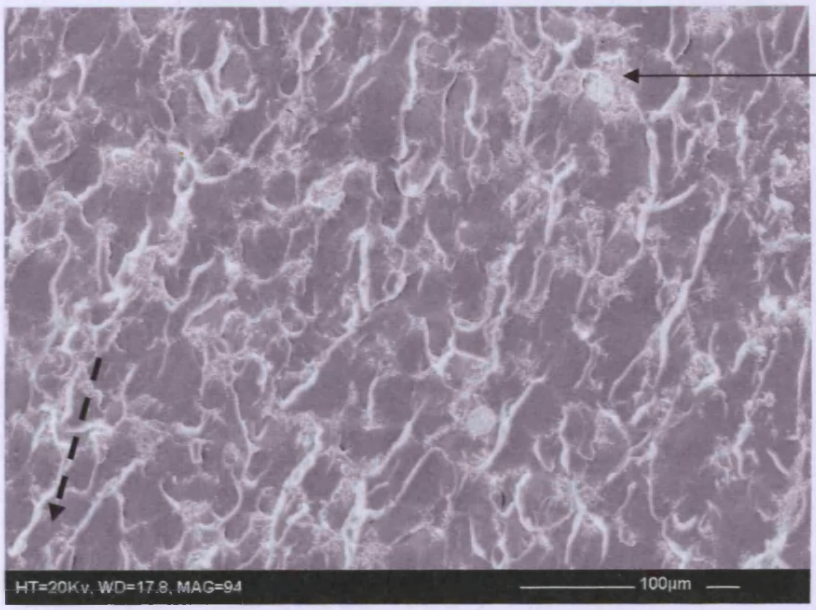

Figure 4.23: Fatigue fracture surface of 100% B866, magnification x 94

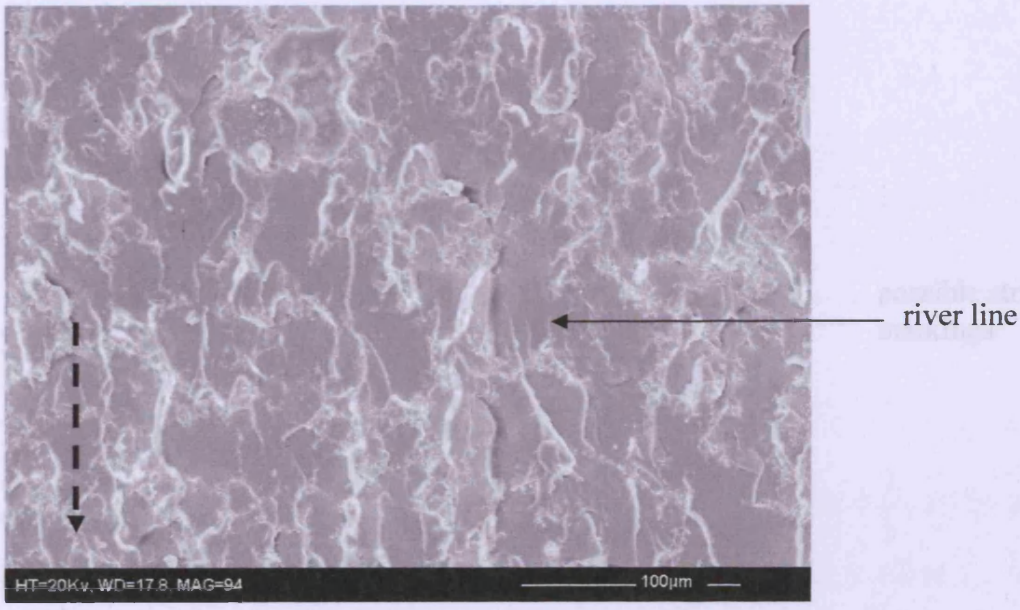

Figure 4.24: Fatigue fracture surface of 100% TS1881, magnification x 94

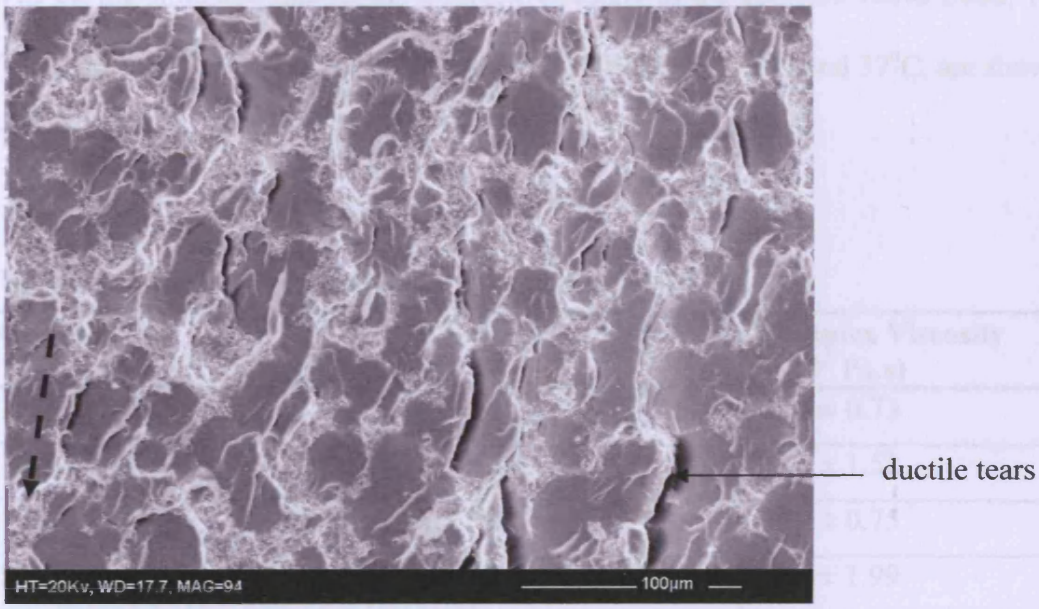

Figure 4.25: Fatigue fracture surface of 100% TS1713, magnification x 94

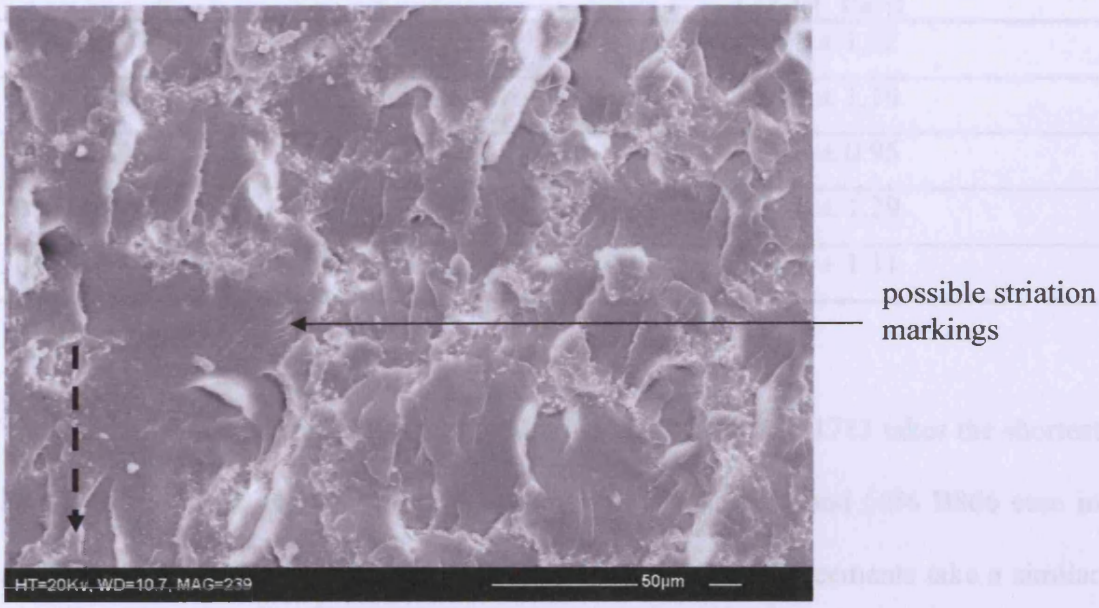

Figure 4.26: Fatigue fracture surface of 100% TS1881, magnification x 239

4.3.5 Rheology

The curing time and maximum complex viscosity of the cements 100% B866, 100% TS1881, 100% TS1713, 50% B866 and 50% TS1881, at 25°C and 37°C, are shown in Tables 4.8 and 4.9.

Table 4.8: Curing time and maximum complex viscosity at 25°C

Cement	Curing Time (minutes)	Complex Viscosity (x 10^3 Pa.s)
100% TS1713	11.7 ± 0.9	57.8 ± 0.73
100% B866	17.5 ± 1.2	75.8 ± 1.52
100% TS1881	16.6 ± 0.6	39.0 ± 0.75
50% B866 - 50% TS1713	13.9 ± 0.7	57.9 ± 1.99
50% TS1881 - 50% TS1713	13.1 ± 0.6	55.8 ± 0.86

Table 4.9: Curing time and maximum complex viscosity at 37°C

Cement	Curing Time (minutes)	Complex viscosity (x 10^3 Pa.s)
100% TS1713	5.0 ± 0.2	58.8 ± 1.02
100% B866	5.9 ± 0.4	59.6 ± 1.19
100% TS1881	5.9 ± 0.2	57.2 ± 0.95
50% B866 - 50% TS1713	5.7 ± 0.3	54.5 ± 1.29
50% TS1881 - 50% TS1713	5.3 ± 0.3	56.3 ± 1.11

The results presented in Table 4.8 show that at 25°C, 100% TS1713 takes the shortest length of time to cure, curing in 11.7 minutes. 50% TS1881 and 50% B866 cure in 13.10 and 13.86 minutes respectively. Even though these two cements take a similar length of time to cure, only the curing rate of 50% B866 is significantly longer than 100% TS1713 ($p<0.01$). The curing rates of both 100% TS1881 and 100% B866 are significantly longer than the other cement formulations ($p<0.0005$), curing in 16.6 and

17.5 minutes respectively. This is almost 1.5 times longer than 100% TS1713.

At 37°C (Table 4.9) all the cements cure at a significantly faster rate ($p<0.0005$), and all cure within approximately one minute of each other (with the average time being 5.6 minutes). Again 100% TS1713 takes the shortest length of time to cure and both 100% B866 and100% TS1881, the longest. There is still, however, a significant difference in the curing rates between the cement containing 100% TS1713 and the cements containing 50% B866 ($p<0.05$), 100% B866 ($p<0.001$) and 100% TS1881 ($p<0.001$).

Changes in complex viscosity and elastic/viscous modulus whilst curing

Figures 4.27 and 4.28 show how the viscosity changes with time for each type of cement at 25°C and 37°C. The changes in elastic/viscous moduli and tan δ of all the experimental cement formulations at 25°C, and of the cements containing 100% B866, 100% TS1881 and 100% TS1713 at 37°C are given in Figures 4.29 - 4.36.

It is clear that at 25°C all the cement formulations have very different viscosity profiles (Figure 4.27). The most striking difference is the range of maximum complex viscosities. 100% B866 has a much greater maximum viscosity (75.8×10^3 Pa.s) than the other cements, along with a correspondingly high maximum elastic modulus, 2.38 MPa (see Figure 4.34). This is consistent with this cements superior flexural modulus and fracture toughness. 100% TS1881 has the lowest maximum viscosity (39.0×10^3 Pa.s) and an equally low maximum elastic modulus (1.24 MPa) when cured, and again this is consistent with this cements poorer flexural properties and fracture toughness as a result of porosity. The maximum viscosity and maximum elastic modulus of cement 100% TS1713 lies in between the two at 57.8×10^3 Pa.s. and 1.81 MPa respectively.

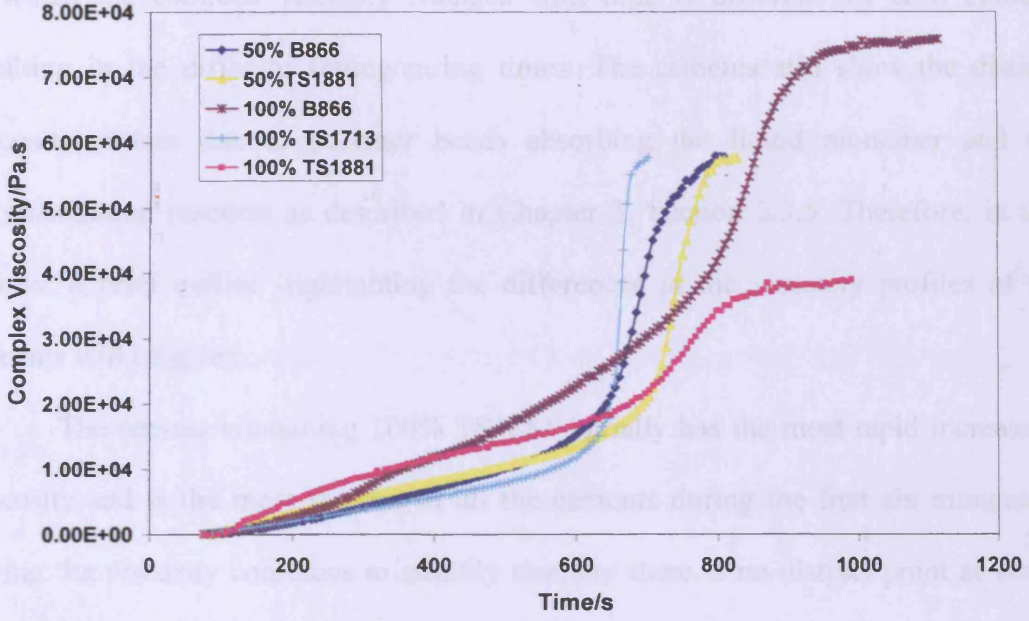

Figure 4.27: Change in complex viscosity during curing at 25°C

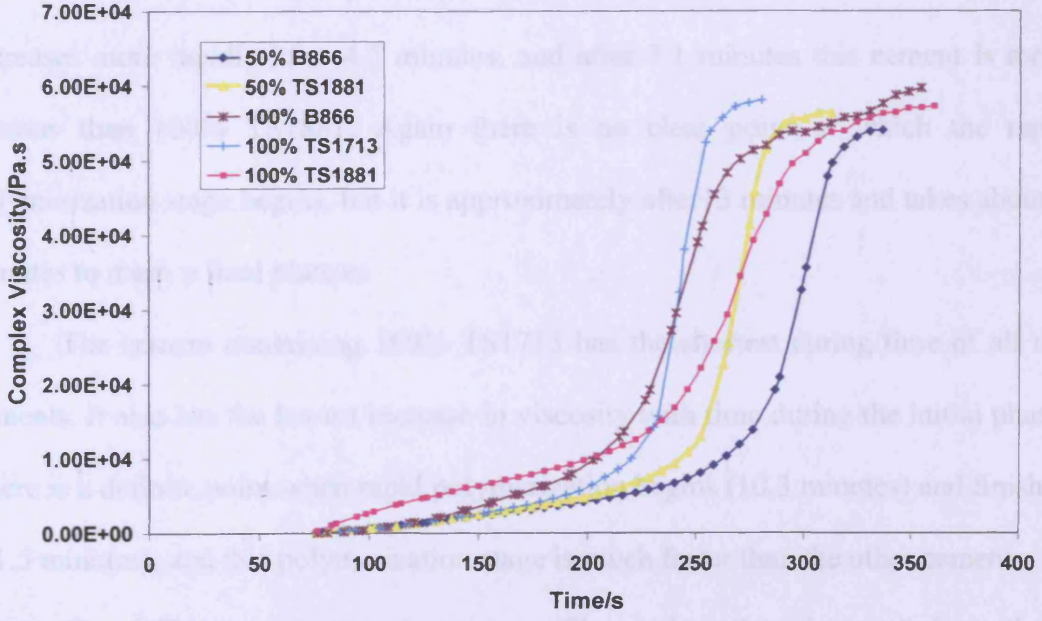

Figure 4.28: Change in complex viscosity during curing at 37°C

As well as having different maximum complex viscosities and elastic moduli, the way in which the complex viscosity changes with time is different for each cement, resulting in the different setting/curing times. The cements still show the distinct viscosity phases due to polymer beads absorbing the liquid monomer and the polymerization reaction as described in Chapter 3, Section 3.3.5. Therefore, in this chapter a brief outline highlighting the differences in the viscosity profiles of the cements will be given.

The cement containing 100% TS1881 initially has the most rapid increase in viscosity and is the most viscous of all the cements during the first six minutes of curing. Its viscosity continues to steadily rise, but there is no distinct point at which the rapid polymerization stage begins. However, it does appear as if the final polymerization stage occurs after 11 minutes, and takes about 3 - 4 minutes, before reaching a final plateau.

The cement containing 100% B866 initially has a very low viscosity, but it increases more rapidly after 4.5 minutes, and after 7.1 minutes this cement is more viscous than 100% TS1881. Again there is no clear point at which the rapid polymerization stage begins, but it is approximately after13 minutes and takes about 3 minutes to reach a final plateau.

The cement containing 100% TS1713 has the shortest curing time of all the cements. It also has the lowest increase in viscosity with time during the initial phase. There is a definite point when rapid polymerization begins (10.3 minutes) and finishes (11.5 minutes), and this polymerization stage is much faster than the other cements.

The differences in the viscosity profiles and setting times of these three cements are most likely to be caused by their different PMMA bead sizes, size distribution and morphology, as well as the presence of the acrylate co-polymer in the

TS1713 polymer. Work by Pascual *et al.*[22] found that increasing the average PMMA bead size and widening the bead size distribution, lead to an increase in setting time. This appears to be the case with 100% TS1881. Conversely, 100% B866 has a smaller range of bead sizes, and from SEM examination (Figure 4.1), a smaller average bead size, but still takes approximately the same length of time to cure as 100% TS1881. The remaining factor differentiating the two types of cements is the surface morphology of the PMMA beads. As mentioned earlier in Sections 4.3.2 and 4.3.3, the irregular morphology of the TS1881 beads increases surface area thereby absorbing more liquid monomer leaving less available monomer for the polymerization reaction. This results in a larger concentration of benzoyl peroxide (initiator) and N, N-dimethyl-p-toluidine (accelerator) reacting with the remaining liquid monomer, thereby increasing not only the polymerization temperature and hence porosity levels, but also the curing rate.[38] This leads to the supposition that had the TS1881 polymer beads a regular surface morphology, hence a smaller surface area, then 100% TS1881 would have taken even longer to cure. This would then correspond with Pascual *et al.*'s work on average bead size and size distribution.[22]

The most interesting effect is that of the bimodal particle size distribution of the TS1713 polymer powder (Figure 4.3). The cement 100% TS1713 has the shortest setting time but the largest average bead size. According to Lewis and Carroll[94] it is not the average particle size which effects curing rates, but the proportion of small and large particles. Lewis and Carroll suggested that having a large number of small particles would increase the length of time of the initial stage by completely dissolving in the liquid monomer, and having a large number of large particles would increase the rate of the rapid polymerization stage. It appears that this maybe the case with the cement, 100% TS1713 with the smaller sized particles causing a long initial

phase with a very gradual increase in viscosity, and the larger sized particles resulting in a sudden, very rapid polymerization reaction. It is this rapid polymerization phase which accounts for the short setting/curing time of 100% TS1713. However, the presence of the methylacrylate co-polymer may also have affected the rate of monomer absorption by the beads, and it is difficult not knowing the proportion of the co-polymer to quantify its effect on curing behaviour.

The effect of combining the B866 or TS1881 powders with TS1713, at 25°C, has been to reduce the overall curing time and the initial increase in viscosity when compared with 100% B866 and 100% TS1881. TS1713 also appears to have a strong influence on the maximum complex viscosity and maximum elastic modulus of both 50% B866 and 50% TS1881. The maximum complex viscosity and maximum elastic modulus of 50% B866 being 57.9 x 10^3 Pa.s and 1.72 MPa respectively (Figure 4.32), and the maximum complex viscosity and maximum elastic modulus of 50% TS1881 being 55.8 x 10^3 Pa.s and 1.81 MPa respectively (Figure 4.33). These values are similar to 100% TS1713.

The change in viscous modulus with time for all the cements at 25°C is also shown in Figures 4.29 - 4.33. Both 100% B866 and 100% TS1881 show a small, but gradual increase reaching a maximum of 0.2 and 0.25 MPa respectively, when the cements reach the rapid polymerization stage, at which point the viscous modulus decreases as the cement becomes a predominantly elastic solid. The viscous modulus of 100% TS1713 also gradually increases while the cement is curing, but then suddenly peaks during the rapid polymerization stage, reaching a maximum of 0.4 MPa before the cement is fully polymerized. Again the change in viscous modulus with time for 50% B866 and 50% TS1881 lies in between 100% B866 and 100% TS1713, and 100% TS1881 and 100% TS1713, respectively.

At 37°C the curing rate is much faster. This is to be expected as the rate of cure is temperature dependent. The change in complex viscosity during curing at 37°C is shown in Figure 4.28. It can be seen that all the cements cure at a very similar rate, 5.6 ± 0.4 minutes. The cements also reach a very similar maximum complex viscosity, 57.3 ± 1.8 x 10^3 Pa.s, and maximum elastic modulus, 1.80 ± 0.05 MPa. For 100% TS1713, 50% B866 and 50% TS1881, the increase in temperature has had no effect on the maximum viscosity, however, it has had an effect on 100% B866 and 100% TS1881.

The maximum viscosity and elastic modulus of 100% B866 at 37°C are now 59.6 x 10^3 Pa.s and 1.84 MPa respectively, and this is much lower than at 25°C. This could be because the cement is curing so rapidly that it does not have time to reach its maximum values. The opposite has occurred for 100% TS1881, its maximum viscosity (57.2 x 10^3 Pa.s) and elastic modulus (1.77 MPa) is much greater at 37°C and this could possibly be because there is now more thermal energy, resulting in a fuller and more complete polymerization. The way the viscous moduli changes with time at 37°C is very similar to the changes observed at 25°C, but obviously take place more rapidly at 37°C.

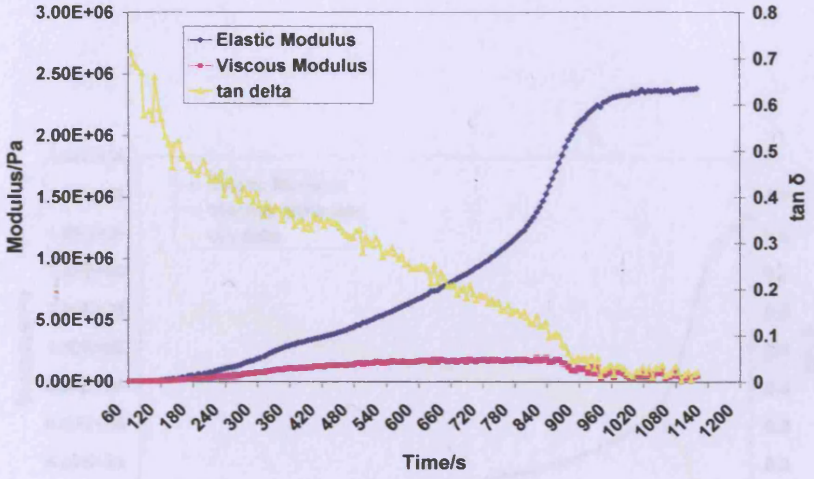

Figure 4.29: Change in elastic/viscous modulus and tan δ of 100% B866 at 25°C

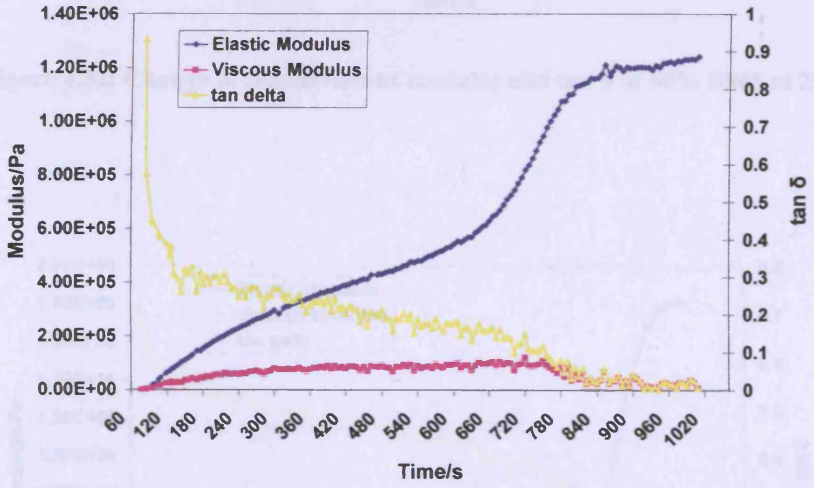

Figure 4.30: Change in elastic/viscous modulus and tan δ of 100% TS1881 at 25°C

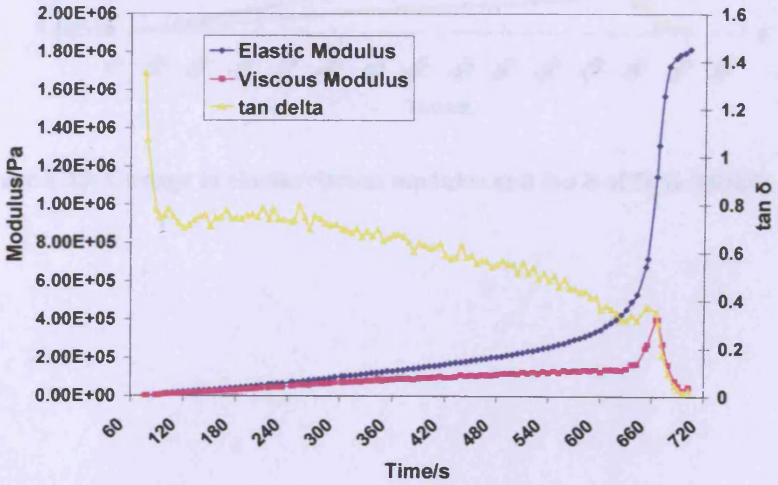

Figure 4.31: Change in elastic/viscous modulus and tan δ of 100% TS1713 at 25°C

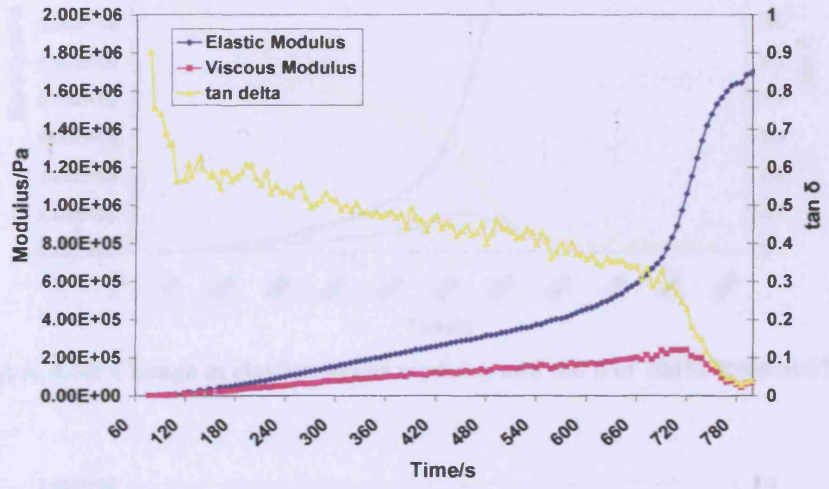

Figure 4.32: Change in elastic/viscous modulus and tan δ of 50% B866 at 25°C

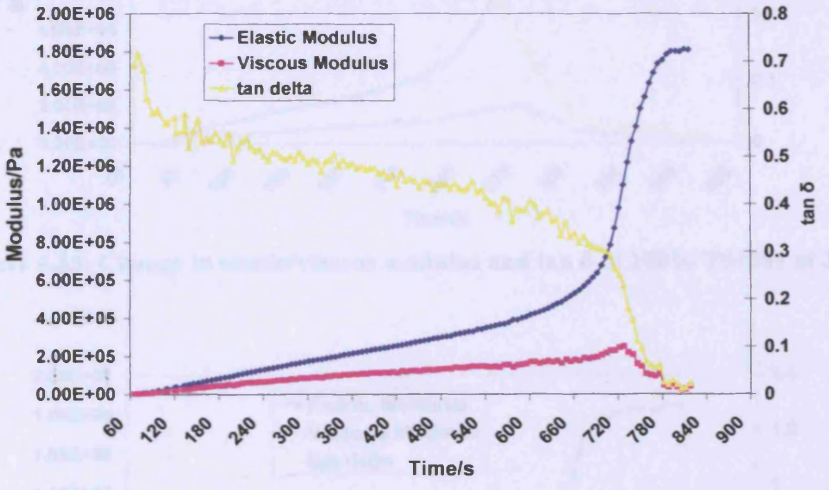

Figure 4.33: Change in elastic/viscous modulus and tan δ of 50% TS1881 at 25°C

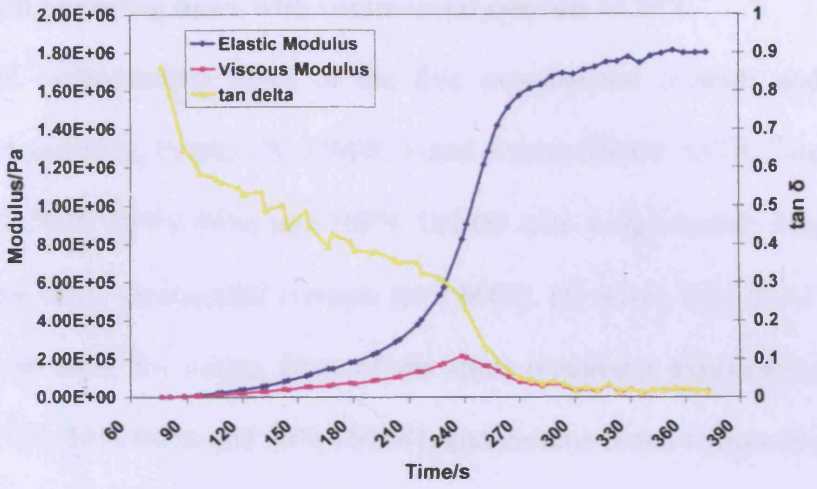

Figure 4.34: Change in elastic/viscous modulus and tan δ of 100% B866 at 37°C

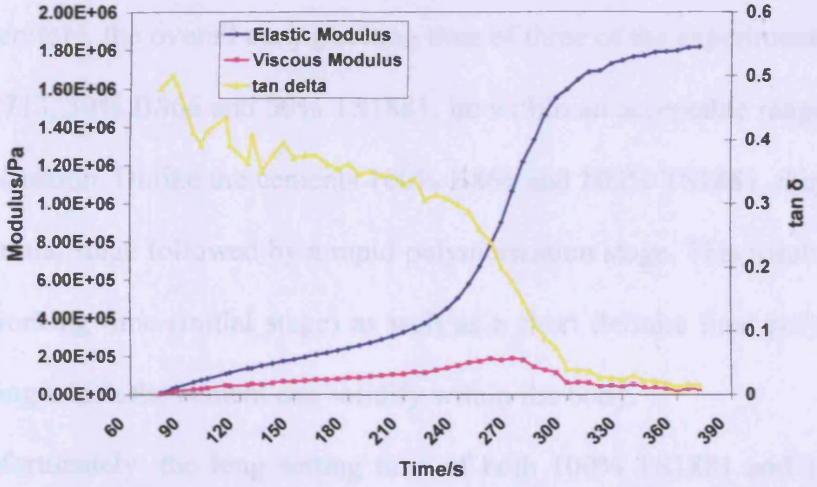

Figure 4.35: Change in elastic/viscous modulus and tan δ of 100% TS1881 at 37°C

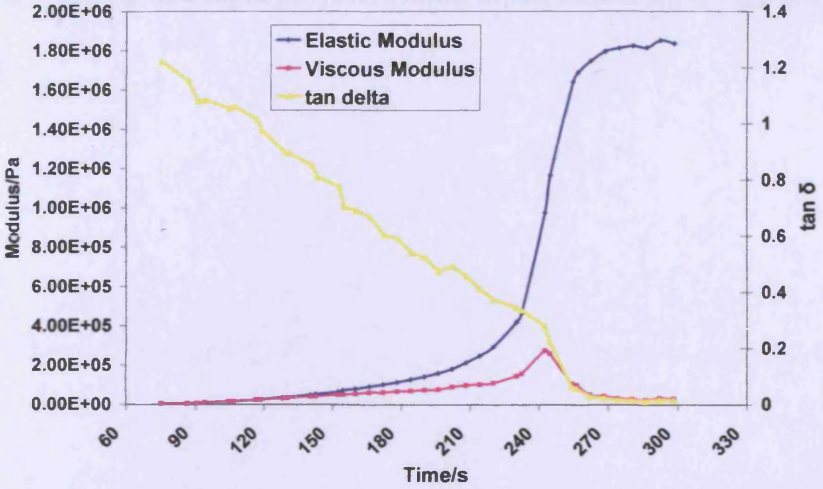

Figure 4.36: Change in elastic/viscous modulus and tan δ of 100% TS1713 at 37°C

Comparison of curing times with commercial cements at 25°C

The overall curing/setting times of the five experimental cements and the three commercial cements; Palacos R, CMW 1 and Cemex ISOPLASTIC, are shown in Figure 4.37. Both 100% B866 and 100% TS1881 take a significantly longer time to cure than the three commercial cements ($p<0.0005$). However, there is no significant difference between the curing rates of the three remaining experimental cements; 100% TS1713, 50% B866 and 50% TS1881, and Palacos R and Cemex ISOPLASTIC ($p>0.05$). All the cements, however, cure at a significantly slower rate than CMW 1 ($p<0.0005$).

Therefore, the overall curing/setting time of three of the experimental cements, 100% TS1713, 50% B866 and 50% TS1881, lie within an acceptable range for use in a clinical situation. Unlike the cements 100% B866 and 100% TS1881, they also have a distinct initial stage followed by a rapid polymerization stage. This results in a clear handling/working time (initial stage) as well as a short definite final polymerization period during which the cement can solidify within the body.

Unfortunately, the long setting time of both 100% TS1881 and 100% B866 (even though 100% B866 has superior rheological properties when cured) as well as their unclear working and rapid polymerization times, makes them both unsuitable for clinical use.

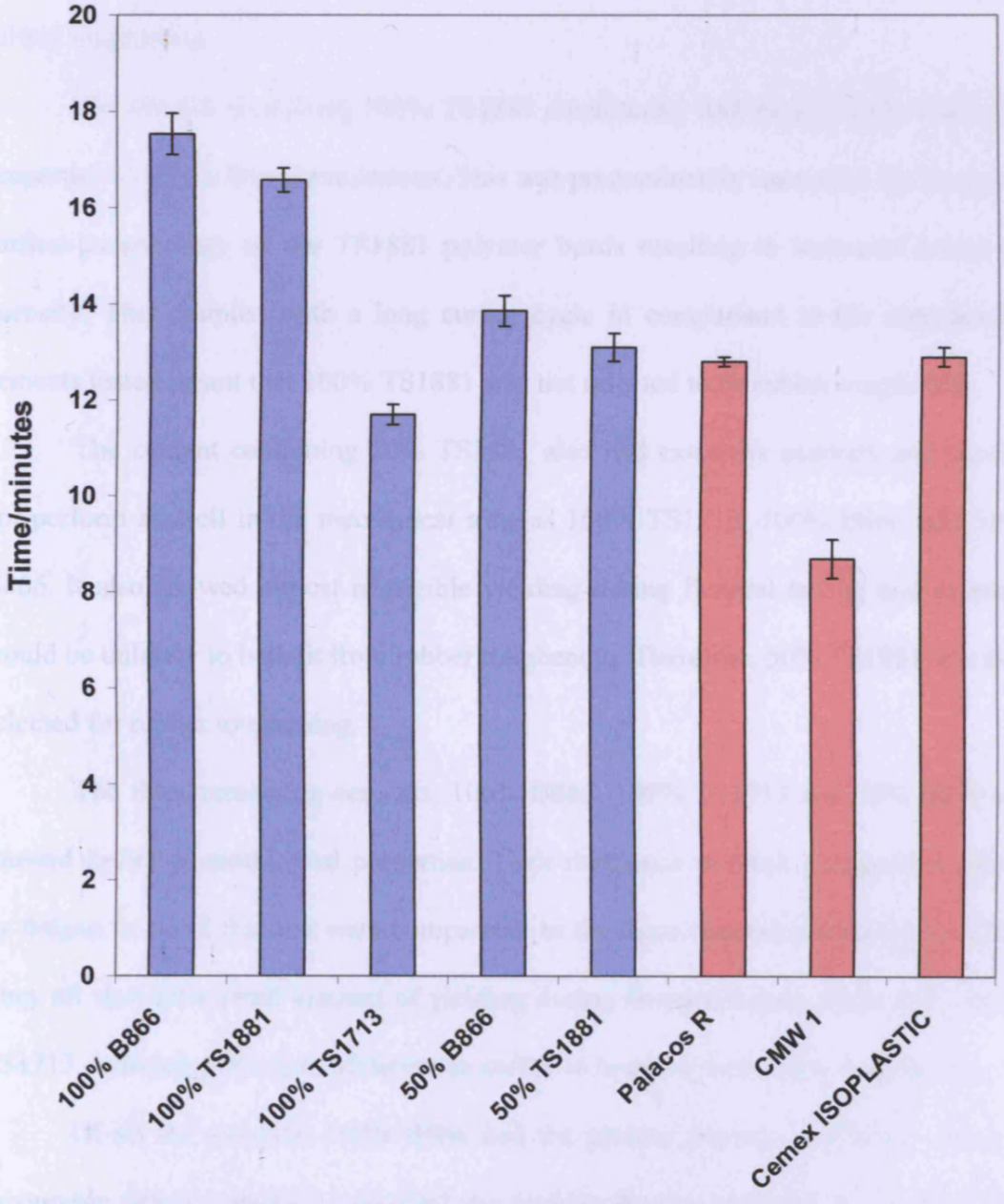

Figure 4.37: Curing times of experimental and commercial cements at 25°C

4.4 CONCLUSIONS

The mechanical and rheological properties of the five different experimental cements; 100% B866, 100% TS1881, 100% TS1713, 50% B866 and 50% TS1881, were examined to determine which two cements would be the most suitable to undergo rubber toughening.

The cement containing 100% TS1881 consistently had the poorest mechanical properties of all the five formulations. This was predominantly caused by the irregular surface morphology of the TS1881 polymer beads resulting in increased levels of porosity. This coupled with a long curing cycle in comparison to the commercial cements tested meant that 100% TS1881 was not selected to be rubber toughened.

The cement containing 50% TS1881 also had extensive porosity and so did not perform as well in the mechanical tests as 100% TS1713, 100% B866 and 50% B866. It also showed almost negligible yielding during flexural testing and as such would be unlikely to benefit from rubber toughening. Therefore, 50% TS1881 was not selected for rubber toughening.

The three remaining cements, 100% B866, 100% TS1713 and 50% B866 all showed desirable mechanical properties. Their resistance to crack propagation either by fatigue or rapid fracture were comparable to the three commercial cements tested. They all showed a small amount of yielding during flexural testing, especially 100% TS1713, indicating that they all have the ability to improve with rubber toughening.

Of all the cements, 100% B866 had the greatest fracture toughness, showed favourable fatigue properties and had the highest flexural modulus. It also had the greatest dynamic shear elastic modulus and complex viscosity. Unfortunately, 100% B866 also had a far longer curing time than the commercial cements and did not

present a clear working or rapid polymerization phase making it unsuitable for use in a clinical situation. Consequently 100% B866 was not selected.

Both the cements, 100% TS1713 and 50% B866, had the same fracture toughness values. In addition, the cement containing 100% TS1713 had the highest flexural modulus and greatest resistance to fatigue crack propagation. Both cements also had curing times comparable to the commercial cements as well as clearly definable working and rapid polymerization times. Therefore, 100% TS1713 and 50% B866 were selected for rubber toughening.

CHAPTER 5

DEVELOPMENT AND TESTING OF RUBBER TOUGHENED BONE CEMENTS

5.1 INTRODUCTION

In the previous chapter experimental cements were developed with equivalent key mechanical and rheological properties in comparison with commercially available bone cements. To improve the fracture toughness of the experimental cements, in order to reduce the risk of brittle fracture, a thermoplastic rubber second phase, acrylonitrile-butadiene-styrene (ABS) powder, was incorporated into the cement. This is known as rubber toughening and allows the cement to yield and deform plastically before eventually fracturing.[9] To promote more efficient toughening/yielding mechanisms, thereby improving fracture toughness yet further, the ABS can be coated with an organo-silane capable of bonding with the PMMA matrix. This creates a stronger interface between the ABS particles and the cement matrix. Although, this increase in toughness results in a corresponding reduction in modulus, the primary objective of this work was to reduce brittle fracture in bone cement.

From the previous chapter, two experimental cement formulations, 100% TS1713 and 50%B866-50%TS1713, were selected to be rubber toughened. Initially, untreated ABS particles were added to both cements in increasing quantities to determine the optimum amount to improve the cements' fracture toughness. This also ascertained which of the two cements showed the greatest response to rubber toughening and would be selected to be toughened with silane-coated ABS particles.

Both experimental cement formulations containing untreated ABS also underwent flexural testing to examine the extent of yielding and decrease in modulus.

Silane-coated ABS particles were then added to the selected cement in the same quantities as the untreated ABS, and the flexural properties, in addition to the fracture toughness, of these new cements were determined.

Incorporating untreated and silane-coated ABS particles into the cement will affect the rheological properties of the cement, therefore these properties were examined over the entire curing process, both at room and body temperature. This would also indicate which type and amount of ABS could be added without compromising the cements' handling/rheological properties.

Finally, by examining the results of all the above tests, the two most favourable quantities of untreated and silane-coated ABS required to improve toughness and to maintain desirable or existing rheological characteristics were established. Cements with these quantities of untreated/silane-coated ABS particles underwent fatigue testing to investigate any improvement in fatigue crack growth behaviour.

5.2 MATERIALS AND METHODS

5.2.1 Materials

The materials used in the development of the rubber reinforced cements are shown in Tables 5.1 - 5.2.

Table 5.1: Materials used in the liquid component

Materials	Manufacturer
Methylmethacrylate stabilised with 10-100 ppm monomethyl ether hydroquinone	Sigma-Aldrich Company Ltd, Dorset, U.K.
N, N-dimethyl-p-toluidine	Sigma-Aldrich Company Ltd, Dorset, U.K.

Table 5.2: Materials used in the powder component

Materials	*Particle sizes	Manufacturer
PMMA co-polymer powder Colacryl® TS1713	38 - 54μ	Lucite International, County Durham, U.K.
Powdered Acrylonitrile Butadiene Styrene	10.3% > 600μ 24.8% = 400-600μ 64.9% < 400μ	Plastic Raw Materials, Merseyside. U.K.
Benzoyl Peroxide	-	Sigma-Aldrich Company Ltd, Dorset, U.K.
Barium Sulphate	-	Sigma-Aldrich Company Ltd, Dorset, U.K.

*Particle sizes given by manufacturer

5.2.2 Preparation of experimental cement formulations

The following experimental cements were formulated:-

(1) Cement with ABS and TS1713 PMMA powder

(2) Cement with ABS and B866 + TS1713 PMMA powder

(3) The most favourable cement selected from (1) and (2), with the ABS being replaced by silane-coated ABS

Cement (1) was based on the experimental cement 100% TS1713 as described in Chapter 4 Section 4.2.3. Five different formulations were made, with 10, 20, 30, 40 and 50% TS1713 PMMA powder being replaced w/w with ABS powder.

Cement (2) was based on the experimental cement 50% B866 - 50% TS1713 also described in Chapter 4 Section 4.2.3. Five different formulations were made, with 10, 20, 30, 40 and 50% of the combined PMMA powders being replaced w/w with ABS powder.

Cement (3) was based on either cement (1) or cement (2), depending on the results of the initial testing, with the ABS powder being replaced with silane-coated ABS.

5.2.3 Surface coating ABS with an organo-silane

The ABS powder was coated with methacryloxypropyltrimethoxy-silane as follows:-

The silane was added with stirring, to a 95% ethanol-5% water solution adjusted to pH 4.5-5.5 with acetic acid, to produce a 2% silane final concentration. This solution was stirred continuously for five minutes to allow hydrolysis and silanol formation. The ABS was added, again with stirring, for 2-3 minutes to become silylated and the solution was decanted. The particles were rinsed with absolute ethanol and left to cure overnight at room temperature.

5.2.4 X-Ray Photoelectron Spectroscopy

To ensure that silylation had taken place, X-ray Photoelectron Spectroscopy (XPS) was employed to detect the presence of silicon on the surface of the treated ABS. Surface spectra were obtained of the ABS both before and after treatment using a Kratos Axis Ultra DLD Spectrometer (Kratos Analytical, Manchester, U.K.) with a monochromatic Al Kα X-ray source, power = 150W, at a pass energy of 160 eV.

5.2.5 Flexural Properties

10 samples for the 3-point bending tests were made by adding 20g of the liquid component to 40g of the powder component, mixing, and manually placing the cement in the moulds as described in Chapter 3, Section 3.2.3. All 3-point bending tests were also carried out as described in Section 3.2.3.

5.2.6 Fracture Toughness

For each type of cement 10 samples were tested as described in Chapter 3, Section 3.2.4. Following testing the fracture surfaces were examined using an SEM as described in Chapter 3, Section 3.2.2.

5.2.7 Rheology

A quantity of 12g of powder was mixed with 6g of liquid (see Chapter 4, Section 4.2.6 for a more detailed composition) and placed between the parallel plates of the rheometer. The method described in Chapter 3, Section 3.2.6 was followed, but for these tests a time of 70 seconds elapsed between start of mixing and the first rheometer reading.

5.2.8 Fatigue

CT specimens were produced using 40g powder component and 20g liquid component. The liquid was added to the powder, hand mixed, and manually placed in the mould as described in Chapter 3, Section 3.2.5. Testing was also carried out as described in Section 3.2.5 and the resultant fracture surfaces were examined using an SEM at 20 or 24 kV as described in Chapter 3, Section 3.2.2.

5.2.9 Statistical Analysis

The same statistical analysis was carried out as described in Chapter 3, Section 3.2.7.

5.3 RESULTS AND DISCUSSION

5.3.1 X-Ray Photon Spectroscopy

X-ray Photon Spectroscopy (XPS) was undertaken to provide evidence that the silane treatment of the ABS particles was successful.

The XPS spectra of the surface of the ABS before and after silylation are shown in Figure 5.1. They clearly show peaks for carbon, nitrogen and surprisingly oxygen and silicon both before and after surface treatment. It is assumed that the oxygen and silicon present on the untreated ABS is due to contamination, possibly during the manufacture of the product. However, as a molar percentage, the amount of silicon has increased from 2.4% (for the untreated ABS) to 5.7% for the treated ABS, and the amount of oxygen has also greatly increased from 5.1% to 14.0%. This indicates that the organosilane is present on the surface of the treated ABS. It is also likely that the oxygen on the surface of the untreated ABS will have helped create a covalent bond between the organosilane and the ABS.

The small peak for fluorine on the spectrum of the treated ABS was due to the glassware containing the treated ABS having been cleaned with a solvent remover.

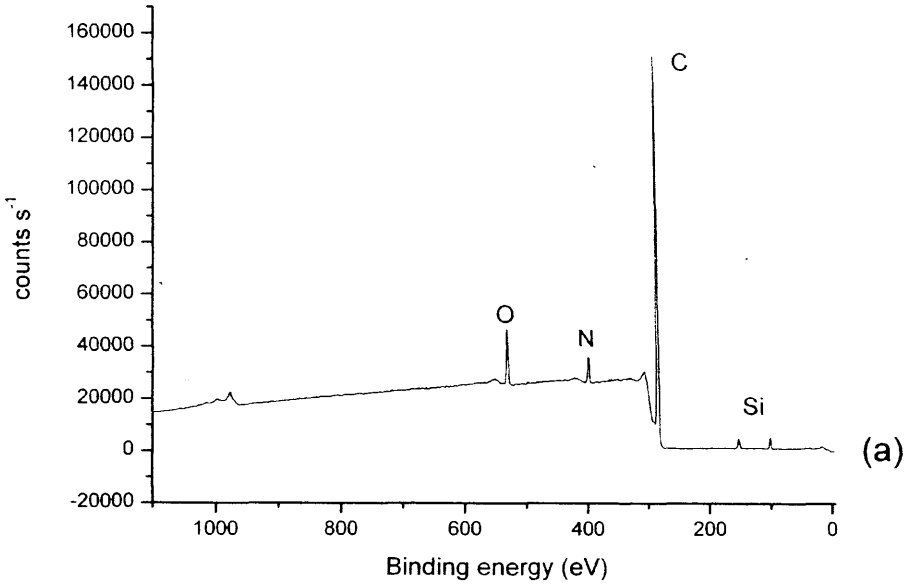

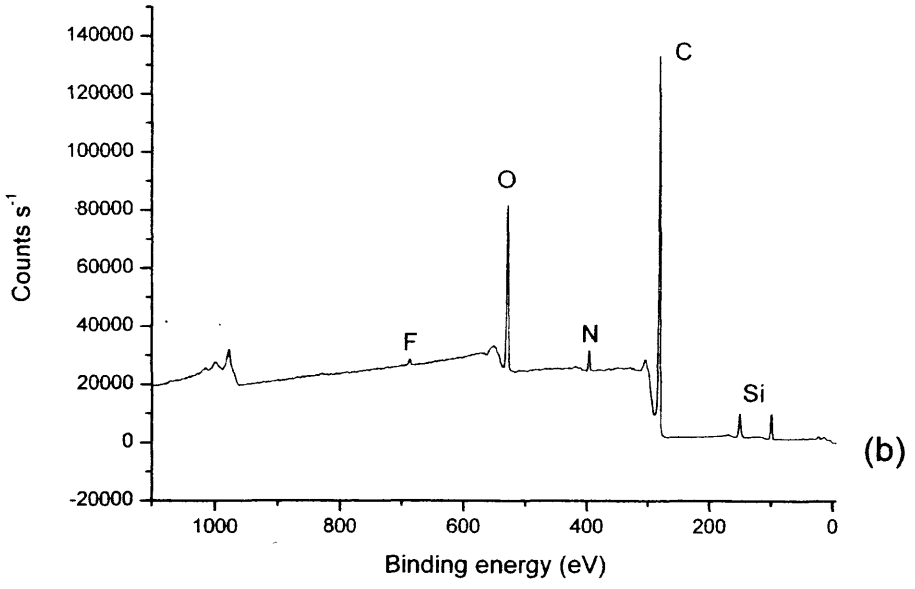

Figure 5.1: XPS spectra (a) before silylation (b) after silylation

5.3.2 Flexural properties of cements containing untreated ABS

Flexural testing was initially carried out on cement (1) i.e. cements containing powdered ABS, and the PMMA powder TS1713; and cement (2) i.e. cements containing ABS, and equal amounts of both TS1713 and B866 PMMA powder.

The flexural strength and moduli of each of these cements are shown in Tables 5.3 and 5.4 as well as the flexural strength and moduli of 100% TS1713 and 50% B866 - 50% TS1713.

Table 5.3: Flexural properties of cements containing ABS and TS1713 PMMA (cement 1)

Cement (1)		**Flexural Strength(MPa)**	**Flexural Modulus (GPa)**
ABS (wt. %)	TS1713 (wt. %)		
0	100	58.80 ± 4.26	2.44 ± 0.09
10	90	59.89 ± 5.99	2.37 ± 0.16
20	80	50.16 ± 5.72	2.00 ± 0.16
30	70	48.43 ± 3.12	1.84 ± 0.08
40	60	46.54 ± 2.22	1.70 ± 0.07
50	50	40.89 ± 2.08	1.50 ± 0.06

Table 5.4: Flexural properties of cements containing ABS and B866 + TS1713 PMMA (cement 2)

Cement (2)			**Flexural Strength (MPa)**	**Flexural Modulus (GPa)**
ABS (wt. %)	B866 (wt. %)	TS1713 (wt. %)		
0	50	50	55.24 ± 5.16	2.46 ± 0.10
10	45	45	55.98 ± 4.03	2.36 ± 0.05
20	40	40	50.56 ± 4.44	1.91 ± 0.18
30	35	35	48.15 ± 1.50	1.78 ± 0.06
40	30	30	46.69 ± 3.00	1.76 ± 0.10
50	25	25	37.80 ± 2.06	1.51 ± 0.12

As expected, the flexural modulus of both types of cement decreases with increasing amounts of ABS with a significant decrease when cements contain 20% or more ABS ($p<0.005$). However, there is no significant difference between the two groups of cements, i.e. between cement (1) and cement (2), when they contain the same percentage of ABS ($p>0.05$).

The flexural strength of both types of cement remains unchanged with the addition of 10% ABS. Further additions of ABS to cement (1) results in a continual significant decrease in strength ($p<0.0005$). Further additions of ABS to cement (2) also results in a continual decrease in strength with a significant decrease found when the cements contain 30% ABS ($p<0.005$), or more ($p<0.0005$). There is no significant difference in strengths between cement (1) and cement (2) at the same percentage levels of ABS.

Figure 5.2 shows the load/displacement curves of cement (1) using one representative sample of each formulation. The decrease in modulus is signified by the reduction of the initial gradient of the curves, and the decrease in strength is signified by the reduction in maximum load. As the strength and modulus of both cements (1) and (2) decreased in a very similar manner only the one graph is shown.

N.B. During the fabrication of the cements there was extreme difficulty in incorporating 50% (i.e. 17.77g) into the cement. Usually, approximately 1-2g of ABS remained in the mixing bowl, therefore it wasn't possible to continue producing cements containing 50% ABS. The cements also became very sticky with any addition of ABS, and adhered to all surfaces they came into contact with, making it very difficult to place the cements in the moulds.

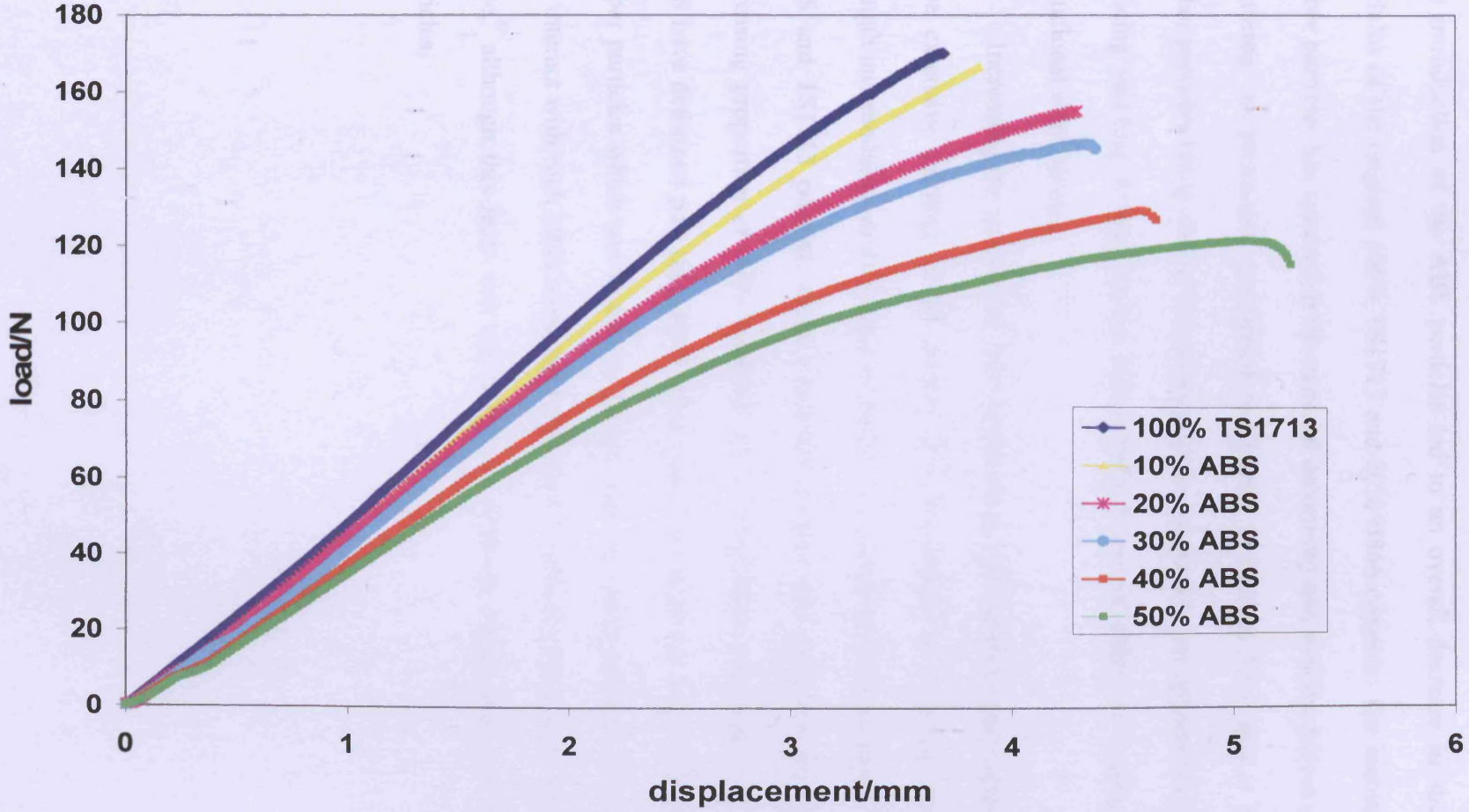

Figure 5.2: Load/displacement curves of TS1713 containing different weight percentages of untreated ABS

Summary of the effect of ABS particles on the flexural properties of the experimental cements

The introduction of the ABS particles led to an overall decrease in strength and modulus of the original 100% TS1713 and 50% B866 cements. The inclusion of the rubber particles has resulted in the material deforming and yielding before eventually fracturing. As previously mentioned in Chapter 2, Section 2.5.1, this is due to the rubber particles being able to extend and deform under a lower applied load as well as inducing yielding throughout the brittle PMMA matrix either by crazing or shear dilatational mechanisms.

Increasing the quantity of ABS means more ABS particles can deform causing more extensive yielding of the matrix, and this results in a greater reduction in strength and modulus, as illustrated by Figure 5.2. Cement (1) i.e. cements containing ABS and TS1713 powder, show increased yielding and therefore elongation with increasing proportion of ABS particles. The formulations containing 30% or more ABS have deformed past their yield point. However, there is a limit to the amount of rubber particles which can be added. If there are too many particles, they can touch and interact with each other reducing the amount of effective yielding which can take place,[9] although this limit was not seen even with the incorporation of 50% ABS particles.

5.3.3 Fracture toughness of cements containing untreated ABS

Testing was initially carried out on cements (1) and (2) and included the cements containing 50% ABS, as these cements had already been produced for flexural testing. Because the results of the flexural testing showed non-linear load/displacement curves, the equivalent curves generated during fracture toughness testing were examined to determine the validity of the fracture toughness test following the procedure outlined in Chapter 2, Section 2.3.2.[8, 59] Although the load/displacement curves did deviate from linearity with the incorporation of ABS they did lie within the acceptable limits required for the determination of fracture toughness and so the test was still valid.

The fracture toughness values of the cements containing ABS are shown in Tables 5.5 and 5.6. These tables also include the fracture toughness of the original 100% TS1713 and 50% B866 cements.

Table 5.5: Fracture toughness of cements containing ABS and TS1713 PMMA (cement 1)

Cement (1)		**K_{1C} (MPa.m$^{1/2}$)**	**Increase in toughness**
ABS (wt. %)	TS1713 (wt. %)		
0	100	2.30 ± 0.12	-
10	90	2.63 ± 0.12	14.3%
20	80	2.71 ± 0.12	17.8%
30	70	2.73 ± 0.12	18.7%
40	60	2.67 ± 0.08	16.1%
50	50	2.37 ± 0.17	3.0%

Table 5.6: Fracture toughness of cements containing ABS and B866 + TS1713 PMMA (cement 2)

Cement (2)			K_{IC} (MPa.m$^{1/2}$)	Increase in toughness
ABS (wt. %)	B866 (wt. %)	TS1713 (wt. %)		
0	50	50	2.30 ± 0.13	-
10	45	45	2.44 ± 0.15	6.1%
20	40	40	2.38 ± 0.14	3.5%
30	35	35	2.25 ± 0.15	-2.2%
40	30	30	2.21 ± 0.21	-3.9%
50	25	25	2.17 ± 0.27	-5.7%

The cement based on 100% TS1713 (see Table 5.5) clearly shows a significant increase in fracture toughness with increasing quantity of ABS, 10% ABS ($p<0.01$), 20% ABS ($p<0.0005$), 30% ABS ($p<0.0005$) reaching a maximum 18.7% increase in toughness with the addition of 30% ABS ($p<0.0005$). Following this there is a slight decrease in fracture toughness with the incorporation of 40% ABS, but it is still significantly greater than the cement TS1713 with no ABS present ($p<0.001$). However, there is no significant increase in toughness with 50% ABS ($p>0.05$).

For the cement containing 50% B866 (Table 5.6) there is a small, but not significant, increase in fracture toughness with the addition of 10% ABS ($p>0.05$) followed by a gradual decrease in toughness with increasing amounts of ABS. The incorporation of 30% ABS or more, actually reduced the fracture toughness of the original 50% B866 cement, but not significantly ($p>0.05$).

Overall, the addition of ABS greatly increased the fracture toughness of 100% TS1713, but not that of cement 50% B866, therefore cement (2) will not be tested further. Silane-coated ABS will now replace the untreated ABS in cement (1). This new cement will be referred to as cement (3).

Summary of the effect of ABS particles on the fracture toughness of experimental cements

The initial addition (i.e. 10%) of untreated ABS particles increased the fracture toughness of both 100% TS1713 and 50% B866 by 14.3% and 6.1% respectively. The rubber particles have effectively toughened the cement by inducing yielding, via shearing and crazing mechanisms, throughout the cement matrix. This means that the mode of fracture, i.e. the way the crack propagates, is no longer brittle but has become more ductile. The cement can now absorb energy by plastically deforming, not only at the crack tip, but throughout the cement. Therefore more fracture energy, G_c, is required for the crack to propagate which leads to an increase in fracture toughness.[8, 56]

With increasing untreated ABS content, the cement is able to undergo more extensive yielding, and hence there should be a further increase in fracture toughness. However, there is a critical amount which can be added before the fracture toughness begins to decrease[104] as a result of interaction between the rubber particles.[9] This can be seen when toughening 100% TS1713, i.e. cement 1 (see Table 5.5).

The fracture toughness of 100% TS1713 increases by 14.3% and 17.8% with the addition of 10% and 20% untreated ABS respectively, reaching a peak increase of 18.7% with 30% ABS. Following this, further additions resulted in a decrease in toughness. However, the cement based on 50% B866 showed a slightly different change in fracture toughness with increasing ABS content (Table 5.6). The maximum/peak, 6.1%, increase in fracture toughness was obtained with only 10% untreated ABS, and was not significant ($p>0.05$). Further additions resulted in a decrease in toughness, eventually reducing the toughness of the material to below that of the original 50% B866 cement.

The reason for the untreated ABS being more effective in toughening 100% TS1713 than 50% B866 is unclear. The only difference between the cements is the different range of bead sizes (see Chapter 4, Section 4.3.1) and proportion of co-polymer. These may somehow limit the effect of the rubber toughening mechanisms. Another explanation could be the size of the rubber particles. Smaller diameter filler particles give rise to a maximum/peak increase in fracture toughness with a small volume fraction of particles, whereas large diameter particles require a larger volume fraction of particles to obtain a peak in fracture toughness. The smaller filler particles also result in a smaller increase in fracture toughness.[104] It is possible that the ABS particles used to toughen 50% B866 could have been smaller than the ABS particles used in 100% TS1713. Even though this seems unlikely, the initial change in fracture toughness of 50% B866 with increasing ABS does appear to follow this concept. The final decrease in fracture toughness could have been caused by rubber particles pulling away from the cement matrix thereby creating new voids. These voids would then act as crack initiation sites allowing new cracks to propagate, further reducing the overall toughness of the cement.

5.3.4 Flexural properties of cement containing silane-coated ABS

The flexural strength and moduli of cement (3) i.e. cement containing the PMMA TS1713 and silane-coated ABS are shown in Table 5.7. Given the problems incorporating 50% untreated ABS into cement (1) and (2), cements were only produced containing 10, 20, 30, and 40% silane-coated ABS.

Table 5.7: Flexural properties of TS1713 containing silane-coated ABS (cement 3)

Cement (3)		**Flexural Strength MPa**	**Flexural Modulus GPa**
Silane-coated ABS (wt %)	TS1713 (wt %)		
0	100	58.80 ± 4.26	2.44 ± 0.09
10	90	55.05 ± 5.58	2.35 ± 0.24
20	80	53.53 ± 2.90	2.07 ± 0.16
30	70	49.93 ± 2.86	1.88 ± 0.09
40	60	45.78 ± 3.61	1.77 ± 0.18

Again, the flexural modulus decreases with increasing amounts of silane-coated ABS. This decrease in modulus becomes statistically significant when 20% or more silane-coated ABS is added ($p<0.0005$). The values of the moduli are very similar to the values obtained with untreated ABS in cement (1) and there is no significant difference between the moduli of cement (3) and cement (1) with the same percentage of ABS ($p>0.05$).

Unlike cement (1), the flexural strength continually decreases with increasing amounts of silane-coated ABS, and a significant decrease is found when 30% silane-coated ABS ($p<0.01$) or 40% silane-coated ABS ($p<0.0005$) is present. Again, there is no significant difference in strength between cement (3) and cement (1) at the ABS percentages.

The change in load and displacement during testing, using one representative

sample of each formulation, is shown in Figure 5.3. Again, the decrease in strength with increasing amount of silane treated ABS, as signified by the reduction in maximum load, as well as the decrease in modulus, signified by the reduction of the initial gradient of the graph, can be seen. Figure 5.3 also shows the increased yielding, and therefore elongation, with increasing proportion of silane-coated ABS. Like the untreated ABS cement formulations shown in Figure 5.2, cements containing 30 and 40% silane treated ABS have deformed past their yield point.

Summary of the effect of silane-coated ABS particles on the flexural properties of an experimental cement

Adding silane-coated ABS particles had predominantly the same effect as adding untreated ABS particles. Again the inclusion of the silane-coated ABS particles resulted in the cement deforming and yielding before fracture. The effect is so similar to the untreated ABS that there is no statistical difference in either the flexural strength or modulus between cements containing silane-coated or untreated ABS particles. This is unexpected as the bonding between the ABS particles and the cement matrix should have required an increased force to break them, thereby increasing flexural strength. It is possible that the influence of the ABS particles on the deformation and yielding of the cement before fracture is so great that even when the particles are bonded to the matrix no significant increase in strength is seen.

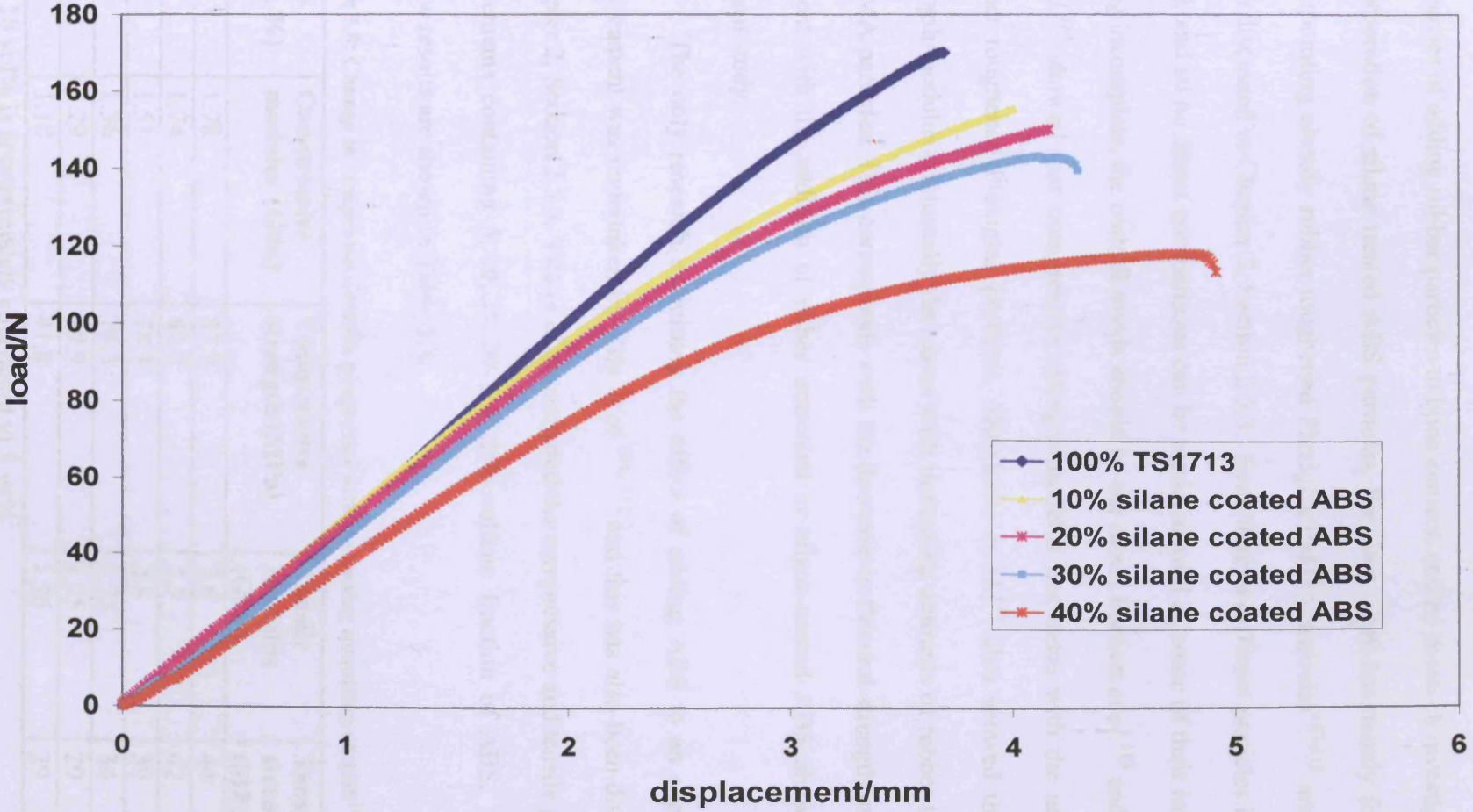

Figure 5.3: Load/displacement curves of TS1713 containing different weight percentages of silane coated ABS

Comparison with previous work by other authors

There has been very little previous work examining the effect on mechanical properties of adding rubber particles to bone cement, and no research investigating the incorporation of silane treated ABS particles. Previous work has mainly focused on incorporating already rubber toughened Plexiglas/PMMA particles[113-115] and this has been discussed in Chapter 2, Section 2.5.3. Even though different particles have been used, and so no direct comparisons can be made, as well as some of their information being incomplete, the overall trends should be the same. Puckett *et al.*[113] and Moseley *et al.*[114] showed that compressive strength/modulus decreases with the addition of rubber toughened Plexiglas particles. Murakami *et al.*[115] also showed that tensile strength/modulus continually decreases with increasing amounts of rubber toughened PMMA particles. This corresponds with the decrease in flexural strength/modulus of cement with the addition of either untreated or silane-coated ABS shown in this present study.

The only research examining the effect of adding ABS to an experimental bone cement was undertaken by Vila *et al.*[111, 112] and this has also been discussed in Chapter 2, Section 2.5.3. Vila *et al* investigated the compressive and tensile properties of cements containing 5, 10, 15, 20 and 25% volume fraction of ABS.

These results are shown in Table 5.8.

Table 5.8: Change in compressive/tensile properties with increasing quantities of ABS[110]

ABS (vol. %)	Compressive modulus (GPa)	Compressive strength (MPa)	Tensile modulus (GPa)	Tensile strength (MPa)
0	1.78	87.9	2.6	44
5	1.74	82.2	2.5	42
10	1.51	78.3	2.3	39
15	1.36	76.3	1.75	34
20	1.29	49.9	1.25	29
25	1.10	41.8	1.25	29

N.B 10 vol% is approximately equivalent to 8 wt%

Their results also show that both the tensile/compressive strengths and moduli decreased with increasing amounts of ABS, until the cement contained 20 volume % ABS. At this point, the further addition of ABS caused the compressive properties to continue decreasing but not the tensile properties, which remained the same.

It is difficult to compare the extent of the decrease in compressive/tensile properties with increasing quantity of ABS determined by Vila *et al.*,[111] with the decrease in flexural properties obtained in this work, as they are different mechanical properties. However, both this study and the work by Vila *et al.* work clearly show how effective ABS particles are in promoting yielding in an otherwise brittle bone cement.

5.3.5 Fracture toughness of cement containing silane-coated ABS

The fracture toughness of cements containing silane-coated ABS (cement 3) are shown in Table 5.9. Again the load/displacement curves generated during testing were examined to confirm that they still followed the criteria to calculate K_{IC}.

Table 5.9: Fracture toughness values of cement (3) containing silane-coated ABS

Cement (3)		**K_{IC} (MPa.m$^{1/2}$)**	**Increase in toughness**
Silane-coated ABS (wt. %)	TS1713 (wt. %)		
0	100	2.30 ± 0.12	-
10	90	2.62 ± 0.27	13.9%
20	80	2.70 ± 0.11	17.4%
30	70	2.87 ± 0.16	24.8%
40	60	3.02 ± 0.16	31.3%

The addition of silane-coated ABS greatly increases the fracture toughness of the original TS1713 cement. There is a continuous significant increase in fracture toughness with increasing amounts of silane-coated ABS ($p<0.005$) resulting in a 31.3% increase in fracture toughness with 40% silane-coated ABS ($p<0.0005$).

Comparison of TS1713 cements containing either untreated or silane-coated ABS

The fracture toughness of the TS1713 cements containing either untreated or silane-coated ABS are shown in Figure 5.4. All the cements have a greater fracture toughness than the original 100% TS1713 cement, with the fracture toughness of TS1713 containing silane-coated ABS continually increasing with increasing amounts of silane-coated ABS. The increase in toughness with 10% and 20% silane-coated ABS, at 13.9% and 17.4% respectively, is very similar to the increase found with 10% and 20% untreated ABS and as such there is no significant difference between their values ($p>0.05$). However, 30% silane-coated ABS increased toughness by 24.8% which greater, though not significantly ($p>0.05$) than the 18.7% increase produced with 30% untreated ABS. Whereas 40% silane-coated ABS increased fracture toughness by 31.3% which is significantly greater ($p=0.001$) than the 16.1% increase found with 40% untreated ABS. As samples were not made of 50% silane-coated ABS, given the earlier problems with incorporating 50% untreated ABS, it is impossible to determine if the fracture toughness would have continued to increase or if it would have peaked with 40% silane-coated ABS.

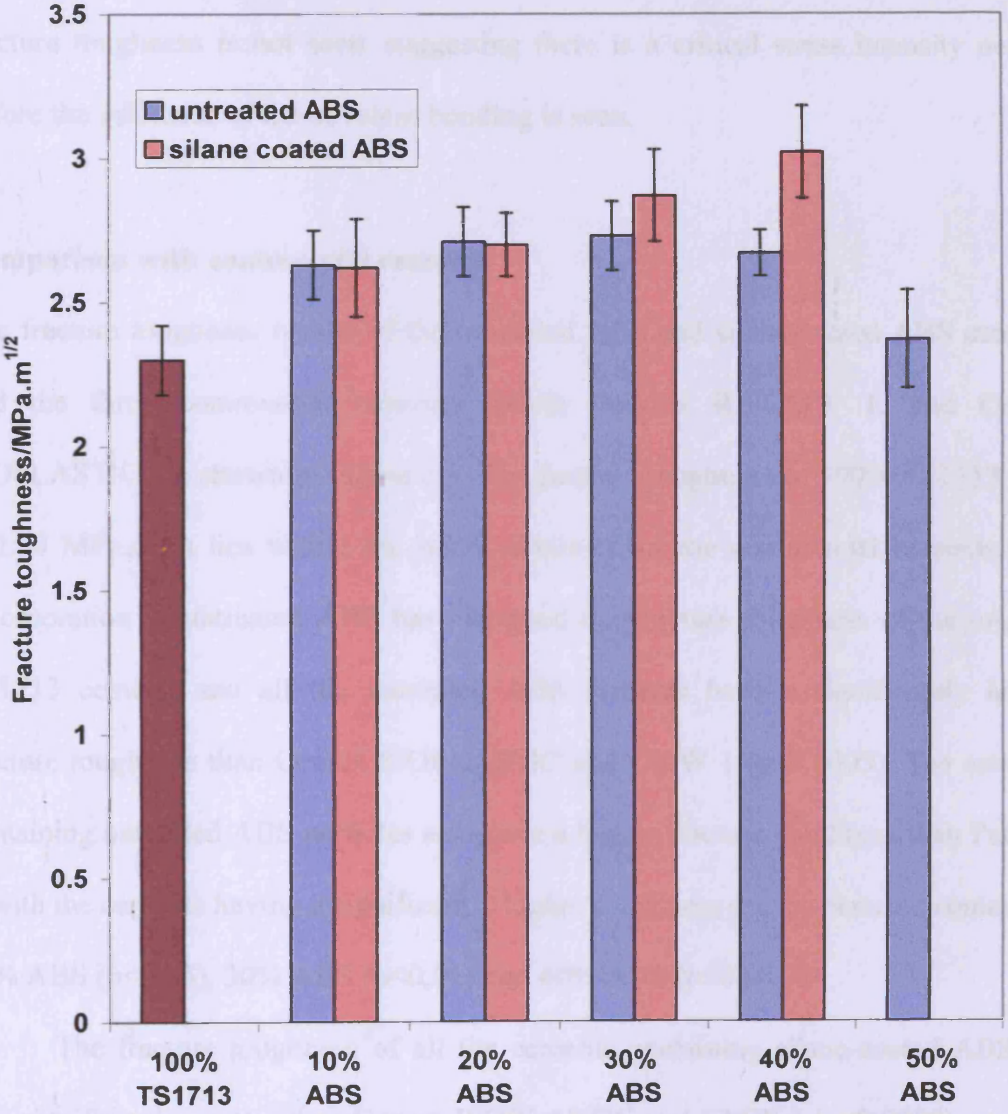

Figure 5.4: Fracture toughness of TS1713 cements containing untreated ABS or silane-coated ABS

It appears that surface treating the ABS with methacryloxypropyltrimethoxy-silane has further improved the fracture toughness of the cement containing 30% and 40% because of the covalent bonding between the ABS particles and the cement matrix. However, with the lower quantities of silane-coated particles this improvement in fracture toughness is not seen, suggesting there is a critical stress intensity needed before the influence of the covalent bonding is seen.

Comparison with commercial cements

The fracture toughness results of the untreated ABS and silane-coated ABS cements and the three commercial cements tested; Palacos R, CMW 1, and Cemex ISOPLASTIC are shown in Figure 5.5. The fracture toughness of 100% TS1713 (K_{IC} = 2.30 MPa.$m^{1/2}$) lies within the range obtained for the commercial cements. The incorporation of untreated ABS has increased the fracture toughness of the original TS1713 cement, and all the untreated ABS cements have a significantly higher fracture toughness than Cemex ISOPLASTIC and CMW 1 ($p<0.0005$). The cements containing untreated ABS particles also have a higher fracture toughness than Palacos R with the cements having a significantly higher toughness are the cements containing 20% ABS ($p<0.05$), 30% ABS ($p<0.01$) and 40% ABS ($p<0.05$).

The fracture toughness of all the cements containing silane-coated ABS are also significantly greater than Cemex ISOPLASTIC and CMW 1 ($p<0.0005$), and the cements having a significantly higher fracture toughness than Palacos R are 20% silane-coated ABS ($p<0.05$), 30% silane-coated ABS ($p<0.005$) and 40% silane-coated ABS ($p<0.0005$).

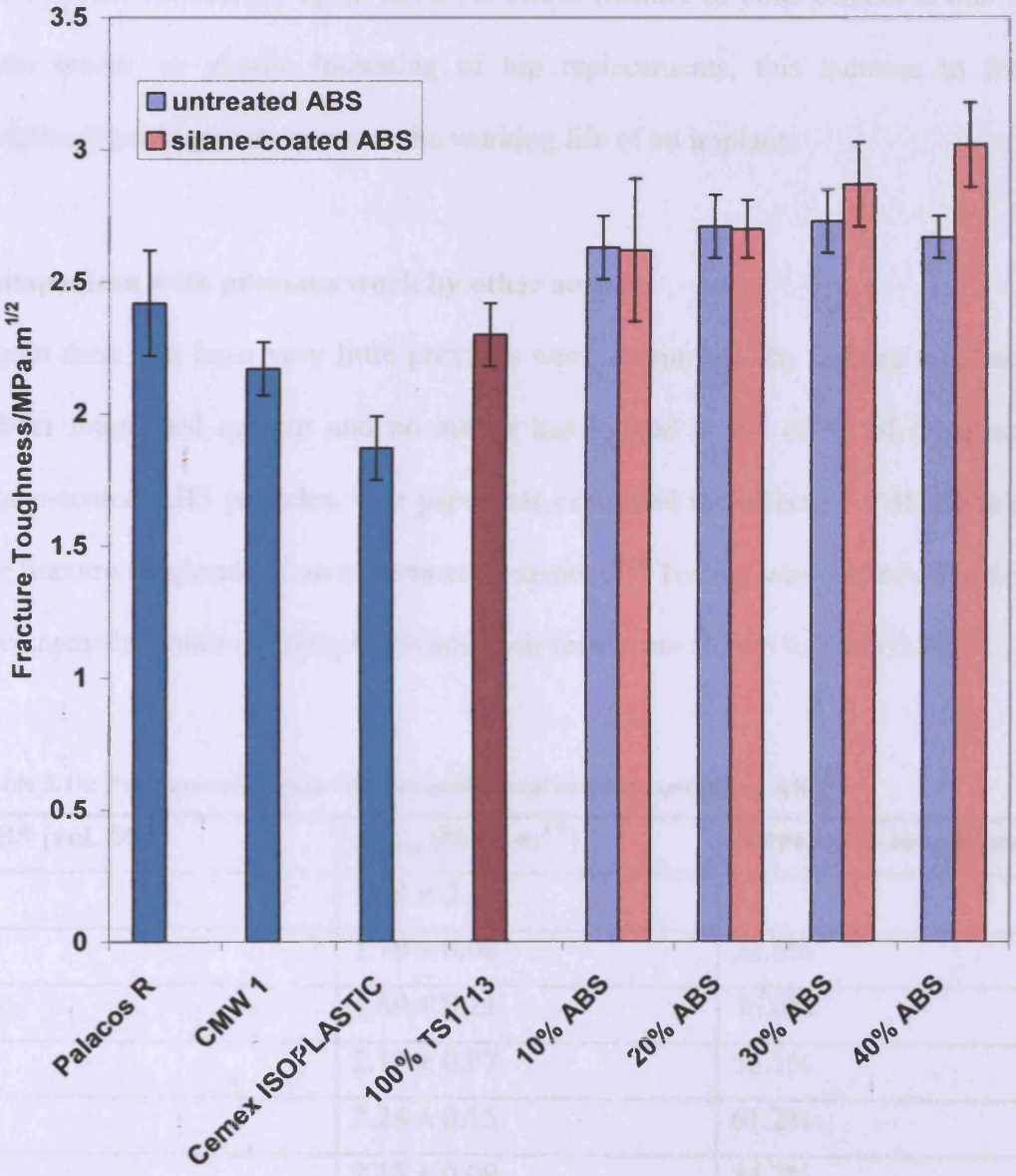

Figure 5.5: Fracture toughness of commercial cements and untreated/silane-coated ABS cements

The addition of 30 and 40% silane-coated ABS had a very pronounced effect on fracture toughness, with 40% silane-coated ABS increasing fracture toughness of the original TS1713 cement by over 30%. This shows, therefore, that the incorporation of 40% silane-coated ABS also has the potential to increase the fracture toughness of commercial cements by up to 30%. As brittle fracture of bone cement is one of the main causes of aseptic loosening of hip replacements, this increase in fracture toughness could greatly increase the working life of an implant.

Comparison with previous work by other authors

Again there has been very little previous work examining the fracture toughness of rubber toughened cement and no author has looked at the effect of incorporating silane-coated ABS particles. One paper has examined the effect of ABS particles on the fracture toughness of an experimental cement.[111] Testing was carried out using CT specimens in tensile opening mode and their results are shown in Table 5.10.

Table 5.10: Fracture toughness of an experimental cement containing ABS[111]

ABS (vol. %)	K_{1max} (MPa.m$^{1/2}$)	Increase in toughness
0	1.39 ± 0.13	-
5	1.70 ± 0.06	22.3%
10	1.89 ± 0.21	36.0%
15	2.17 ± 0.07	56.1%
20	2.24 ± 0.15	61.2%
25	2.15 ± 0.09	54.7%

Their results also show fracture toughness increasing with increasing ABS content, reaching a peak increase of 61.2% with 20% ABS. Following this there was a decrease in fracture toughness with 25% ABS. The quantity of ABS required in their experimental cements to achieve the maximum increase in fracture toughness was 20%. This lies in between the quantity required for maximum toughness in 100% TS1713 (30% ABS) and 50% B866 (10% ABS). Their experimental cements also had a much greater increase in toughness with the incorporation of ABS than were obtained in this study. These differences can be accounted for by the different brand and hence particle sizes, of the ABS (ABS T-723) and PMMA powder (Rostal), as well as the different testing method employed. The particles sizes of the ABS are unknown, but the average particle size of the PMMA beads are 60μm which is larger than the average PMMA beads used in 100% TS1713 and 50% B866, with no indication given of the range.

Other authors[115, 116] have shown an increase in fracture toughness with the addition of rubber-toughened PMMA particles into commercial cement. Murakami *et al.*[115] found that the fracture toughness of CMW increased by 16.5% with the addition of 50% rubber toughened PMMA and Perek and Pilliar[116] showed that the fracture toughness of Zimmer continually increased when 10, 20, 30 and 40% rubber-toughened PMMA was added. Although not directly relevant, their work does indicate that incorporating some form of rubber compound will increase the fracture toughness of bone cement.

SEM examination of fracture surfaces following fracture toughness testing

Figure 5.6 shows the fracture surface of TS1713 containing 30% untreated ABS particles and it is very different from the fracture surface obtained with no ABS present (Chapter 4, Figure 4.19). Here the surface is very rough with no cleaved PMMA beads, implying that the cement has deformed in a more ductile like manner. The ABS particles have essentially acted as stress concentrators which facilitate local yielding resulting in the uneven surface. There are whole PMMA beads present, and the crack has preferentially propagated through the PMMA matrix around the PMMA beads and ABS particles. As the crack has undertaken a more convoluted path through the cement thereby increasing its surface area, more energy is required for crack propagation which corresponds with its high fracture toughness value.

The fracture surface of TS1713 containing 40% untreated ABS (Figure 5.7) clearly shows the ABS particles protruding from its surface. The corresponding fracture surface would therefore contain voids where the ABS particles had pulled out of the surface. The ABS particles themselves have a slightly irregular dimpled surface morphology. Again the fracture surface is rough and no cleaved PMMA beads can be seen, suggesting the crack has propagated in a more tortuous manner which would correspond with its high fracture toughness value.

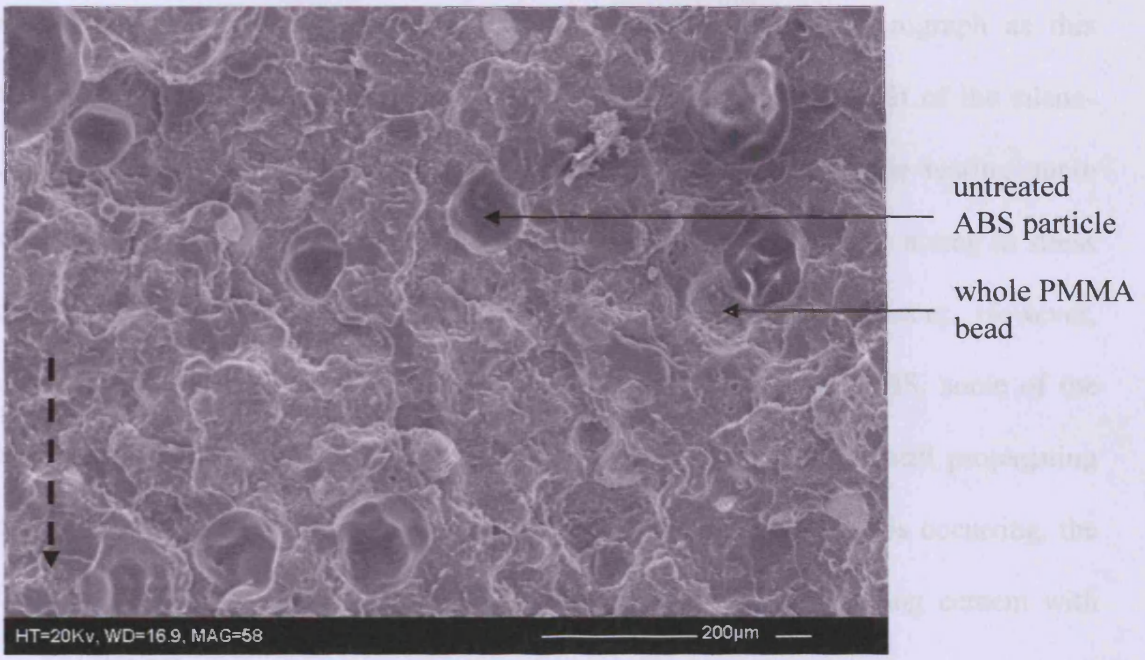

Figure 5.6: Fracture surface of TS1713 cement containing 30% untreated ABS magnification x 58. Direction of crack propagation is indicated by the dashed arrow.

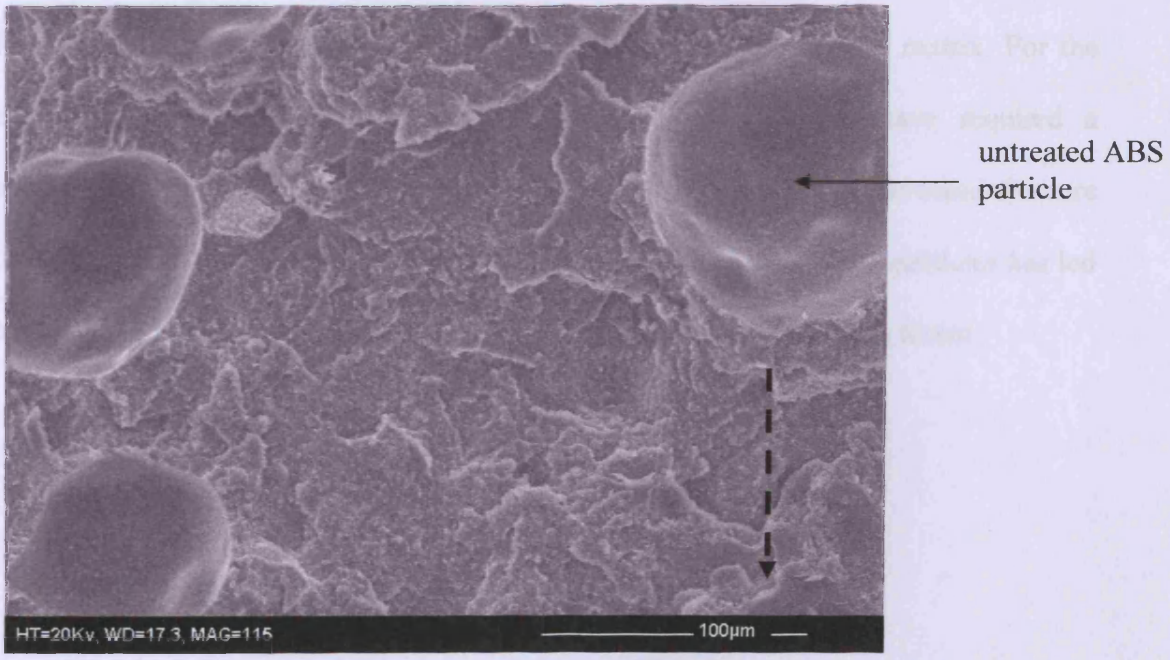

Figure 5.7: Fracture surface of TS1713 cement containing 40% untreated ABS magnification x 115

Figure 5.8 shows the fracture surface of cement TS1713 containing 30% silane-coated ABS. There are no ABS particles shown on this particular micrograph as this micrograph best represents changes in the PMMA matrix as a result of the silane-coated ABS particles. The fracture surface very rough with ductile tearing again showing that the ABS particles have promoted plastic deformation by acting as stress concentrators, resulting in the crack propagating in a tortuous manner. However, unlike the fracture surfaces of the cements containing untreated ABS, some of the PMMA beads have been cleaved, and this shows that the crack is still propagating directly through the PMMA beads in some areas. Even though this is occurring, the fracture toughness of this cement was greater than the corresponding cement with untreated ABS.

The fracture surface of the cement TS1713 with 40% silane-coated ABS is shown in Figure 5.9, and again this surface is very rough as a result of plastic deformation. The main feature of this surface is the cleaved ABS particle. This shows how well the silane-coated ABS particle has bonded to the cement matrix. For the crack to propagate directly through the ABS particle would have required a substantial increase in fracture energy, G_c, and this in turn has increased fracture toughness. The combination of plastic deformation and cleaved ABS particles has led to this cement having the highest fracture toughness of all the cements tested.

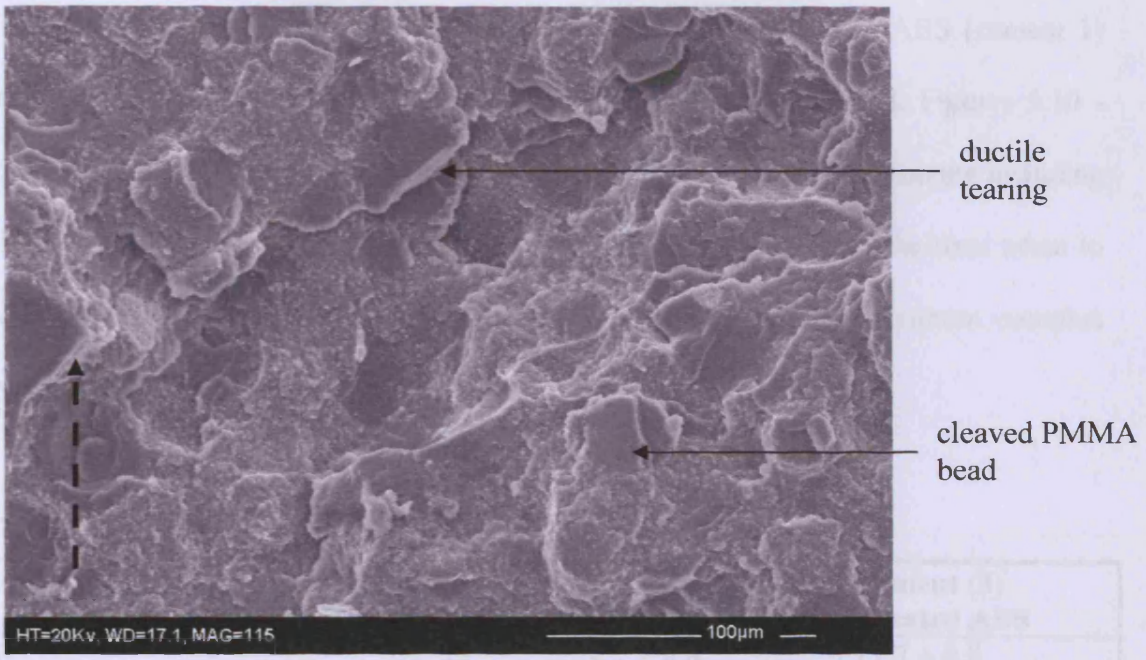

Figure 5.8: Fracture surface of TS1713 cement containing 30% silane-coated ABS magnification x 115

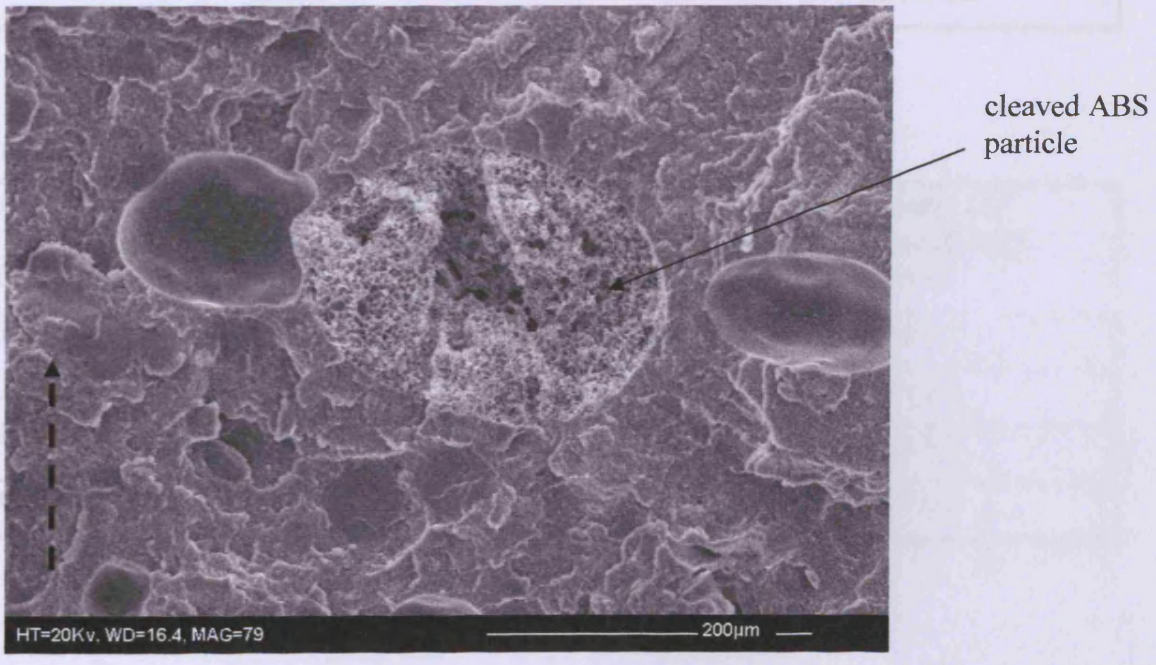

Figure 5.9: Fracture surface of TS1713 cement containing 40% silane-coated ABS magnification x 77

5.3.6 Rheology

The rheological properties of cements containing 10, 20, 30, 40% ABS (cement 1) and 10, 20, 30, 40% silane-coated ABS (cement 3) were examined. Figures 5.10 - 5.13 show how the complex viscosity changes with time for all the cements including 100% TS1713 both at 25°C and 37°C. Tables 5.11 and 5.12 show the time taken to cure at both temperatures and Tables 5.13 and 5.14 show the maximum complex viscosity of each cement

Table 5.11: Curing time in minutes at 25°C

ABS (%)	TS1713 (%)	Cement (1) Untreated ABS	Cement (3) Treated ABS
0	100	11.7 ± 0.8	11.7 ± 0.8
10	90	13.1 ± 0.1	13.7 ± 0.3
20	80	12.2 ± 0.2	13.0 ± 0.2
30	70	11.6 ± 0.2	12.8 ± 0.3
40	60	10.8 ± 0.1	12.4 ± 0.2

Table 5.12: Curing time in minutes at 37°C

ABS (%)	TS1713 (%)	Cement (1) Untreated ABS	Cement (3) Treated ABS
0	100	4.9 ± 0.2	4.9 ± 0.2
10	90	5.5 ± 0.2	5.9 ± 0.2
20	80	5.4 ± 0.1	5.6 ± 0.2
30	70	5.7 ± 0.1	5.7 ± 0.1
40	60	5.7 ± 0.1	6.0 ± 0.1

Table 5.13: Maximum complex viscosity/Pa.s x 10^3 at 25°C

ABS (%)	TS1713 (%)	Cement (1) Untreated ABS	Cement (3) Treated ABS
0	100	57.7 ± 0.73	57.7 ± 0.73
10	90	60.1 ± 0.09	76.9 ± 0.81
20	80	58.0 ± 1.05	78.0 ± 1.51
30	70	59.0 ± 0.27	75.1 ± 0.97
40	60	58.3 ± 0.92	76.4 ± 1.87

Table 5.14: Maximum complex viscosity/Pa.s x 10^3 at 37°C

ABS (%)	TS1713 (%)	Cement (2) Untreated ABS	Cement (3) Treated ABS
0	100	59.0 ± 0.79	59.0 ± 0.79
10	90	56.5 ± 1.08	76.2 ± 1.27
20	80	57.7 ± 0.69	75.6 ± 1.70
30	70	57.4 ± 0.26	76.4 ± 1.00
40	60	58.7 ± 0.93	75.3 ± 1.32

The results show that at 25°C, 100% TS1713 takes 11.7 minutes to cure, and reaches a maximum complex viscosity of 57.7 Pa.s. The addition of 10% untreated ABS, significantly increases the curing time to 13.1 minutes ($p<0.0005$). By further increasing the amount of ABS present, the overall curing time gradually decreases, with 40% untreated ABS taking 10.8 minutes to cure. For all of these cements (cement 1), the maximum complex viscosity remained unchanged (i.e. approximately 60 x 10^3 Pa.s). This and the change in viscosity with time for these cements are shown in Figure 5.10.

The effect of adding 10% silane-coated ABS to the original TS1713 cement is shown in Figure 5.11. Again, the time taken to cure (13.7 minutes) has significantly

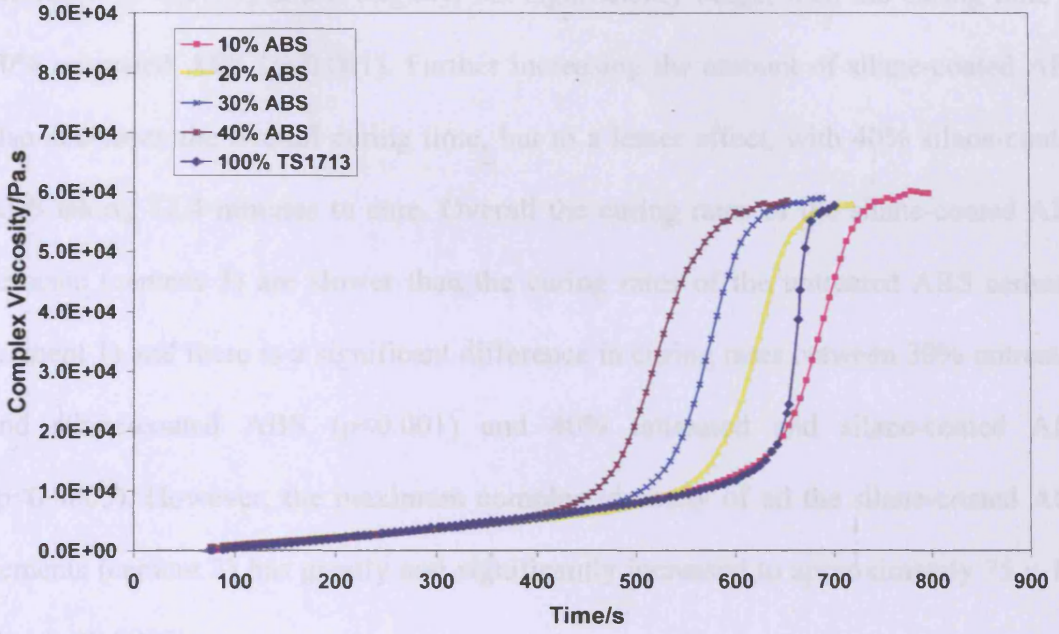

Figure 5.10: Change in complex viscosity during curing of cements containing untreated ABS at 25°C

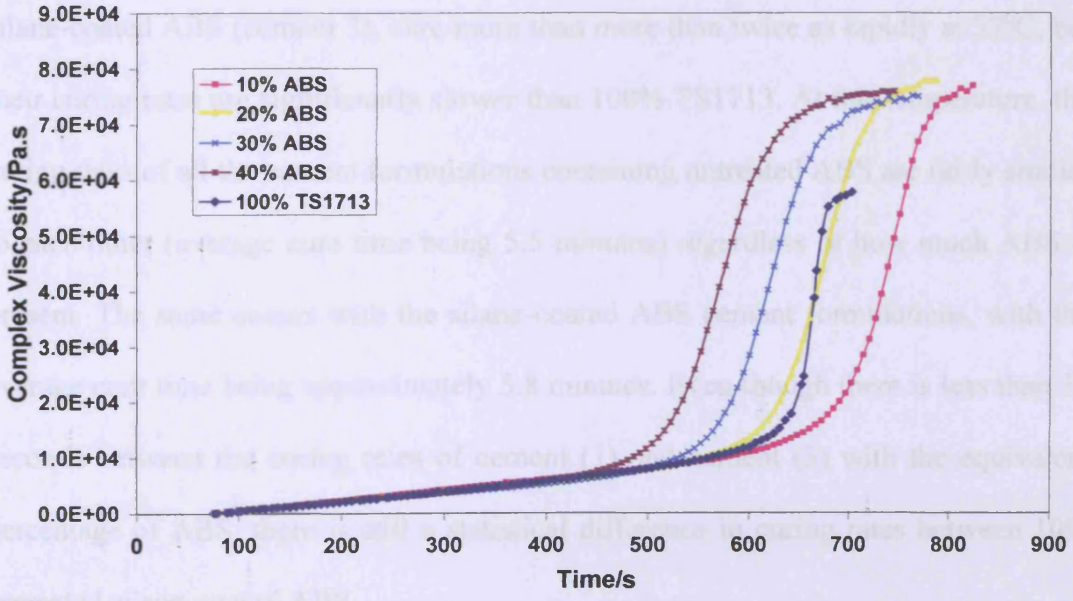

Figure 5.11: Change in complex viscosity with time of cements containing silane-coated ABS at 25°C

increased ($p<0.0005$) and is slightly, but significantly longer than the curing time of 10% untreated ABS ($p<0.001$). Further increasing the amount of silane-coated ABS also decreases the overall curing time, but to a lesser effect, with 40% silane-coated ABS taking 12.4 minutes to cure. Overall the curing rates of the silane-coated ABS cements (cement 3) are slower than the curing rates of the untreated ABS cements (cement 1) and there is a significant difference in curing rates between 30% untreated and silane-coated ABS ($p<0.001$) and 40% untreated and silane-coated ABS ($p<0.0005$). However, the maximum complex viscosity of all the silane-coated ABS cements (cement 3) has greatly and significantly increased to approximately 75×10^3 Pa.s ($p<0.0005$).

As expected, at 37°C, all the cements cure at a significantly much faster rate, $p<0.0005$, (see Table 5.10). 100% TS1713 cures almost 2.5 times as rapidly at 37°C, taking only 4.9 minutes. Both the cements containing untreated ABS (cement 1), and silane-coated ABS (cement 3), cure more than more than twice as rapidly at 37°C, but their curing rates are significantly slower than 100% TS1713. At this temperature, the curing rates of all the cement formulations containing untreated ABS are fairly similar to each other (average cure time being 5.5 minutes) regardless of how much ABS is present. The same occurs with the silane-coated ABS cement formulations, with the average cure time being approximately 5.8 minutes. Even though there is less than 30 seconds between the curing rates of cement (1) and cement (3) with the equivalent percentage of ABS, there is still a statistical difference in curing rates between 10% untreated silane-coated ABS.

The maximum complex viscosity of all the cements, however, remains unchanged by the increase in temperature (see Figures 5.12 and 5.13).

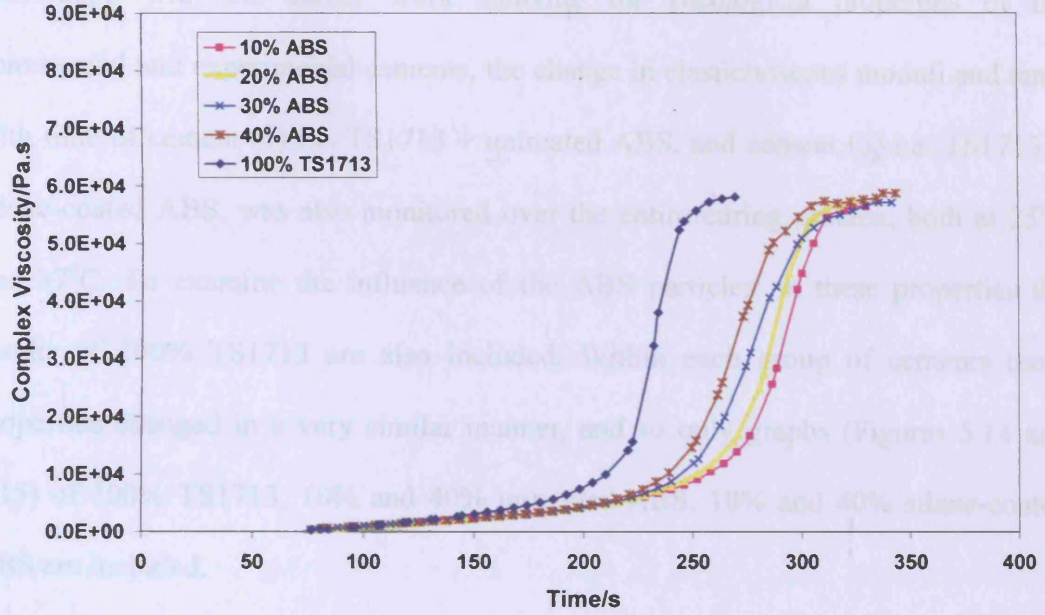

Figure 5.12: Change in complex viscosity during curing of cements containing untreated ABS at 37°C

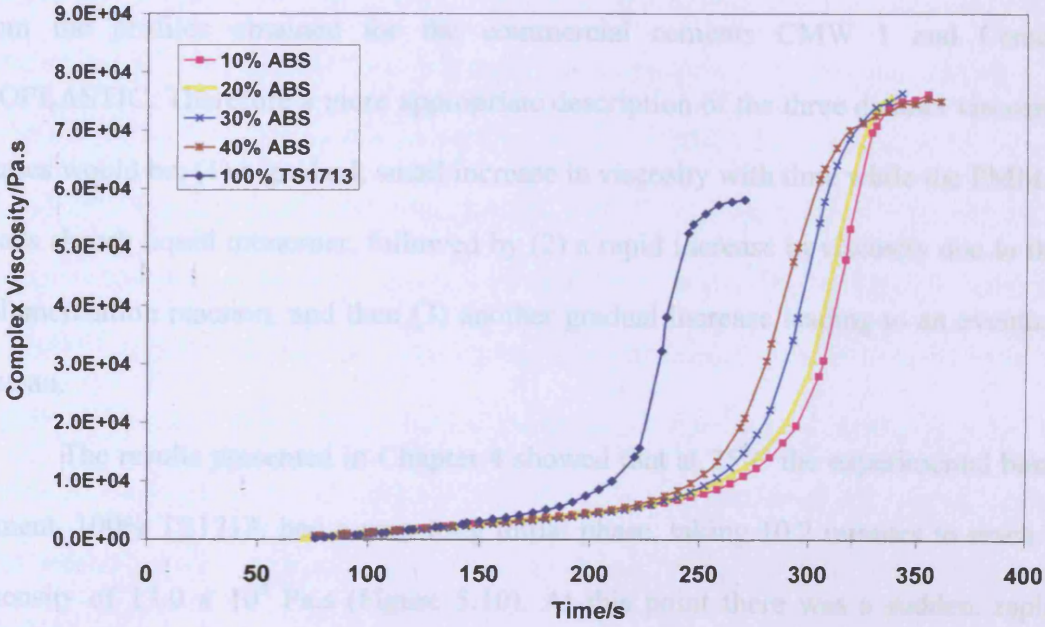

Figure 5.13: Change in complex viscosity during curing of cements containing silane-coated ABS at 37°C

Continuing with the earlier work studying the rheological properties of the commercial and experimental cements, the change in elastic/viscous moduli and tan δ with time of cement (1) i.e. TS1713 + untreated ABS, and cement (3) i.e. TS1713 + silane-coated ABS, was also monitored over the entire curing process, both at 25°C and 37°C. To examine the influence of the ABS particles on these properties the results of 100% TS1713 are also included. Within each group of cements these properties changed in a very similar manner, and so only graphs (Figures 5.14 and 5.15) of 100% TS1713, 10% and 40% untreated ABS, 10% and 40% silane-coated ABS are included.

Analysis of rheological properties

The viscosity profiles of all the cements (Figures 5.10-5.13) are very similar to each other, and the commercial cement Palacos R. However, they are significantly different from the profiles obtained for the commercial cements CMW 1 and Cemex ISOPLASTIC. Therefore a more appropriate description of the three distinct viscosity phases would be; (1) a gradual, small increase in viscosity with time while the PMMA beads absorb liquid monomer, followed by (2) a rapid increase in viscosity due to the polymerization reaction, and then (3) another gradual increase leading to an eventual plateau.

The results presented in Chapter 4 showed that at 25°C the experimental bone cement, 100% TS1713, had a very long initial phase, taking 10.2 minutes to reach a viscosity of 13.0 x 10^3 Pa.s (Figure 5.10). At this point there was a sudden, rapid increase in viscosity as the cement polymerized (cured) taking only a further 70 seconds to reach a viscosity of 56.3 x 10^3 Pa.s. This was followed by a final small increase in viscosity over a very short time period (20 seconds).

Adding 10% untreated ABS to the cement had no effect on the initial increase

in viscosity, it still took 10.2 minutes to reach 13.0 x 10^3 Pa.s (see Figure 5.10). However, the second rapid increase in viscosity (the polymerization reaction) was more gradual, taking almost twice as long (120 seconds) to reach a viscosity of 56.8 x 10^3 Pa.s. The final gradual increase in viscosity was also more pronounced, this time taking a further 50 seconds to reach its maximum viscosity of 60.1 x 10^3 Pa.s. Given that the second and third viscosity phases (curing phases) were longer, the overall curing rate was longer when the cement contains 10% untreated ABS.

Figure 5.10 also shows the effect of adding 20%, 30% and 40% untreated ABS on the viscosity and overall curing rate. For all of these cement formulations, the second and third viscosity phases were very similar to the second and third phases of the 10% ABS cement. However, increasing the amount of ABS present decreased the initial viscosity phase, leading to a decrease in the overall curing time. It is evident that the introduction of ABS particles into the cement has affected both the initial increase in viscosity and the final polymerization reaction. The decrease in the initial viscosity phase was due to the change in the 2:1 PMMA powder/liquid monomer ratio. Replacing part of the PMMA powder with ABS means there is less PMMA powder reacting with the same amount of liquid monomer. This effectively leads to the PMMA beads swelling more rapidly and so decreasing the overall curing time. It is also likely that the presence of ABS particles is somehow inhibiting or slowing down the benzoyl peroxide initiator and/or N, N-dimethyl-p-toluidine accelerator from reacting with the liquid monomer, which results in the final polymerization reaction taking longer.

The viscosity profiles of the cements containing silane-coated ABS at 25°C (see Figure 5.11) are very similar to those obtained for the untreated ABS. The most striking difference was the increase in the maximum viscosity, almost 80 x 10^3 Pa.s compared with 60 x 10^3 Pa.s for the untreated ABS. Pre-treating the ABS has

incorporated a methacrylate functional silane onto the surface of the rubber particles. This methacrylate portion chemically interacts with the cement taking part in the polymerization reaction and enables the ABS to become a chemically bonded reinforcing agent. This interaction of the silane-coated ABS particles leads to an increase in the viscosity of the cement in comparison to the untreated ABS. The maximum viscosity of the cements with silane-coated ABS was slightly greater than the commercial cements Palacos R, CMW 1 and Cemex ISOPLASTIC.

At 37°C all the cements cure at a much faster rate which is to be expected. The increase in temperature causes the polymer beads to absorb the liquid monomer and swell more rapidly, as well as increasing the rate of polymerization. The change in viscosity with time at 37°C of 100% TS1713 and the cement formulations containing untreated ABS and silane-coated ABS are shown in Figures 5.12 and 5.13 respectively.

The viscosity profile of 100% TS1713 at 37°C is essentially very similar to the 25°C profile except the initial increase in viscosity region was much shorter. This is also true for all the untreated and treated ABS formulation cements, however, as the curing reaction is now so much faster, the difference in the rate of cure within each cement formulation group is much smaller, leading to all the untreated ABS cements curing in approximately 5.5 minutes and all the treated ABS cements curing in 5.8 minutes. This shows that the increase in temperature has a much larger effect on the rate of cure than any change in the powder PMMA/liquid monomer ratio.

The changes in elastic/viscous modulus and tan δ with time (Figures 5.14 and 5.15) follow a similar trend to the previous cements tested i.e. both the elastic (storage) modulus and viscous (loss) modulus initially increase with time, with the elastic modulus increasing much more rapidly as the cement changes from being a viscous liquid to an elastic solid. The peak in the viscous modulus occurs during the

transition of the cement and more details about this behaviour is given in Chapter 3, Section 3.3.5.

For 100% TS1713, the initial increase in the viscous and elastic modulus were very similar to those obtained for Palacos R, but the final stage of curing, with the sudden peak in viscosity modulus and rapid increase in elastic modulus, was similar to CMW 1. However, the maximum elastic modulus was approximately 1.8 x 10^6 Pa compared to 2.4 x 10^6 Pa for commercially available cements.

By adding untreated ABS the changes in elastic/viscous moduli show the same characteristics as Palacos R over the entire curing process. There was also no change in the maximum elastic modulus, it remains at 1.8 x 10^6 Pa. The profiles are very similar for all this group of cements (and so only the graphs of the cements containing 10% ABS and 40% ABS are shown here), but obviously take place faster with increasing amounts of ABS due to an increased ratio of monomer to PMMA powder.

Adding silane-coated ABS increased the maximum elastic modulus to 2.5 x 10^6 Pa, which is comparable with, if not greater than, the maximum elastic modulus for commercial cements. Again this is due to the methacrylate portion of the silane coupling agent bonding with the polymeric matrix, thereby acting as a reinforcing agent. The changes in elastic/viscous moduli for this group of cements also show the same characteristics as Palacos R over the whole curing process.

The curing rates of all the experimental cements are comparable with commercially available cements, both at 25°C and 37°C. However, only the cements containing silane-coated ABS have a maximum viscosity and maximum elastic modulus similar to the commercial cements, CMW 1, Palacos R and Cemex ISOPLASTIC, with 40% silane-coated ABS showing the closest rheological/handling properties to Palacos R

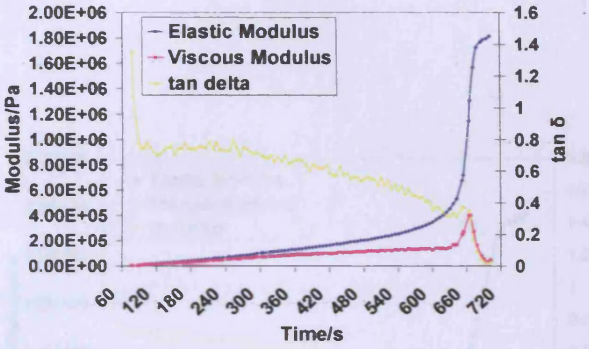

Figure 5.14a: 100% TS1713 at 25°C

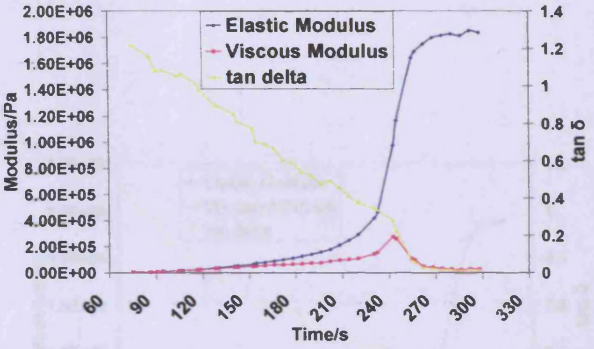

Figure 5.14b: 100% TS1713 at 37°C

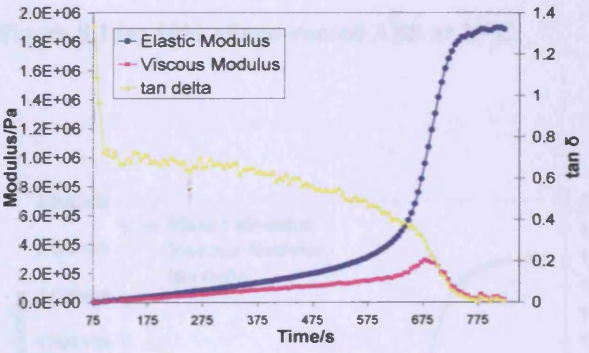

Figure 5.14c: 10% untreated ABS at 25°C

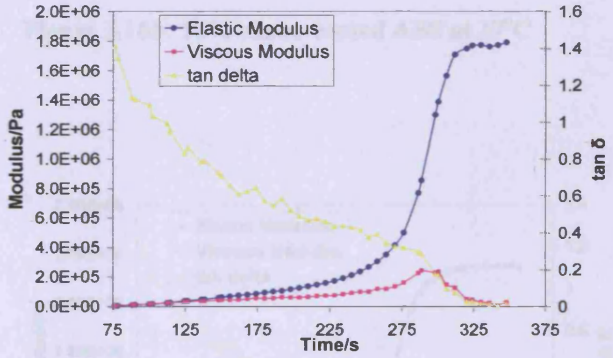

Figure 5.14d: 10% untreated ABS at 37°C

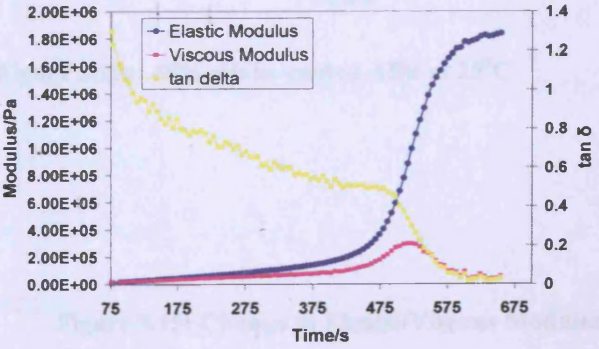

Figure 5.14e: 40% untreated ABS at 25°C

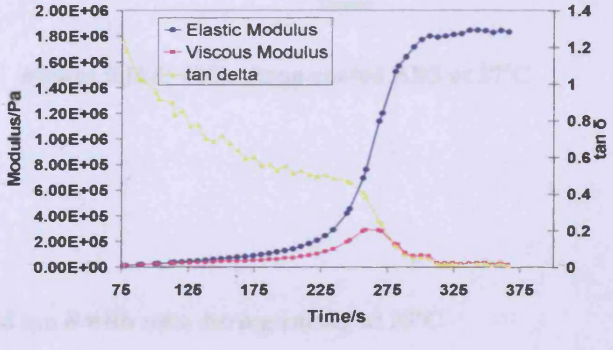

Figure 5.14f: 40% untreated ABS at 37°C

Figure 5.14: Change in Elastic/Viscous Modulus and tan δ with time during curing at 25°C and 37°C of 100% TS1713, and cements containing 10% and 40% untreated ABS

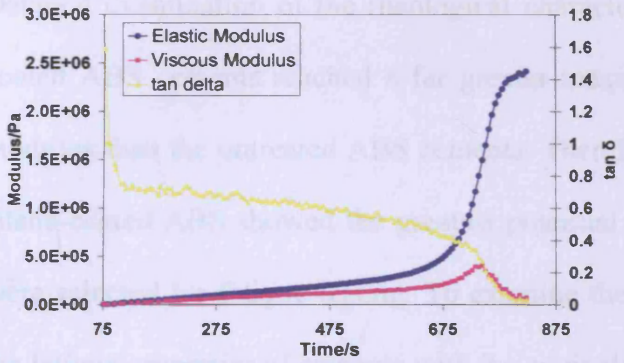

Figure 5.16a: 10% silane-coated ABS at 25°C

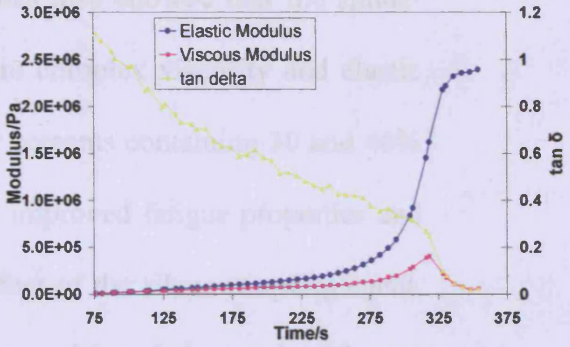

Figure 5.16b: 10% silane-coated ABS at 37°C

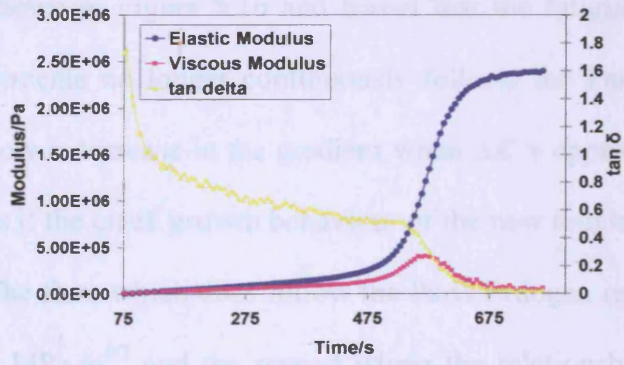

Figure 5.16c: 40% silane-coated ABS at 25°C

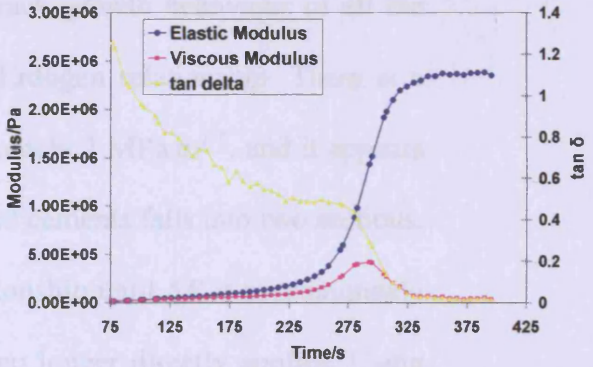

Figure 5.16d: 40% silane-coated ABS at 37°C

Figure 5.15: Change in Elastic/Viscous Modulus and tan δ with time during curing at 25°C and 37°C of cements containing 10% and 40% silane-coated ABS

5.3.7 Fatigue

The results from the fracture toughness testing revealed that the cements containing 30 and 40% silane-coated ABS had the greatest improvement in fracture toughness. Detailed examination of the rheological characteristics also showed that the silane-coated ABS cements reached a far greater maximum complex viscosity and elastic modulus than the untreated ABS cements. Therefore cements containing 30 and 40% silane-coated ABS showed the greatest potential for improved fatigue properties and were selected for fatigue testing. To examine the effect of the silane coupling agent, the fatigue properties of cements with the equivalent quantities of untreated ABS were also tested.

The results of the fatigue testing of one sample of each type of cement are shown in Figure 5.16 and reveal that the fatigue crack growth behaviour of all the cements no longer continuously follows the Paris Erdogan relationship. There is a now a decrease in the gradient when ΔK = approximately 2 MPa.m$^{1/2}$, and it appears as if the crack growth behaviour of the new toughened cements falls into two sections. The first, which does follow the Paris Erdogan relationship until ΔK = approximately 2 MPa.m$^{1/2}$ and the second where the relationship no longer directly applies. Using Figure 5.25, the fatigue crack growth rate parameters have been calculated over the stress intensity factor range 0.5 - 2.0 MPa.m$^{1/2}$ which is approximately the same stress intensity range in which the fatigue cracks propagated through the commercial and experimental cements. The resultant crack propagation parameters of all the samples are shown in Table 5.15 along with the average parameters for the cement 100% TS1713.

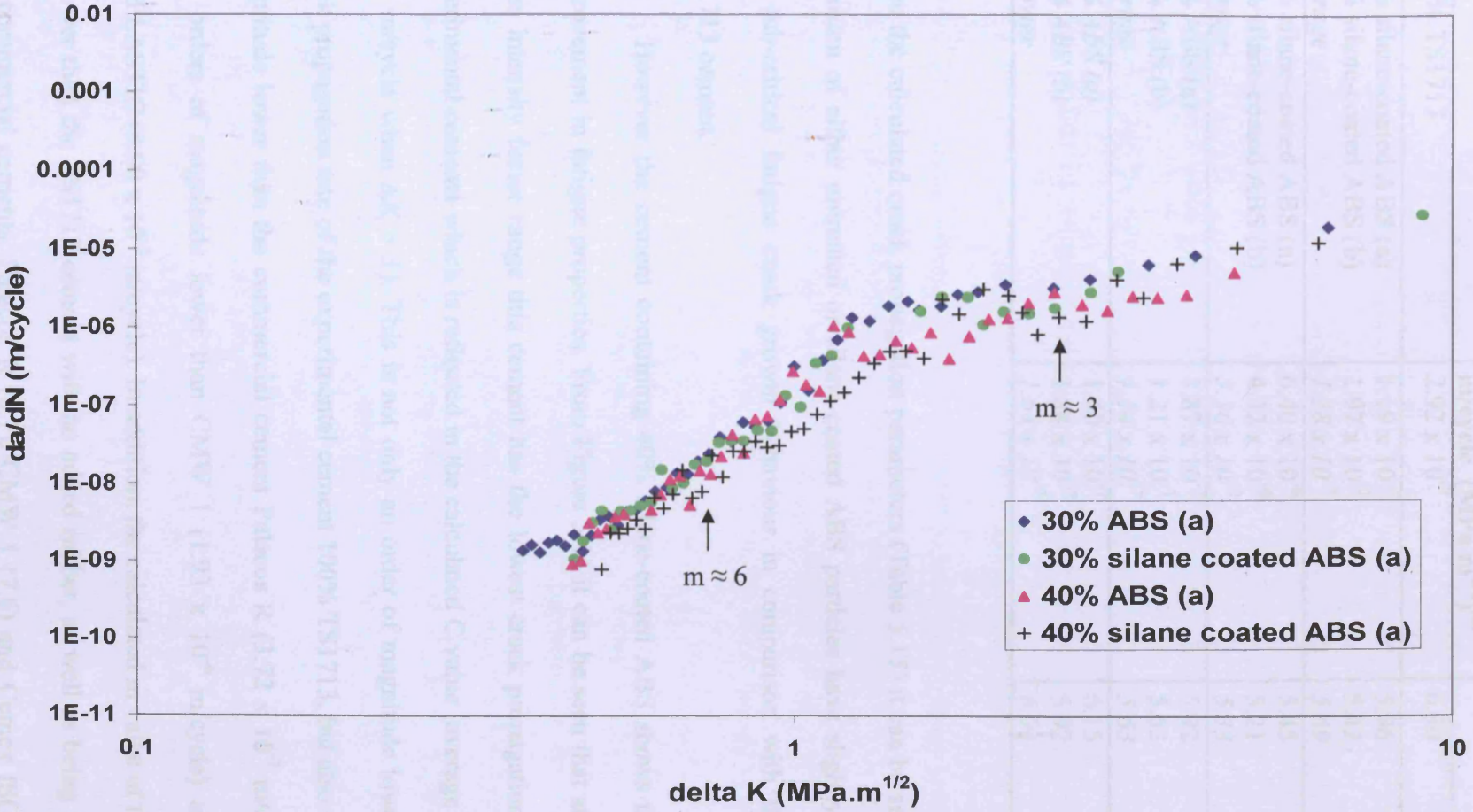

Figure 5.16: Fatigue crack growth rate, d*a*/d*N*, plotted against the stress intensity range, delta *K*, for cements containing 30% and 40% untreated/silane coated ABS

Table 5.15: Fatigue crack propagation rate parameters

Cement	Crack growth rate, C, m/cycle $(MPa\ m^{1/2})^{-m}$	m	R^2
100% TS1713	2.92×10^{-7}	6.30	0.99
30% silane-coated ABS (a)	1.19×10^{-7}	5.96	0.95
30% silane-coated ABS (b)	1.97×10^{-7}	5.42	0.93
Average	*1.58×10^{-7}*	*5.69*	
40% silane-coated ABS (a)	6.40×10^{-8}	5.45	0.98
40% silane-coated ABS (b)	4.32×10^{-8}	5.21	0.95
Average	*5.36×10^{-8}*	*5.33*	
30% ABS (a)	1.87×10^{-7}	5.92	0.98
30% ABS (b)	1.21×10^{-7}	5.63	0.96
Average	*1.54×10^{-7}*	*5.63*	
40% ABS (a)	1.40×10^{-7}	6.15	0.95
40% ABS (b)	1.88×10^{-7}	5.92	0.91
Average	*1.64×10^{-7}*	*6.04*	

From the calculated crack propagation parameters (Table 5.15) it can be seen that the inclusion of either untreated or silane-coated ABS particles have slightly improved the sub-critical fatigue crack growth behaviour in comparison with the original TS1713 cement.

However the cement containing 40% silane-coated ABS shows the greatest improvement in fatigue properties. From Figure 5.16 it can be seen that at any given stress intensity factor range this cement has the lowest crack propagation of all the experimental cements which is reflected in the calculated C value (average C = 5.36×10^{-8} m/cycle when $\Delta K = 1$). This is not only an order of magnitude lower than the crack propagation rate of the experimental cement 100% TS1713, but also an order of magnitude lower than the commercial cement Palacos R (3.72×10^{-7} m/cycle), and two orders of magnitude lower than CMW 1 (1.93×10^{-6} m/cycle) and Cemex ISOPLASTIC (8.90×10^{-6} m/cycle). In addition, the calculated m value of this cement is lower than the TS1713 cement with no added rubber, as well as being lower than the commercial cements, Palacos R (6.7), CMW 1 (7.6) and Cemex ISOPLASTIC

(7.4). This signifies that the incorporation of 40% silane-coated ABS particles is also reducing the acceleration of the propagating crack.

The crack growth behaviour of the cements containing 30% untreated ABS, 40% untreated ABS or 30% silane-coated ABS during this initial section, may only show a as small improvement in comparison with 100% TS1713, but it is still more favourable than the three commercial cements.

The most interesting fatigue behaviour is during the second section of the graph i.e. when the stress intensity factor range lies between 2 and 9 MPa.m$^{1/2}$. Usually unstable crack growth occurs resulting in the fracture of bone cement before ΔK = 2 MPa.m$^{1/2}$. [60, 73] However, the cements containing 30 and 40% untreated or silane-coated ABS particles are able to withstand much higher stress intensities, and whilst the crack propagation rate still increases it does so at a much slower rate (m $\approx$ 3), finally fracturing when ΔK is between 5 and 9 MPa.m$^{1/2}$. These cements, therefore, have a far superior fatigue resistance than any of the experimental or commercial cements tested.

It appears as if the maximum stress intensity factor (K_{max}) has to reach a certain critical level (given by the inflection on the graph) before the triaxial stress concentrations at the equators of the rubber particles are sufficient to induce crazing and planar dilatation bands throughout the cement matrix. These crazes and planar dilatation bands (toughening mechanisms) result in a reduction in the crack propagation rate.

The critical maximum stress intensity factor when the toughening mechanisms begin to take effect is approximately 1.5 MPa.m$^{1/2}$, and this is when the cement without rubber particles, i.e. 100% TS1713, is on the verge of fracture. In the ABS toughened cements, crack propagation continues until the maximum stress intensity

factor reaches between 6 MPa.m$^{1/2}$ (40% untreated ABS) and 10 MPa.m$^{1/2}$ (30% silane-coated ABS) when fracture finally occurs. Effectively there has been a dramatic increase in the fatigue resistance of the cement, with the cements showing a minimum three-fold and maximum five-fold increase in fatigue resistance.

It is difficult to determine at this preliminary stage which type or amount of ABS particles would be the most effective to use. However the fact that all four cement formulations containing either untreated or silane-coated ABS particles have shown greatly improved fatigue properties is very encouraging. It is reasonable to say therefore, that these results could have huge implications for bone cement used in a clinical situation. The ABS containing cements can not only withstand longer, faster growing cracks thereby increasing the fatigue life of the cement, but can also tolerate much larger stresses. This means that when in use, for example in a hip prosthesis, the cement could survive a sharp increase in stress as a result of a fall, which would otherwise lead to fracture of the cement.

Given the novelty of this work it is not possible to directly compare these fatigue results with work by other authors. There is no published data on the addition of ABS particles in these quantities or on the addition of silane-coated ABS particles. However, Vila *et al.*[112] did examine the fatigue crack growth rate of an experimental cement containing 10 vol.% ABS and even though their results showed an improvement in the fatigue parameters their cement fractured when $\Delta K \approx 1$ MPa.m$^{1/2}$. The most likely explanation for this is that not enough ABS was incorporated into the cement to induce extensive toughening mechanisms.

5.3.8 SEM examination of fracture surfaces following fatigue testing

Figure 5.17 shows the fatigue fracture surface of 30% untreated ABS during the second stage of fracture (i.e. the non-Paris Erdogan section) and therefore is the most interesting micrograph. Not only does it have large areas of uneven matrix which show that the ABS particles are inducing local yielding, therefore promoting a more ductile mode of fracture, but it also has large areas of cleaved PMMA beads. These are particularly noticeable in the top right hand corner of the micrograph. The cleaved PMMA beads indicate that the crack is taking a more direct route through the cement probably as a result of the more rapid rate of fracture occurring during this section.

Two rubber particles are clearly visible, and a microcrack can be seen generating from the left rubber particle. A large amount of ductile tearing can be seen radiating from the rubber particles into the matrix and show that the crack has propagated on different planes.

The micrograph of the fatigue fracture surface of 40% untreated ABS (Figure 5.18) has been taken from the Paris Erdogan section where less rapid crack propagation has taken place. Therefore there are less cleaved PMMA beads and the surface is very uneven showing a large amount of ductile tearing. At this slow rate of fracture the crack has mainly propagated through the matrix and around the PMMA beads. There is, however, a microcrack visible and this may be a deformed pore already present in the sample.

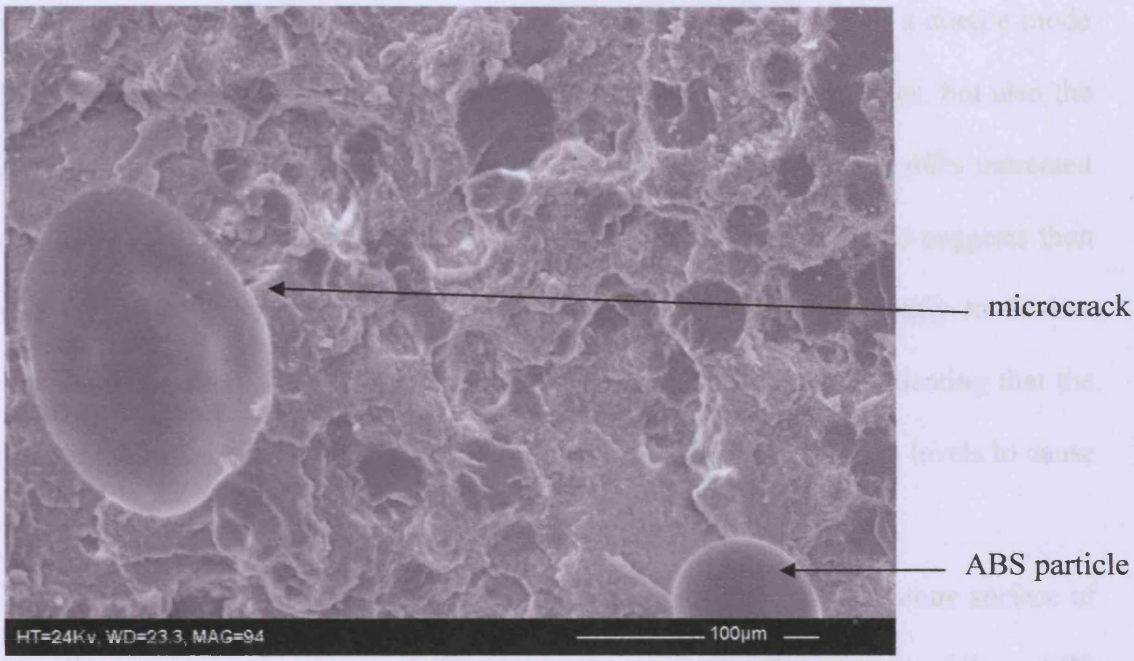

Figure 5.17:Fatigue fracture surface of 30% untreated ABS magnification x 94

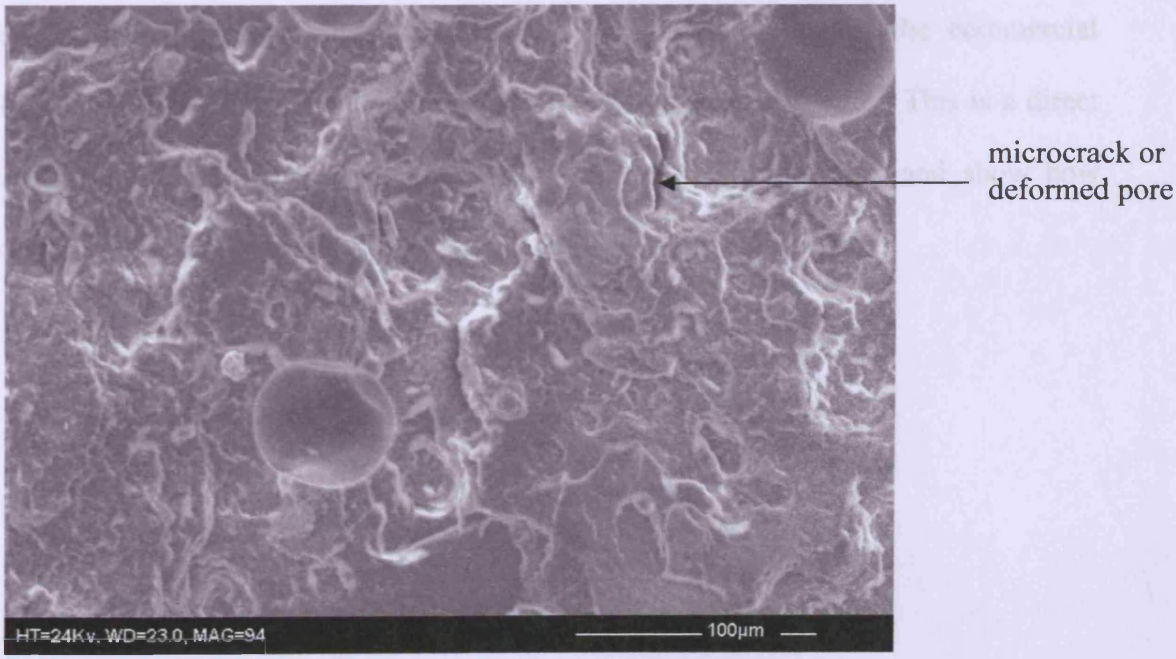

Figure 5.18: Fatigue fracture surface of 40% untreated ABS magnification x 94

The fracture surface of 30% silane-coated ABS (Figure 5.19) has also been taken from the Paris Erdogan region. The surface is very uneven and shows a ductile mode of crack propagation signifying not only the effect of the ABS particles, but also the slow rate of crack propagation. Unlike the fracture surfaces of 30 and 40% untreated ABS there appear to be 'troughs' near two of the rubber particles. This suggests than the rate of crack propagation has temporarily slowed down sufficiently to deviate from its preferential path. One of the rubber particles has cracked indicating that the stress levels at the equator of this particle has reached sufficiently high levels to cause fracture and this will have facilitated more local yielding.[106]

Two cracked ABS particles dominate the micrograph of the fracture surface of 40% silane-coated ABS (Figure 5.20). Again the stresses at the equators of these ABS particles must have been great enough to cause the particles to rupture and this would relieve stresses in the surrounding matrix, resulting in localised yielding.

All the fatigue fracture surfaces show how much more uneven and ductile the fatigue crack propagation is through these cements than either the commercial (Figures 3.13-3.15) or the experimental cements (Figures 4.23-4.25). This is a direct consequence of the rubber particles inducing plastic deformation, and show how effective these particles are in increasing the ductility of bone cement.

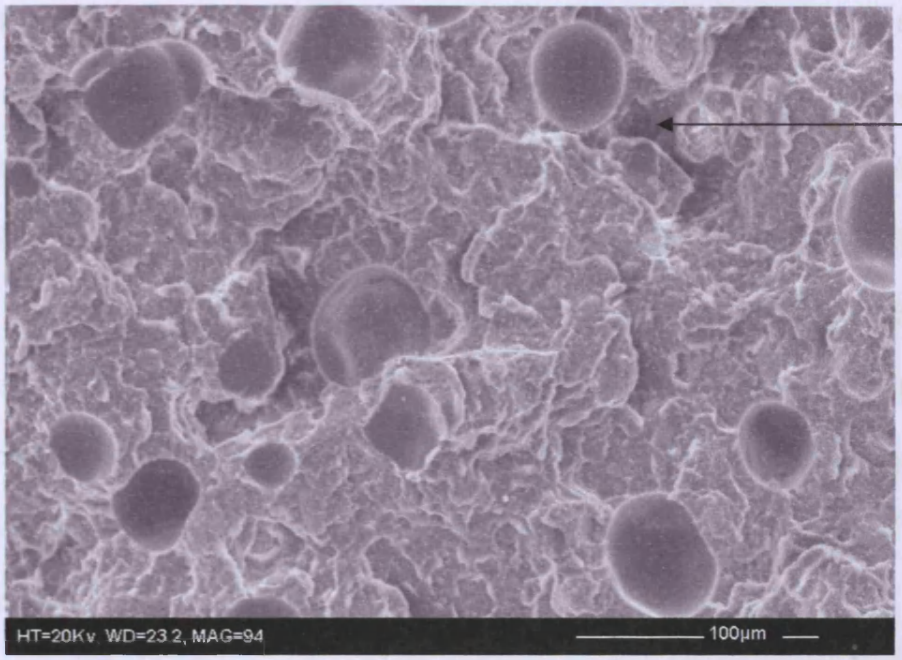

Figure 5.19: Fatigue fracture surface of 30% silane-coated ABS magnification x 94

Figure 5.20: Fatigue fracture surface of 40% silane-coated ABS magnification x 120

5.4 CONCLUSIONS

The objective of this chapter was to determine the effectiveness of the inclusion of untreated ABS particles in increasing the fracture toughness of bone cement, thereby improving the resistance of the bone cement to brittle fracture, and to establish if fracture toughness could be further enhanced by using silane-coated ABS particles.

The incorporation of either 10, 20, 30 or 40% untreated ABS particles did improved fracture toughness and so increased the resistance of an experimental bone cement to brittle fracture. The inclusion of 30% ABS resulted in the greatest increase in fracture toughness with K_{IC} values increasing from 2.30 MPa.m$^{1/2}$ (with no ABS present) to 2.73 MPa.m$^{1/2}$.

The incorporation of 10, 20, 30 or 40% silane-coated ABS particles also improved fracture toughness with 30% silane-coated ABS resulting in a greater increase in fracture toughness (K_{IC} = 2.87 MPa.m$^{1/2}$) than the equivalent percentage of untreated ABS particles. Fracture toughness was further improved with the incorporation of 40% silane-coated ABS (K_{IC} = 3.02 MPa$^{1/2}$)

The addition of 10, 20, 30 or 40% untreated or silane-coated ABS particles increased fracture toughness but caused a decrease in the flexural strength and modulus of the experimental cement. The flexural strengths and moduli continually decreased with increasing quantity of ABS particles. Obviously a compromise will have to be made between increased fracture resistance and any decreases in flexural properties.

The integration of 30% and 40% untreated or silane-coated ABS particles also dramatically improved fatigue crack propagation behaviour during the latter stages of propagation with a remarkable three-fold increase in fatigue resistance. Cements were

able to withstand a maximum stress intensity factor of at least 6 $MPa.m^{1/2}$, and therefore the risk of premature fracture by fatigue could be significantly reduced.

Adding untreated/silane-coated ABS particles also affected the rheological behaviour of acrylic cement. The incorporation of 10% untreated ABS as 25°C increased the overall curing rate from 11.7 minutes to 13.1 minutes. However, further additions of untreated ABS reduced the curing rate, with the cement containing 40% untreated ABS curing in 10.8 minutes. The same effect on curing rates was found when using silane-coated ABS, with cement containing 10% silane-coated ABS curing in 13.7 minutes and cement containing 40% surface treated ABS curing in 12.4 minutes.

The addition of untreated ABS particles did not change the maximum shear viscosity and maximum shear elastic modulus of the acrylic cement. However, silane-coated ABS particles greatly increased the maximum complex viscosity and maximum elastic modulus by approximately 35% and 33% respectively.

The use of either untreated ABS or silane-coated ABS particles has improved the fracture resistance of an experimental cement and further conclusions are found in the following chapter.

CHAPTER 6

CONCLUSIONS AND FURTHER WORK

6.1 CONCLUSIONS

This research confirms that the addition of ABS particles does improve the resistance of an experimental acrylic bone cement to brittle fracture. In addition, the innovative step of surface treating the ABS particles with the organosilane coupling agent, methacryloxypropyltrimethoxy-silane, can further improve fracture resistance.

The incorporation of untreated ABS particles increased fracture toughness of the experimental cement. The ABS particles effectively toughened the cement by promoting yielding and plastic deformation throughout the cement matrix via shearing and/or crazing mechanisms. This resulted in a 19% increase in fracture toughness with the incorporation of 30% untreated ABS particles.

Using silane-coated ABS particles further increased fracture toughness. The methacrylate portion of the organosilane agent present on the surface of the ABS particles chemically interacted with the cement during polymerization enabling the ABS to become chemically bonded to the cement matrix. This promoted more efficient toughening mechanisms and consequently the fracture toughness increased by 31% with the integration of 40% silane coated ABS.

The most striking effect of the incorporation of untreated and silane coated ABS was the changes they brought about in the fatigue crack propagation behaviour of the experimental cement. There was at least a three fold increase in the maximum stress intensity factor during the later stages of crack propagation which illustrates that the cement has the potential to withstand longer, faster growing cracks.

Furthermore, it appears as if the maximum stress intensity factor has to reach a critical level before the stress concentrations are sufficient to induce the shearing/crazing toughening mechanisms. It was, however, not possible to differentiate between the effect of the two types of ABS particles employed.

The incorporation of untreated or silane-coated ABS particles increased fracture toughness and fatigue resistance but also caused a corresponding decrease in the flexural strength and modulus. Therefore a compromise will have to be made between improvements in fracture resistance and any decrease in flexural properties.

This research also showed that adding 20% or more, untreated or silane-coated ABS particles decreased the handling time and therefore setting time of the original experimental cement. However, the setting times remained comparable to commercially available cements. The addition of silane-coated ABS particles also increased the maximum viscosity of the acrylic cement by 35% and maximum elastic modulus by approximately 33%.

The enhanced critical mechanical properties of acrylic cement toughened with ABS or silane coated ABS reveal that the cement is no longer so susceptible to brittle fracture. The fracture toughness and fatigue resistance of the toughened cements have improved so extensively that when in clinical use, for example as a fixating agent in a hip replacement, the cement is likely to be able to survive a sudden impact such as a person falling over. It is also more likely to be able to endure longer cracks before eventually fracturing and this will increase the working life of the implant. This shows that there is future potential in using acrylic cement toughened with ABS or silane-coated ABS particles.

6.2 FURTHER WORK

There are several areas in which this research can be extended. More investigation is needed to determine the critical quantity of untreated/silane coated ABS particles required to obtain the dramatic improvements seen in the fatigue properties during the latter stages of stable crack propagation. This may also highlight any differences in the fatigue behaviour as a result of the silane coupling agent.

Following on from this, it would be interesting to examine the fatigue crack growth behaviour of the new cements containing untreated or silane-coated ABS following a sudden increase in load, which would be equivalent to a person falling over. An overload can be applied during fatigue testing and the effect on the crack growth rate monitored.

During the course of testing it became clear that the surface morphology and size distribution of the PMMA beads has an influence on the cements' polymerization behaviour and therefore mechanical properties. Only a few authors have correlated the effect of bead sizes and bead size distribution on both curing behaviour and the resultant mechanical properties of the fully cured cement. Therefore further examination of these factors together would provide a more complete picture of the influences of bead sizes and bead size distribution on mechanical properties.

Finally, in order to enable the use of the new experimental cements in a clinical situation, their overt tackiness during the initial mixing stage would have to be addressed.

REFERENCES

1. Saha, S. and Pal, S. Mechanical properties of bone cement: a review. *Journal of Biomedical Materials Research*, 1984, **18**, pp.435-462.

2 Kohn, D. H. and Ducheyne, P. Materials for bone and joint replacement. In *Materials Science and Technology A comprehensive treatment.* Cahn, R.W., Haasen, P., Kramer, E.J. ed. Vol. 14, VCH, Weinheim, 1992.

3. Jasty, M. *et al.* The initiation of failure in cemented femoral components of hip arthroplasties. *Journal of Bone and Joint Surgery*, 1991, **73B**, pp.551-558.

4. Lennon, A. B. and Prendergast, P. J. Residual stress due to curing can initiate damage in porous bone cement: experimental and theoretical evidence. *Journal of Biomechanics*, 2002, **35**, pp.311-321.

5. Orr, J. F. *et al.* Shrinkage stresses in bone cement. *Biomaterials*, 2003, **24**, pp. 2933-2940.

6. Lu, X. and Topoleski, L. D. T. A controlled-notch specimen to study fatigue crack initiation in bone cement. *Journal of Biomedical Materials Research (Applied Biomaterials)*, 2000, **53**, pp.505-510.

7. Ishihara, S. *et al.* On fatigue lifetimes and fatigue crack growth behaviour of bone cement. *Journal of Materials Science: Materials in Medicine*, 2000, **11**, pp.661-666.

8. McCrum, N. G. *et al. Principles of Polymer Engineering.* 2nd edition, Oxford University Press, Oxford, 1997.

9. Young, R. J. and Lovell, P. A. *Introduction to Polymers.* 2nd edition, Chapman & Hall, London, 1991.

10. Rosen, S. L. *Fundamental Principles of Polymeric Materials.* 2nd edition, John Wiley & Sons, Inc, New York, 1993.

11. Charnley, J. Anchorage of the femoral head prosthesis to the shaft of the femur. *Journal of Bone and Joint Surgery*, 1960, **42B**, pp.28-30.

12. Lewis, G. Properties of acrylic bone cement: state of the art review. *Journal of Biomedical Materials Research*, 1997, **38**, pp.155-182.

13. Amar, A. R. *et al.* Percutaneous transpedicular polymethylmethacrylate vertebroplasty for the treatment of spinal compression fractures. *Neurosurgery*, 2001, **49**, pp.1105-1115.

14. Hukins, D. W. L. Manchester University, Lecture notes on biomaterials and biomechanics, 1994.

15. Cowie, J. M. G. *Polymers: Chemistry & physics of modern materials*. 2nd edition, Nelson Thornes Ltd, Cheltenham, 2001.

16. Park, J. B. Acrylic bone cement: in vitro and in vivo property-structure relationship-a selective review. *Annals of biomedical engineering*, 1983, **11**, pp.297-312.

17. Belkoff, S. M. and Molloy, S. Temperature measurement during polymerization of polymethylmethacrylate cement used for vertebroplasty. *Spine*, 2003, **28(14)**, pp.1555-1559.

18. Meyer, P. R. *et al.* On the setting properties of acrylic bone cement. *Journal of Bone and Joint Surgery*, 1973, **55A**, pp.149-156.

19. Haas, S.S. *et al.* A characterisation of polymethylmethacrylate bone cement. *Journal of Bone and Joint Surgery*, 1975, **57A**, pp.380-391.

20. Nicholas, M. K. D. *et al.* Analysis of the rheological properties of bone cement. *Journal of Materials Science: Materials in Medicine*, 2007, **18**, pp.1407-1412.

21. Madigan, S. *et al.* Influence of two changes in the composition of an acrylic bone cement on some of its properties: the case of surgical simplex® P. *Journal of Materials Science*, 2006, **41**, pp.5758-5759.

22. Pascual, B. *et al.* New aspects of the effect of size and size distribution on the setting parameters and mechanical properties of acrylic bone cements. *Biomaterials*, 1996, **17**, pp.509-516.

23. Vazquez, B. *et al.* Optimization of benzoyl peroxide concentration in an experimental bone cement based on poly(methyl methacrylate). *Journal of Materials Science: Materials in Medicine*, 1997, **8**, pp.455-460.

24. Pascual, B. *et al.* Modified acrylic bone cement with high amounts of ethoxytriethyleneglycol methacrylate. *Biomaterials*, 1999, **20**, pp.453-463.

25. Brauer, G. M. *et al.* Dependence of curing time, peak temperature and mechanical properties on the composition of bone cement. *Journal of Biomedical Materials Research*, 1986, **20**, pp.839-852.

26. Wixson, R. L. *et al.* Vacuum mixing of acrylic bone cement. *Journal of Arthroplasty*, 1987, **2**, pp.141-149.

27. Rimnac, C. M. *et al.* The effect of centrifugation on the fracture properties of acrylic bone cements. *Journal of Bone and Joint Surgery*, 1986, **68A**, pp.281-287.

28. Macaulay, M. D. *et al.* Differences in bone-cement porosity by vacuum mixing, centrifugation, and hand mixing. *Journal of Arthroplasty*, 2002, **17**, pp.569-575.

29. Muller, S. D. *et al.* The dynamic volume changes of polymerising poly-methyl methacrylate bone cement. *Acta Orthopaedica Scandinavica*, 2002, **73(6)**, pp.684-687.

30. Dunne, N. J. *et al.* The relationship between porosity and fatigue characteristics of bone cement. *Biomaterials*, 2003, **24(2)**, pp.239-245.

31. Gilbert, J. L. *et al.* A theoretical and experimental analysis of polymerization shrinkage of bone cement: A potential major source of porosity. *Journal of Biomedical Materials Research*, 2000, **52**, pp.210-218.

32. Dunne, N. J. and Orr, J. F. Influence of mixing techniques on the physical properties of acrylic bone cement. *Biomaterials*, 2001, **22**, pp.1819-1826.

33. Askeland, D.R. *The science and engineering of materials.* 2nd edition, Chapman and Hall, London, 1990.

34. Harper, E. J. and Bonfield, W. Tensile characteristics of ten commercial acrylic bone cements. *Journal of Biomedical Materials Research*, 2001, **58**, pp.605-616.

35. Puska, M. A. *et al.* Mechanical properties of oligomer-modified acrylic bone cement. *Biomaterials*, 2003, **24**, pp.417-425.

36. Noble, P.C. Selection of acrylic bone cements for use in joint replacement. *Biomaterials*, 1983, **4**, pp.94-100.

37. Kurtz, S. M. *et al.* Static and fatigue mechanical behavior of bone cement with elevated barium sulfate content for treatment of vertebral compression fractures. *Biomaterials*, 2005, **26**, pp.3699-3712.

38. Kusy, R. P. Characterization of self-curing acrylic bone cements. *Journal of Biomedical Materials Research*, 1978, **12**, pp.271-305.

39. Kuhn, K-D. Bone Cements: *Up-To-Date Comparison of Physical & Chemical Properties of Commercial Materials*. Springer, Berlin, 2000.

40. Robinson, R. P. *et al.* Mechanical properties of poly(methyl methacrylate) bone cements. *Journal of Biomedical Materials Research*, 1981, **15**, pp.203-208.

41. Weber, S. C. and Bargar, W. L. A comparison of the mechanical properties of simplex, zimmer, and zimmer low viscosity bone cements. *Biomaterials, Medical Devices and Artificial Organs*, 1983, **11(1)**, pp.3-12.

42. Linden, U. Mechanical properties of bone cement. *Clinical Orthopaedics and Related Research*, 1991, **272**, pp.274-278.

43. Combs, S. P. and Greenwald, A. S. The effects of barium sulphate on the polymerization temperature and shear strength of surgical simplex p. *Clinical Orthopaedics and Related Research*, 1979, **145**, pp. 287-291.

44. Taitsman, J. P. and Saha, S. Tensile strength of wire-reinforced bone cement and twisted stainless-steel wire. *Journal of Bone and Joint Surgery, American Volume*, 1977, **59**, pp.419-425.

45. Jasper, L. E. *et al.* Material properties of various cements for use with vertebroplasty. *Journal of Materials Science: Materials in Medicine*, 2002, **13**, pp.1-5.

46. Lautenschlager, E. P. *et al.* Mechanical properties of bone cements containing large doses of antibiotic powders. *Journal of Biomedical Materials Research*, 1976, **10**, pp.929-938.

47. Taylor, D. *et al.* The effect of stress concentrations on the fracture strength of polymethylmethacrylate. *Materials Science and Engineering A*, 2004, **382**, pp.288-294.

48. Pascual, B. *et al.* Influence of the modification of P/L ratio on a new formulation of acrylic bone cement. *Biomaterials*, 1999, **20**, pp.465-474.

49. Vallo, C.I. Influence of load type on flexural strength of a bone cement based on PMMA. *Polymer Testing*, 2002, **21**, pp.793-800.

50. Ishihara, S. *et al.* The static and cyclic strength of a bone-cement bond. *Journal of Materials Science: Materials in Medicine*, 2002, **13**, pp.449-455.

51. Higgs, W. A. J. *et al.* Evaluating acrylic and glass-ionomer cement strength using the biaxial flexure test. *Biomaterials*, 2001, **22**, pp.1583-1590.

52. Vallo. C. I. Flexural strength distribution of a PMMA-based bone cement. *Journal of Biomedical Materials Research (Applied Biomaterials)*, 2002, **63**, pp.226-236.

53. Lewis, G. *et al.* Influence of the radiopacifier in an acrylic bone cement on its mechanical, thermal, and physical properties: Barium sulphate-containing cement versus iodine-containing cement. *Journal of Biomedical Materials Research Part B: Applied Biomaterials*, 2004, **73B**, pp.77-87.

54. Liu, C. *et al.* Some failure modes of four clinical bone cements. *Proeedings of the Instution of Mechanical Engineers Part H*, 2001, **215**, pp.359-366.

55. Griffith, A. A. The phenomena of rupture and flow in solids. *Philosophical Transactions of the Royal Society of London*, 1921, **221A**, pp. 163-198.

56. Kinloch, A. J. and Young, R. J. *Fracture Behaviour of Polymers*. Elsevier Applied Science Publishers, London and New York, 1985.

57. Ward, I. M. *Mechanical Properties of Solid Polymers*. 2nd edition, John Wiley & Sons, Chichester, 1979.

58. Crawford, R. J. *Plastics Engineering*. 2nd edition, Pergamon Press, Oxford, 1990.

59. International Standard ISO 13586. Plastics - Determination of fracture toughness (G_{IC} et K_{IC}) - Linear elastic fracture mechanics (LEFM) approach, 2000.

60. Ginebra, M. P. *et al.* Mechanical performance of acrylic bone cements containing different radiopacifying agents. *Biomaterials*, 2002, **23**, pp.1873-1882.

61. Vallo, C. I. *et al.* Mechanical and fracture behaviour evaluation of commercial acrylic bone cements. *Polymer International*, 1997, **43**, pp.260-268.

62. Beaumont, P. W. R. The strength of acrylic bone cements and acrylic cement-stainless steel interfaces. *Journal of Materials Science*, 1977, **12**. pp.1845-1852.

63. Lewis, G. Apparent fracture toughness of acrylic bone cement: effect of test specimen configuration and sterilization method. *Biomaterials*, 1999, **20**, pp.69-78.

64. Higgs, W. A. J. *et al.* Comparison of the material properties of PMMA and glass-ionomer based cements for use in orthopaedic surgery. *Journal of Materials Science: Materials in Medicine*, 2001, **12**, pp.453-460.

65. Gilbert, J. L. *et al.* Self-reinforced composite poly(methyl methacrylate): static and fatigue properties. *Biomaterials*, 1995, **16**, pp.1043-1055.

66. Alberts, L, R. *et al.* Mechanical and strength properties of a low and high viscosity PMMA cements, vacuum mixed, room temperature and prechilled components. *Transactions of the 25th Annual Meeting of the Society for Biomaterials,* 1999, p.388.

67. Lewis, G. Effect of loading rate on the apparent fracture toughness of acrylic bone cement. *Bio-Medical Materials and Engineering*, 2002, **12**, pp.149-155.

68. Lewis, G. and Bhattaram, A. Influence of a pre-blended antibiotic (gentamicin sulfate powder) on various mechanical, thermal, and physical properties of three acrylic bone cements. *Journal of Biomedical Applications*, 2006, **20**, pp.377-408.

69. Davies, J. P. and Harris, W. H. Effect of hand mixing tobramycin on the fatigue strength of Simplex P. *Journal of Biomedical Materials Research*, 1991, **25**, pp.1409-1414.

70. James, S. P. *et al.* A fractographic investigation of PMMA bone cement focusing on the relationship between porosity reduction and fatigue life. *Journal of Biomedical Materials Research*, 1992, **26**, pp.651-662.

71. Johnson, J. A. *et al.* On factors influencing the fatigue of acrylic bone cement. *12th Annual Meeting of the Society for Biomaterials*, May, 1986.

72. Freitag, T. A. and Cannon, S. L. Fracture characteristics of acrylic bone cements. II. Fatigue. *Journal of Biomedical Materials Research*, 1977, **11**, pp.609-624.

73. Molino, L. N. and Topoleski, L. D. T. Effect of $BaSO_4$ on the fatigue crack propagation rate of PMMA bone cement. *Journal of Biomedical Materials Research*, 1996, **31**, pp.131-137.

74. Suresh, S. *Fatigue of Materials*. 2nd edition, Cambridge University Press, Cambridge, 2003.

75. Hertzberg, R. W. and Manson, J. A. *Fatigue of Engineering Plastics*. Academic Press, London, 1980.

76. Murphy, B. P. and Prendergast, P. J. On the magnitude and variability of the fatigue strength of acrylic bone cement. *International Journal of Fatigue*, 2000, **22**, pp.855-864.

77. Dunne, N. J. *et al.* The relationship between porosity and fatigue characteristics of bone cement. *Biomaterials*, 2003, **24**, pp.239-245.

78. Lewis, G. *et al.* Effect of test frequency on the in vitro fatigue life of acrylic bone cement. *Biomaterials*, 2003, **24**, pp.1111-1117.

79. Lewis, G. and Janna, S. I. Effect of fabrication pressure on the fatigue performance of Cemex XL acrylic bone cement. *Biomaterials*, 2004, **25**, pp.1415-1420.

80. Krause, W. *et al.* Fatigue properties of acrylic bone cements: S-N, P-N, and P-S-N data. *Journal of Biomedical Materials Research: Applied Biomaterials*, 1988, **22**, pp.221-244.

81. Johnson, J. A. *et al.* Fatigue of acrylic bone cement - Effect of frequency and environment. *Journal of Biomedical Materials Research*, 1989, **23**, pp.819-831.

82. Nguyen, N. C. *et al.* Reliability of PMMA bone cement fixation: fracture and fatigue crack-growth behaviour. *Journal of Materials Science: Materials in Medicine*, 1997, **8**, pp.473-483.

83. Wright, T. M. and Robinson, R. P. Fatigue crack propagation in polymethylmethacrylate bone cements. *Journal of Materials Science*, 1982, **17**, pp.2463-2468.

84. Askew, M. J. *et al.* Fracture toughness and crack propagation rates of bone cements and a polyisobutylene-toughened polymethylmethacrylate material. *The 20th Annual Meeting of the Society for Biomaterials*, April 5-9, 1994, Boston, pp.417.

85. Baleani, M. *et al.* The effect of gentamicin sulphate on the fracture properties of a manually mixed bone cement. *Fatigue and Fracture of Engineering Materials and Structures*, 2007, **30**, pp.479-488.

86. Barnes, H. A. *et al. An introduction to rheology*. Elsevier, Amsterdam, 1998.

87. Van Krevelen, D. W. *Properties of polymers*. 3rd edition, Elsevier, Amsterdam, 1997.

88. Verdonschot, N. and Huiskes, R. Creep properties of three low temperature-curing bone cements: A preclinical assessment. *Journal of Biomedical Materials Research*, 2000, **53**, pp.498-504.

89. Lee, A. J. C. *et al.* Factors affecting the mechanical and viscoelastic properties of acrylic bone cement. *Journal of Materials Science: Materials in Medicine*, 2002, **13**, pp.723-733.

90. Liu, C. *et al.* Creep behavior comparison of CMW1 and palacos R-40 clinical bone cements. *Journal of Materials Science: Materials in Medicine*, 2002, **13**, pp.1021-1028.

91. Nicholas, M. K. D. The viscoelastic properties of bone cement. MSc. dissertation, Manchester, 1994.

92. Dunne, N. J. and Orr, J. F. Curing characteristics of acrylic bone cement. *Journal of Materials Science: Materials in Medicine*, 2002, **13**, pp.17-22.

93. Krause, W. R. *et al.* The viscosity of acrylic bone cements. *Journal of Biomedical Materials Research*, 1982, **16**, pp.219-243.

94. Lewis, G. and Carroll, M. Rheological properties of acrylic bone cement during curing and the role of the size of the powder particles. *Journal of Biomedical Materials Research*, 2002, **63**, pp.191-199.

95. Farrar, D. F. and Rose, J. Rheological properties of PMMA bone cements during curing. *Biomaterials*, 2001, **22**, pp.3005-3013.

96. Hernandez, L. *et al.* Preparation of acrylic bone cements for vertebroplasty with bismuth salicylate as radiopaque agent. *Biomaterials*, 2006, **27**, pp.100-107.

97. Kotha, S. P. *et al.* Fracture toughness of steel-fibre-reinforced bone cement. *Journal of Biomedical Materials Research*, 2004, **70A**, pp.514-521.

98. Saha, S. and Warman, M. L. Compressive and shear properties of graphite reinforced bone cement. *Orthopaedic Transactions*, 1979, **3**, p.164.

99. Wright, T. M. and Trent, P. S. Mechanical properties of aramid fibre-reinforced acrylic bone cement. *Journal of Materials Science*, 1979, **14**, pp.503-505.

100. Topoleski, L. D. *et al.* Flow intrusion characteristics and fracture properties of titanium-fibre-reinforced bone cement. *Biomaterials*, 1998, **19**, pp.1569-1577.

101. Kotha, S. P. *et al.* Improved mechanical properties of acrylic bone cement with short titanium fiber reinforcement. *Journal of Materials Science: Materials in Medicine*, 2006, **17**, pp.1403-1409.

102. Vallo, C. I. Influence of filler content on static properties of glass-reinforced bone cement. *Journal of Biomedical Materials Research*, 2000, **53**, pp.717-727.

103. Ackley, M. A. and Monroe, E. Alumina as a filler for bone cement: a feasibility study. *Biomaterials*, 1980, **1**, pp.217-221.

104. Richardson, M. O. W. *Polymer Engineering Composites*. Applied Science Publishers Ltd, London, 1977.

105. Bucknall, C. B. *et al.* Rubber toughening of plastics. Part 7. Kinetics and mechanisms of deformation in rubber-toughened PMMA. *Journal of Materials Science*, 1984, **19**, pp.2064-2072.

106. Lovell, P. 2001. A. Rubber-toughened plastics: Strategies for their preparation and evaluation. <URL:http://www.academic.sun.ac.za/unesco/PolymerED2001/Contributions/AbstUNESCO/Lovell.pdf?> [Accessed 6th February 2007].

107. Todo, M. *et al.* Toughening mechanisms of rubber toughened PMMA. *JSME International Journal Series A - Solid Mechanics and Material Engineering*, 1999, **42**, pp.585-591.

108. Dow Corning. 2000. A guide to silane solutions from dow corning <URL:http//www.dowcorning.com/content/publishedit/SILANE-GUIDE.pdf?DCWS=Silanes%20Solutions&DCWSS=> [Accessed: 3rd October 2006].

109. Witucki, G. L. A silane primer: Chemistry and applications of alkoxy silanes. *Journal of Coatings Technology*, 1993, **65**, pp.57-60.

110. Arkles, B. Tailoring surfaces with silanes. *Chemtech*, 1977, **7**, pp.766-778.

111. Vila, M. M. *et al.* Effect of porosity and environment on the mechanical behavior of acrylic bone cement modified with acrylonitrile-butadiene-styrene particles:I. Fracture toughness. *Journal of Biomedical Materials Research (Applied Biomaterials)*, 1999, **48**, pp.121-127.

112. Vila, M. M. *et al.* Effect of porosity and environment on the mechanical behavior of acrylic bone cement modified with acrylonitrile-butadiene-styrene particles: Part II. Fatigue crack propagation. *Journal of Biomedical Materials Research (Applied Biomaterials)*, 1999, **48**, pp.128-134.

113. Puckett, A. D. *et al.* Improved orthopaedic bone cement formulations based on rubber toughening. *Critical Reviews in Biomedical Engineering*, 2000, **28(3&4)**, pp.457-461.

114. Moseley, J. P. *et al.* The development and characterization of a fracture-toughened acrylic for luting total joint arthroplasties. *Journal of Biomedical Materials Research*, 1999, **47**, pp.529-536.

115. Murakami, A. *et al.* Rubber-modified bone cement. *Journal of Materials Science*, 1988, **23**, pp.2029-2036.

116. Perek, J. and Pilliar, R. M. Fracture toughness of composite acrylic bone cements. *Journal of Materials Science: Materials in Medicine*, 1992, **3**, pp.333-344.

117. International Standard ISO 178, Plastics - Determination of flexural properties. 1993.

118. Schering Corporation, U.S.A. 1994, Palacos LV-40 instructions and data sheet.

119. British Standard Institute, Draft for Development, Method for determination of threshold stress intensity factors and fatigue crack growth rates in metallic material. 1999.

120. Bland, M. *An Introduction to Medical Statistics*. 2nd edition, Oxford University Press, Oxford, 1997.

121. Ginebra, M. P. *et al.* Effect of size distribution of the PMMA beads on the fatigue crack propagation of acrylic bone cements. *Transactions of the 16th European Conference on Biomaterials*, London, U.K. 2001, pp. T20.